Phase Transitions in Polyampholytic Polymers and Hydrogels

by

Anthony Evan English

B.A.Sc., Simon Fraser University (1987)
M.A.Sc., University of Toronto (1989)

Submitted to the Harvard-MIT Division of Health Sciences and Technology
in partial fulfillment of the requirements for the degree of

Doctor of Philosophy in Medical Engineering and Medical Physics

at the

MASSACHUSETTS INSTITUTE OF TECHNOLOGY

March 1996

Author .....
Harvard-MIT Division of Health Sciences and Technology
March 26, 1996

Certified by .....
Toyoichi Tanaka
Professor of Physics
Thesis Supervisor

Accepted by .....
Martha L. Gray
Chairman, Departmental Committee on Graduate Students

Phase Transitions in Polyampholytic Polymers and Hydrogels

by

Anthony Evan English

Submitted to the Harvard-MIT Division of Health Sciences and Technology
on March 20, 1996, in partial fulfillment of the
requirements for the degree of
Doctor of Philosophy in Medical Engineering and Medical Physics

Abstract

Polyampholytes represent a class of ionic copolymer containing positive, negative and even neutral monomers. The unique physical properties of polyampholytes that arise from Coulombic interactions between polymeric and solvent ions make them of interest to both the scientific and engineering community. This study presents an experimental and analytical investigation of the phase behavior of polyampholytic polymers and hydrogels as a function of thermal energy, ionic screening length, solvent interactions, and elastic forces. Using massively parallel supercomputer simulations the thermal phase transitions of individual polyampholyte chains have been examined and the extrapolation of these simulations to real physical systems is critically examined. Based on an experimental study of acrylamide polyampholytic hydrogels, the role of ion dissociation equilibria and counter ion shielding has been investigated. By considering the non-equilibrium swelling transitions of polyampholytes it is shown, in contradiction to a number of recent experimental, analytical and computational studies, that acid and base dissociation equilibria plays a fundamental role in the thermodynamic behavior of these materials. The properties of balanced and slightly unbalanced polyampholytes are compared to polyelectrolyte systems.

Thesis Supervisor: Toyoichi Tanaka
Title: Professor of Physics

Acknowledgments

To my supervisor, Dr. Toyoichi Tanaka, I owe a special thanks for giving me the opportunity to work in laboratory built on twenty years of his experience and for helping me fund my work during difficult economic times. Much of my work I have based on the earlier studies of a good friend and colleague of mine, Dr. Xiaohong Yu. Initiating a new series of experimental protocols is perhaps one of the most difficult phases of any new research endeavor. As a result, Dr. Yu's contribution cannot be underestimated. I also owe a special thanks to Dr. Alan Grodzinsky, Dr. José Manzanares and Dr. Salvador Mafé for contributing to the theoretical foundations of my work. In addition, I wish to acknowledge Dr. Vijay Pande for his time in helping me with the computer resources I needed to do much of my work. I will remember Alexander Grosberg for his genuine interest as an acting mentor and for including me in collaborations with others and for helping give me the opportunity to present my work at a conference I would have overlooked. My colleagues, Rose Du, Zhonghua Pei, Dr. Michal Orkisz, Kevin Wasserman, Changang Wang, and Hua Yang I owe a special thanks for both their scientific input and comradery. To Dr. Steven Leeb and Ahmed Mitwalli I thank for their creative ideas and suggestions and for reminding me that I'm still an engineer at heart. I wish to acknowledge the generous fellowship support from Raytheon corporation and Rhône-Poulenc Rorer that made it possible for me to attend MIT. For the few times I was able to spend with my family during the years of my studies I am grateful. In particular, I will never forget Elissa and Audrey for their laughter which still echoes down the infinite corridor.

Contents

List of Figures

Chapter 1

Introduction

Polyampholytes represent a special class of ionic copolymers which contain positive, negative and even neutral monomers. The unique physical properties of these materials that arise from Coulombic interactions between polymeric and solvent ions make them of interest to both the scientific and engineering community. Synthetic polyampholytes are now emerging as a model for understanding the thermodynamic behavior of proteins, biomolecules and other forms of soft condensed matter. The phase transitions these materials can undergo in response to small changes in external stimuli make them of potential use as artificial muscles or micro actuators, controlled drug release systems, and materials for separation and filtration processes. Studies into the equilibrium and non-equilibrium phase behavior of polyampholytes are therefore expected to lead to wide applications in chemical, agricultural and medical technologies

1.1 Historical Perspective

Since a polyampholyte consists of charged monomers immersed in a solvent medium, it is no surprise that many analytic treatments have their foundations based on ionic solution theory. Ionic solution theory, like much of polymer physics, arose

out of the many methods used to treat imperfect gases and simple fluids. It was through the work of McMillan and Mayer[McM45] that the formal procedures for treating imperfect gases using virial expansions and integral equations was extended to ionic solutes in solution. It is interesting to note that the intractability of the long range Coulombic forces in ionic solutions first lead Debye and Hückel[Deb23,Lan58] in 1923 to develop their potential theory. The Debye-Hückel theory describes the thermodynamic behavior of an ionic solution by defining the mean electrostatic potential in the vicinity of a reference ion. It wasn't until 1950, however, that Mayer[May50] developed a cluster expansion theory for ionic solutions that established the Debye-Hückel approximation as a first order correction in an infinite series expansion.

The shortcoming of many of the ionic solution series expansion methods is that beyond the Debye-Hückel approximation calculations become non-trivial very rapidly. As a result, many analytic descriptions of polyampholytes are based on the concept of a Debye-Hückel plasma which is limited to low ion concentrations. In 1980 Edwards, King and Pincus[Edw80] proposed one of the first theoretical descriptions of polyampholyte phase transition phenomena using the Debye-Hückel theory. Their model predicted that polymers which carry a balanced number of positive and negative charges exhibit a phase transformation from an extended random flight configuration to a condensed microphase. Higgs and Joanny[Hig91] included the third virial coefficient in a Debye-Hückel model where both charged monomers and small ions contribute to the electrostatic screening. Baker et al.[Bak95] and Yu[Yu93] have used Debye-Hückel models with correction factors to explain their data. Using a modified Flory theory Dobrynin et al.[Dob95] used Debye-Hückel interactions to model polyampholyte swelling transitions as a function of temperature and charge offset.

The total number of experimental studies of synthetic polyampholytes is relatively small. The important contributions by Corpart et al.[Cor93], Skouri et al.[Sko94],

Baker et al.[Bak94,Bak95], Annaka et al.[Ann92,Ann94], and Yu[Yu93] represent a significant fraction of polyampholyte studies which have been performed to date. Of particular interest has been the transition from collapsed balanced polyampholyte behavior to swollen unbalanced polyampholyte or polyelectrolyte behavior with increasing polymer charge offset. Figure 1-1, for example, shows the data obtained from one study[Yu93] of polyampholytic hydrogel swelling that clearly illustrates the transition from collapsed polyampholyte behavior to swollen unbalanced polyampholyte behavior. In particular, the flat swelling transition observed near the balance point, shown in Fig. 1-2, has been the subject of a number of recent investigations. In a series of four publications, Kantor et al.[Kan92,Kan94,Kan95a,Kan95b] made a thorough study of the swelling properties of isolated short chain polyampholytes with a lattice simulation. Kantor et al. found that a critical charge offset was required to cause swelling and concluded that the flat region shown in Fig. 1-2 was the result of charge offset alone.

The growth in the development in random system theories has inspired a number of new analytical and computational studies that have been aimed specifically at understanding the role of disorder in polyampholytes. Qian et al.[Qia88] investigated randomly charged polyampholyte chains in a θ solvent using replica field theory. Gutin et al.[Gut95] also considered randomness in polyampholyte models. Using a Blume Emery Griffiths Ising spin lattice model Aalberts et al.[Aal94] were able to reproduce the flat swelling transition region shown in Fig. 1-2. The microscopic model of Aalberts et al. considered the charge distribution randomness as random fields producing competing quenched random interactions in a spin system. The internal pH was assumed equal to that of the surrounding bath.

Due to the very slow kinetics found in spin glass systems, recent computational, analytical and experimental studies of polymer based polyampholyte transitions have also considered these systems advantageous from the point of view of their rapid kinetic response[Yu93,Kan92]. This thesis shows that the kinetic response

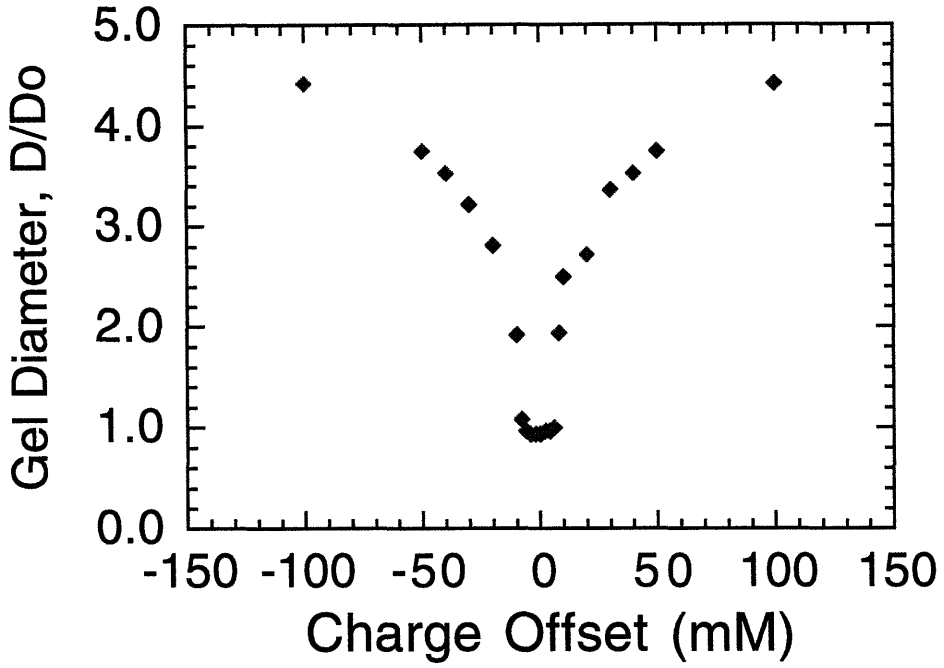

Figure 1-1: Polyampholyte swelling versus charge offset. Previous experimental studies of polyampholyte phase behavior showed a symmetric swelling distribution around the balance point. The diameter measurements of cylindrical hydrogels were scaled to the diameter at which the hydrogel was cast (Do).

of these materials is far longer than realized and is an important part of both the experimental and theoretical understanding of these materials. In fact, most of the data presented in Figs. 1-1 and 1-2, which has been used in support of three extensive studies[Yu93,Kan92,Kan94,Kan95a,Kan95b,Aal94], has not reached thermodynamic equilibrium.

1.2 Thesis Outline

An interesting aspect of polyampholytes in aqueous solutions that has been repeatedly overlooked in most recent studies are the effects of ion dissociation. There has been no careful study of the hydrogen and hydroxide ion equilibria of synthet-

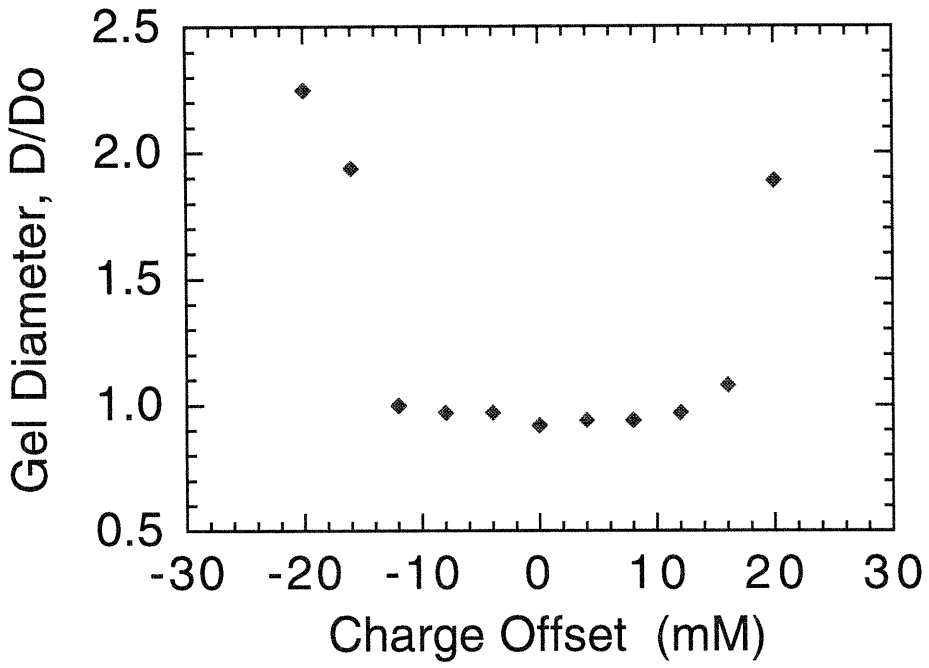

Figure 1-2: Polyampholyte swelling near the charge balance point. Near the polyampholyte charge balance point a flat swelling transition was observed. The diameter measurements of cylindrical hydrogels were scaled to the diameter at which the hydrogel was cast (Do).

ic polyampholytes which bear both positive and negative charges. In fact many studies have completely ignored the role of counter ions altogether. By not considering the long equilibration times one is in essence ignoring ion dissociation effects when polyampholytes are prepared under certain conditions. This thesis shows that despite the importance of most of these recent experimental and theoretical investigations, ion dissociation is an effect that cannot be overlooked even for monomeric groups with highly dissociable ionic groups. The purpose of this thesis is thus not to undermine, but to complement the results of these previous studies.

Chapter 2 examines the properties of isolated polyampholytes using a dynamic Monte Carlo simulation and analytical arguments. The coil globule transition temperature is found using heat capacity estimates from the simulations. The nature

of the coil globule transition in balanced polyampholytes is described and compared to other analytic studies. The scaling behavior of the radius of gyration as a function of temperature and polymer length is also obtained. This chapter then discusses the implications of ignoring counter ions in these models. In particular, the extrapolation of these models to real physical systems is critically examined.

Chapter 3 presents a detailed analytical and experimental study of the equilibrium and non-equilibrium properties of polyelectrolyte hydrogels. Since polyelectrolytes contain charge groups of only one sign their properties are extremely important for comparing and contrasting the behavior of polyampholytes with both positive and negative charges. In particular, the charged monomer used in this study is a dissociable acid group that produces very clearly the swelling characteristic of a polyelectrolyte with dissociable ionic monomer groups.

In chapter 4 the role of counter ions and ion dissociation in establishing the equilibrium swelling of balanced and unbalanced polyampholytic hydrogels is investigated experimentally and theoretically. The swelling dependence on both the net charge offset and the external bath salt concentration is examined using an acrylamide based polyampholytic hydrogel. By careful consideration of the swelling kinetics, this chapter illustrates the effects of ion dissociation equilibria and counter ion shielding in polyampholytic hydrogels near their balance point where both polyelectrolyte and polyampholyte effects are present. The theory presented in this chapter considers a Flory type swelling model where the Coulombic interactions between fixed ions in the hydrogel resemble those of an ionic solid with a Debye screening factor. Theoretical predictions from this model are shown to be in qualitative agreement with experimental results.

The role of counter ions and ion dissociation in establishing the equilibrium swelling of balanced and unbalanced polyampholytic hydrogels with variable concentrations of neutral monomeric spacers is investigated in chapter 5. The competing solvent, elastic, polyelectrolyte, and polyampholyte effects over a wide range of

bath salt concentrations and monomeric composition is illustrated. It will be shown that dissociable monomeric groups with very high dissociation constants can still show swelling patterns consistent with ion association at low ionic strengths.

This thesis will demonstrate that many of the interactions that have been used to explain real experimental data are often masked by ion dissociation effects at low ionic strengths and high monomeric ion concentrations. It will be shown how dissociation effects can easily be overlooked in many cases simply because the associated kinetcs can be very long. This thesis will also describe the disadvantages of the Debye-Hückel approximation in polyampholytes where the polyion and small ion concentrations are on the order of 1 M. It will be shown that very simple Donnan models, which have been in existence for over fifty years, can still provide valuable insight into ionic polymeric systems in aqueous solutions.

Chapter 2

Polyampholytic Polymer Phase Transitions

Abstract

The thermal phase behavior of isolated polyampholyte polymers in a good solvent is examined using a dynamic Monte Carlo simulation and analytical arguments. It is shown computationally that polyampholytes with an equal number of positive and negative charges exhibit a well defined first order phase transition from an extended coil configuration to an ordered crystalline structure. A heat capacity peak between the random coil configuration and a Debye-Hückel globular structure was not observed. The important role of counter ions in unbalanced polyampholyte behavior is discussed.

2.1 Introduction

Polyampholyte polymers consist of a linear sequence of positive and negative monomers. Balanced polyampholytes have an equal number of positive and negative monomers while unbalanced polyampholytes have an excess of one type of charged monomer. A polyelectrolyte polymer is a polyampholyte with charge groups of only one sign. The many body Coulombic interactions which dominate the behavior of polyampholytes near the balance point in a good solvent create a very complicated

set of interactions which are still not very well understood.

The study of isolated polyampholyte polymers has received much theoretical interest. Edwards and King[Edw80] first showed that the electrostatic interactions within a balanced random polyampholyte lead to a collapse transition from a random flight configuration to a condensed microelectrolyte with Debye-Hückel structure. Higgs and Joanny[Hig91] analyzed polyampholyte phase behavior using scaling arguments and the uniform expansion method based on the assumption that the ionic distribution was also that of Debye-Hückel plasma. Gutin and Shakhnovich[Gut95] investigated random polyampholyte chains near the balance point using scaling arguments and concluded that Coulombic interactions between charged monomers leads to globule formation in balanced polyampholytes and elongated structures in unbalanced polyampholytes.

Due to the complicated Coulombic interactions within polyampholyte polymers the application of numerical simulations to these systems has received much consideration. Based on dynamic Monte Carlo simulations, Kantor et al.[Kan92] have made a very thorough study of polyampholyte phase transitions using a modified Coulomb potential. The results of Kantor et al. show that a charge offset of $\sqrt{N}$, where N is the number of monomers, is required to produce polyampholyte swelling. De Souza et al.[DeS93] used a Monte Carlo simulation to study polyampholyte transitions using a screened Coulomb potential and found that balanced polyampholytes collapse and unbalanced polyampholytes swell. Using a lattice Monte Carlo simulation based on random fields and a three state Ising spin model, Aalberts et al.[Aal94] observed similar phase behavior near the polyampholyte balance point. Victor and Imbert[Vic93] performed a Monte Carlo study of alternating polyampholytes and concluded that a coil to crystalline lattice theta transition describes these polymeric materials.

The objective of this study is to examine the equilibrium phase behavior of isolated polyampholyte polymers as a function of temperature using a dynamic

Monte Carlo algorithm and analytical arguments based on the restricted primitive Coulombic interaction model[Out74]. Heat capacity measurements are obtained and the computed thermodynamic parameter variability due to both changes in the quenched charged sequence and numerical artifacts is illustrated. It is shown computationally that polyampholytes with an equal number of positive and negative charges exhibit a well defined first order phase transition from an extended coil configuration to an ordered crystalline structure. Since a Debye-Hückel structure globular conformation does not represent a totally collapsed configuration it is interesting to note that these simulations do not produce a heat capacity peak between the random coil configuration and Debye-Hückel globular structures described using previous analytic approaches.

2.2 Lattice Simulations

2.2.1 Polyampholyte Model

The polyampholyte model in this study consists of a dynamic Monte Carlo lattice algorithm based on the bond fluctuation method[Car88]. This algorithm has the advantage of combining the simplicity of lattice Monte Carlo methods with those of continuous Brownian dynamics. The monomer positions are discretized to a three dimensional lattice with the polymer connectivity implemented by restricting the maximum separation between neighboring monomers to four lattice units. Hard sphere excluded volume interactions are simulated by not allowing any pair of monomers to come closer than two lattice units.

In three dimensions the Coulombic energy between two monomers is of the form

$$U(r) = \frac{z_1 z_2 e^2}{4\pi\epsilon r}, \tag{2.1}$$

where z_i represent the valence of monomer charge i, e the unit charge, r the monomer

separation distance, and ϵ is the solvent permittivity. For the purpose of simulation it is convenient to define a set of reduced parameters. For a given temperature the charge coupling is

$$\gamma = \frac{e^2}{4\pi\epsilon a k_B T} = \frac{l_B}{a}, \tag{2.2}$$

where a is the lattice unit distance, k_B the Boltzmann constant, T the absolute temperature, and l_B the Bjerrum length. The dimensionless reduced temperature is

$$T^* = \frac{1}{\gamma}. \tag{2.3}$$

The reduced Coulombic potential for an ensemble of monomers is therefore

$$U^*(r'_{ij}) = \sum_{ij} \frac{z_i z_j}{r'_{ij}}, \tag{2.4}$$

where r'_{ij} is the separation distance between monomers i and j in lattice units.

2.2.2 Method

For each Monte Carlo time step an attempt is made to move every monomer by one lattice unit in a random direction. The monomers are selected at random and based on the Metropolis criterion[Met53] each movement is accepted or rejected. For a given temperature a polymer of length N is thermalized for 250 N^2 Monte Carlo time steps and then the first two moments of the squared radius of gyration and energy per monomer are estimated from the next 250 N^2 Monte Carlo time steps. Based on the internal energy variance, $\Delta U(T^*)$, and temperature the specific heat capacity is calculated using

$$C_v(T^*) = \frac{\Delta U(T^*)}{(T^*)^2}. \tag{2.5}$$

The equilibrium behavior of polymer chains of lengths between four and sixty four monomers were examined as a function of temperature. Simulations were performed for a total of twelve different temperatures. Each polymer was thermalized at a temperature of ten Monte Carlo degrees and then cooled gradually by reducing the temperature by a factor of two. For each different polymer length different charge sequences were examined for variability in the measured Monte Carlo parameters.

2.3 Results and Discussion

2.3.1 Neutral Polyampholytes

Figure 2-1 shows that the heat capacity, $C_v(T^*)$, of balanced polyampholytes at each length exhibits a well defined peak indicating the existence of a first order phase transition at $T^* \approx 0.04$ degrees. Each curve represents a different balanced quenched charge sequence. It was found through repeated simulations that although the heat capacity peak occurred at a well defined temperature, the height of the peak itself varied from one simulation to another. Obtaining a specific heat capacity scaling law was, therefore, not feasible with this algorithm. Any heat capacity temperature dependence was not observed as a function of polymer length or quenched sequence within the kinetic constraints of the simulation.

The heat capacity peak indicates that the charge coupling at the transition point is approximately 25. It is interesting to note that this value is significantly higher than that obtained by Victor and Imbert[Vic93] using the algorithm of Wall and Mandel[Wal75]. Based on the covalent radius of carbon in its sp3 configuration, the distance between two carbons on a real polymer backbone is approximately 1.6 $\mathring{A}$ and the separation between monomer groups is thus approximately 3.2 $\mathring{A}$. At room temperature with an aqueous solvent the Bjerrum length is about 7 $\mathring{A}$. This implies that the charged coupling and reduced temperature in a real polymeric system are

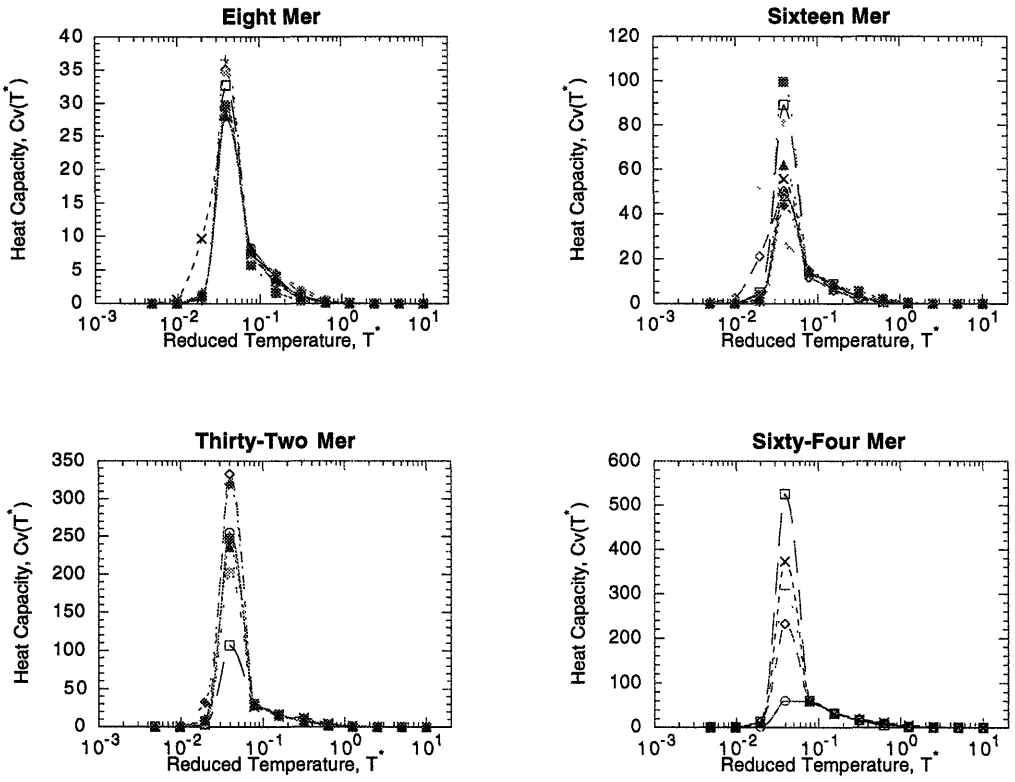

Figure 2-1: Balanced polyampholyte heat capacity versus reduced temperature. The maximum heat capacity occurs at a well defined temperature for all sequences and chain lengths.

of the order of unity. A charge coupling of 25 at room temperature would indicate an intermonomer distance of $l_B/25 = 0.28$ $\AA$ which is much smaller than most real polymeric systems.

Figures 2-2 and 2-3 show the squared radius of gyration and energy per monomer as a function of temperature for balanced polyampholytes of different lengths and charge sequences. At very high temperatures the thermal energy completely dominates the electrostatic interactions and the polymer behaves as a neutral chain in a good solvent. As a result, at high temperatures the energy per monomer becomes a specific function of the charge sequence. One would expect that in the limit of infinite polymer lengths random sequences will not show differences in energy at high

temperatures. In the neighborhood of 0.1 degrees the energy per monomer for all charge sequences becomes almost identical. In this temperature range the average distribution of ions is very similar. As the chain length increases this temperature interval where similar behavior occurs also increases. Lowering the temperature below the transition point results in a separation of energy levels as the conformations become trapped in local energy minima.

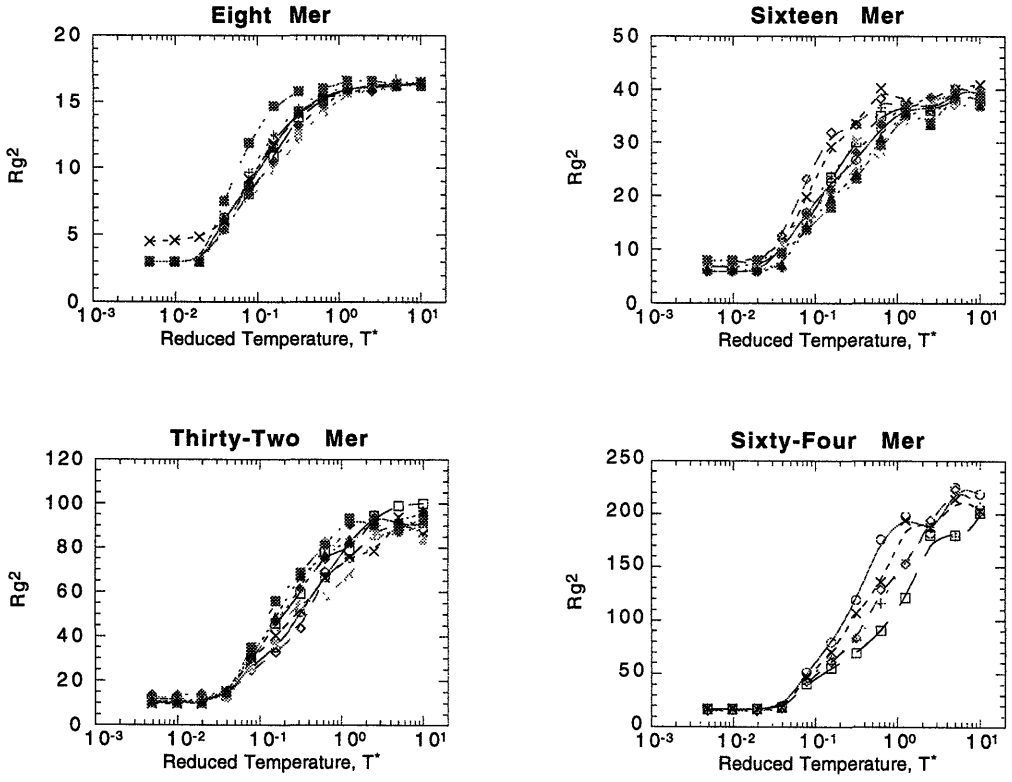

Figure 2-2: Balanced polyampholyte squared radius of gyration versus reduced temperature. Balanced polyampholytes exhibit a collapse transition as the temperature is lowered.

The trend in the average energy per monomer over the different quenches shows a systematic decrease with increasing polymer chain length. The asymptotic value can be understood in terms of the cohesive energy per ion of an infinite lattice.

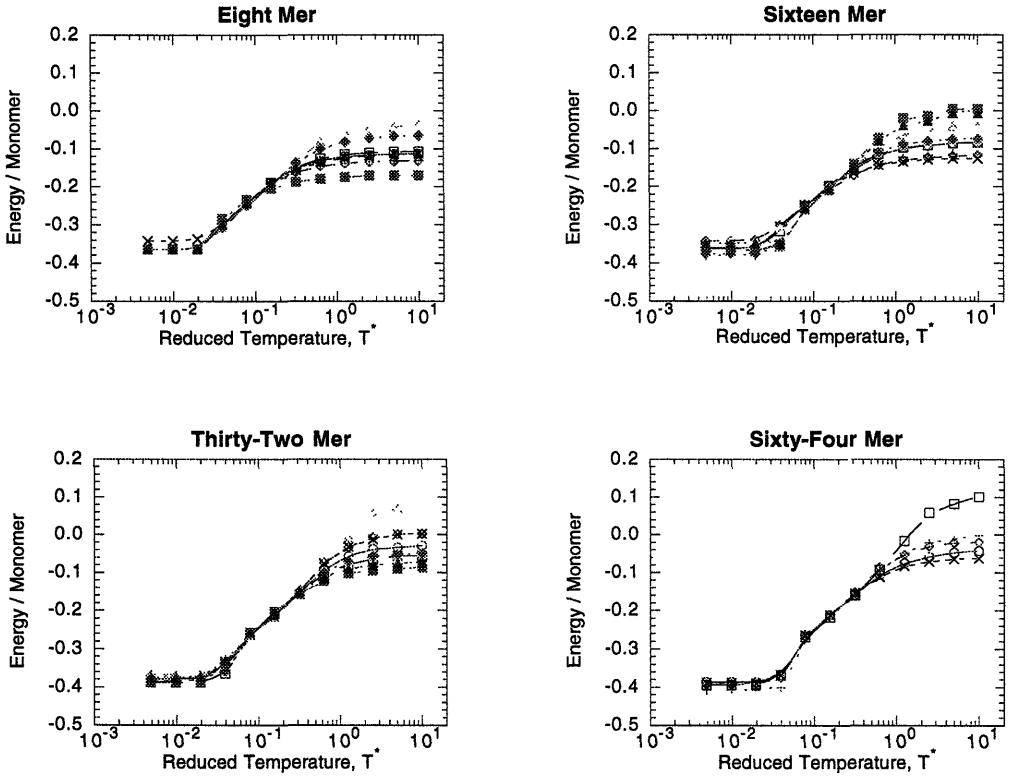

Figure 2-3: Balanced polyampholyte energy per monomer versus reduced temperature.

Recall that for ionic crystals the cohesive energy is given by

$$\Delta F_{lattice} = -\frac{A}{2} N \frac{e^2}{4\pi\epsilon a}, \tag{2.6}$$

where A is the Madelung constant of order unity[Kit86]. In terms of reduced units the free energy is

$$\Delta F^*_{lattice} = -\frac{A}{2} N \frac{1}{a} \tag{2.7}$$

where a is the excluded volume distance which in this simulation is 2. For a sodium chloride cubic structure the Madelung constant is 1.75 giving an asymptotic limit

of -0.4375 for the frozen energy conformation. For a poorly arranged lattice the Madelung constant is 1 and the corresponding asymptotic energy is -0.25. This simply states that an ordered alternating array of positive and negative ions in the ground state will give the lowest energy while more disordered arrangements of the ions will give higher energy values. In all the simulations performed using balanced polyampholyte chains the ground states resemble ionic crystalline forms. The finite polymer length is the main reason for not reaching the asymptotic ground state energy limit.

Figure 2-4 shows the variability that results when the same polymer charge sequence is simulated using different random number sequences. The heat capacity varied from one simulation to another when the simulation was repeated with the same polymer. The conformation of the ground state also varied from simulation run to simulation run. Repeated attempts to renature to a unique ground state failed. The energy per monomer as a function of temperature, however, showed very repeatable results using the interaction potential described in the methods section. The largest variability among the different charge sequences occurs at high temperatures. In all cases the effects of Coulombic interactions become important when the reduced temperature is approximately unity.

Figure 2-5 shows that balanced polyampholytes exhibit coil, globule[1] and frozen cubic sodium chloride structures at high, medium and low temperatures. At low temperatures the polyampholyte freezes into an alternating positive and negative charge configuration along higher order planes in most cases. During some simulation runs more unstable states were obtained at low temperatures if the polymer was cooled rapidly.

The globule phase occurs just above the transition temperature. The description of this phase using the concept of a Debye-Hückel electrolyte is problematic since

[1]By the definition of a globular phase[Lif78] it may be more appropriate to consider the crystalline configuration as the globule phase.

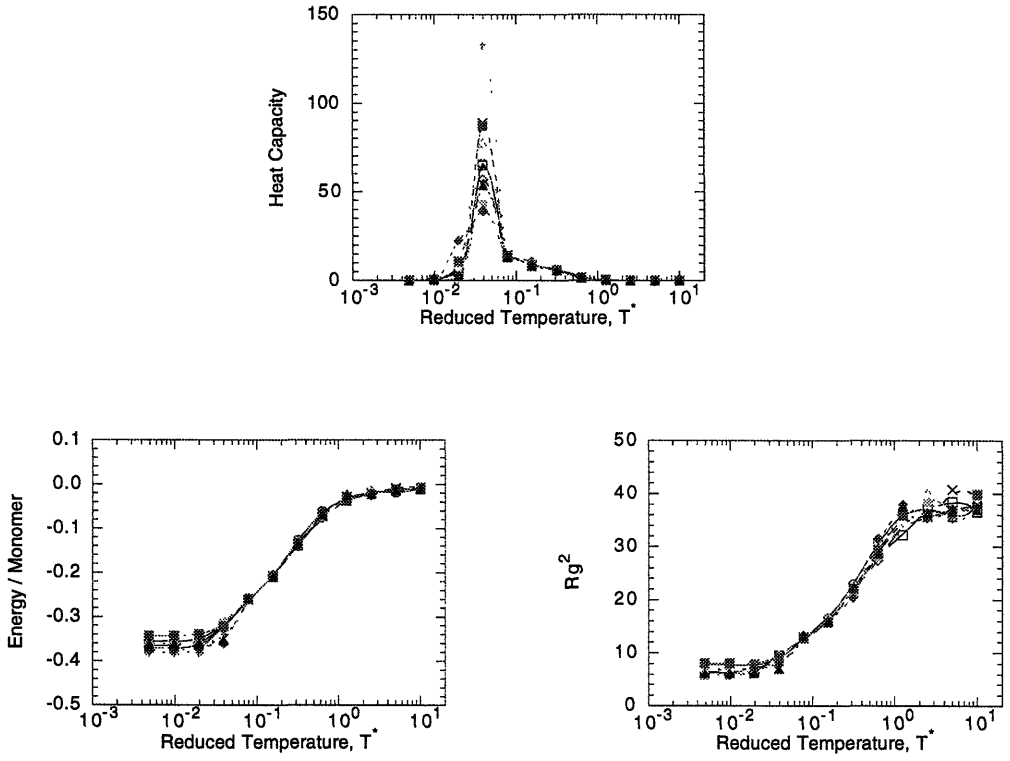

Figure 2-4: Heat capacity, squared radius of gyration and energy per monomer variability versus reduced temperature for a single balanced polyampholyte sequence.

the temperature is far to low to justify such an approximation. At the transition temperature the polyampholyte has a partially crystalline sodium chloride structure. The frozen conformation shown in Fig. 2-5 illustrates the phantom bond network associated with this model since only maximum bond lengths and excluded volume interactions are considered during the simulation runs. The bond restriction of this algorithm gives the polymer chain much flexibility to find a low energy state at low temperatures. The fact that bond cuts are allowed in this algorithm has the advantage of decreasing the equilibrium time. More conformations are accessible in a shorter number of Monte Carlo steps if bond cuts are allowed.

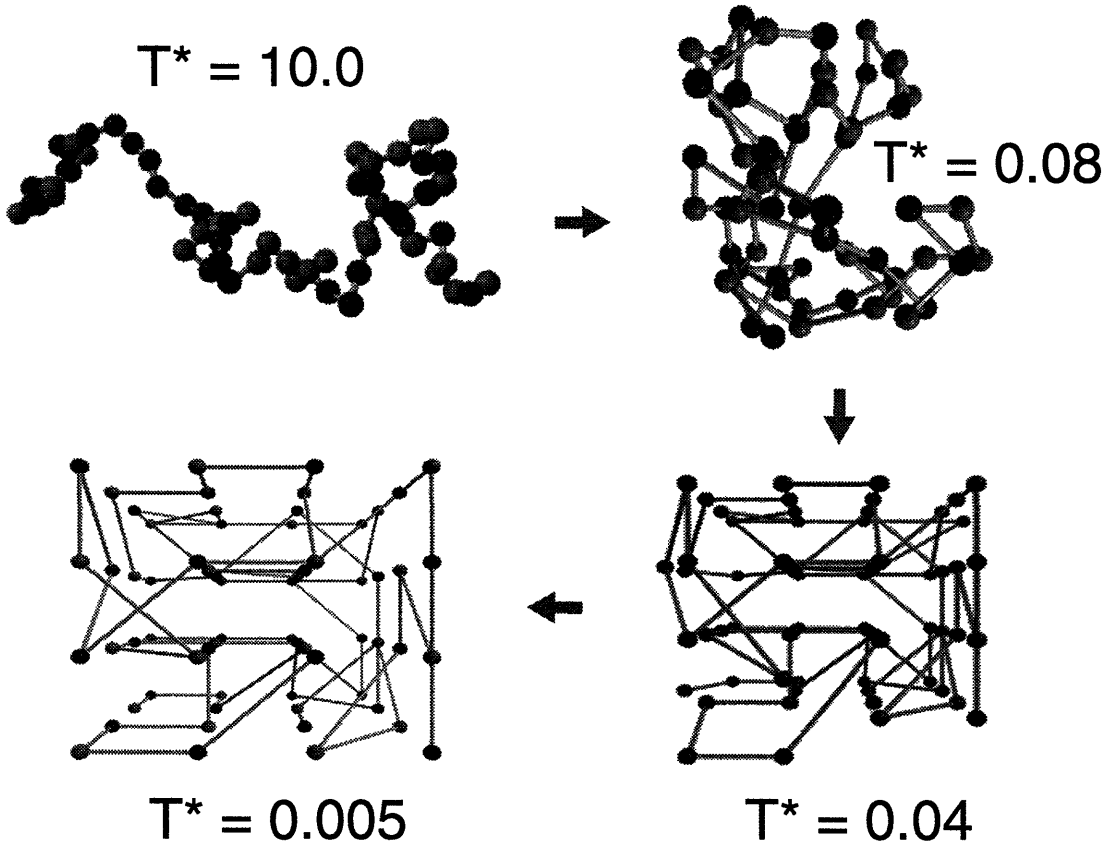

Figure 2-5: Simulated collapse transition of neutral polyampholyte polymer. At high Monte-Carlo temperatures the polyampholyte exists as an extended coil. Lowering the temperature causes the polyampholyte to form a globular structure. At the transition temperature a half melted crystalline structure forms. Below the transition temperature a regular NaCl lattice structure results.

2.3.2 Scaling Properties of Neutral Polyampholytes

As a standard for comparing the scaling properties of balanced polyampholytes it is important to understand the scaling of polymer chains with only neutral monomers. Figure 2-6 shows the radius of gyration scaling for polymer chains with only neutral monomers. The error bars represent the standard deviation of the radius of gyrations obtained during each simulation run. The standard deviation of the mean over twenty simulation runs is also shown in Fig. 2-6. Figure 2-6 shows that ensemble mean fluctuations are significantly smaller than the fluctuations en-

countered during a single simulation run. With a constant maximum bond limit of four lattice units, excluded volumes of $\sqrt{2}$, $\sqrt{3}$ and 2 produce scaling exponents of $\nu = 0.55264$, $\nu = 0.60845$ and $\nu = 0.6159$ respectively. The universal exponent, $\nu_o \approx 0.588$, for excluded volume interactions in three dimensions falls within these values. These values are, however, greater than the Gaussian θ point temperature value of $\nu = \nu_\theta = \frac{1}{2}$. Polymer simulations based on these excluded volume interactions, therefore, give scaling exponents corresponding to good solvents.

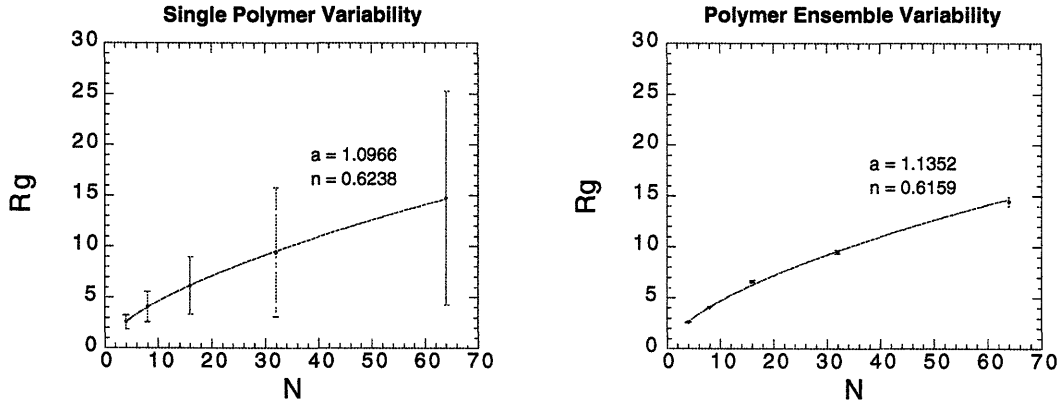

Figure 2-6: Scaling behavior of uncharged polymers. The error bars in the first graph represent the standard deviation of the radius of gyration over each simulation run for a single polymer. In the second graph the error bars represent the standard deviation and over an ensemble of twenty polymers.

The fact that the scaling behavior of uncharged homopolymers can be varied simply by changing the excluded volume interaction is an interesting point. Previous studies based on this algorithm concluded that the small scaling exponent obtained ($\nu = 0.55$) was due to the crossover between Gaussian and self-avoiding behaviors in these relatively short chains[Kan92]. Simple inspection of this algorithm for excluded volumes of $\sqrt{2}$ show that bond cuts easily occur. The relatively short length of the chains in these studies do not appear to be completely responsible for this behavior. It has been shown that with this simulation algorithm the scaling behavior can be varied from near Gaussian to self avoiding simply by increasing the

monomer excluded volume without altering the chain lengths. In the limit of very long chains, however, the universal value of 3/5 should be obtained for all these different constraints.

Figure 2-7 shows the scaling exponent of an ensemble of random balanced polyampholytes as a function of temperature. The Flory temperature for the random polyampholyte examined with this model is approximately 0.33 degrees. Below 0.1 degrees scaling exponents were difficult to obtain due to the long equilibration times.

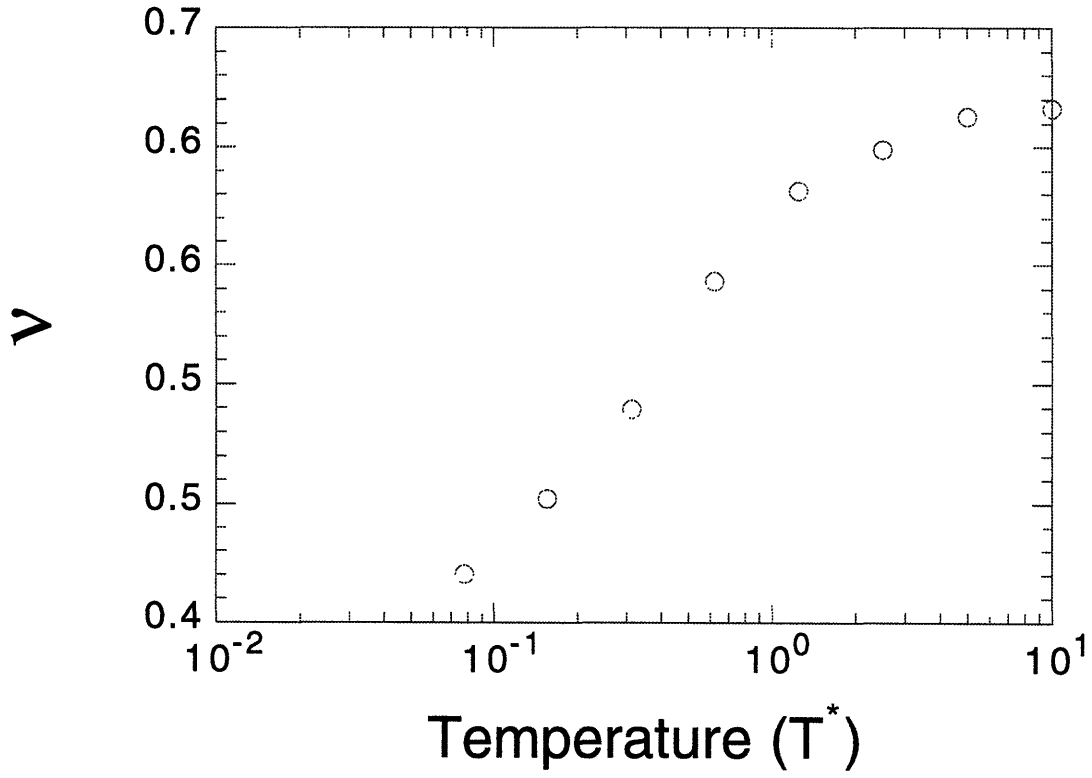

Figure 2-7: Scaling behavior of random balanced polyampholyes versus temperature. The θ temperature is approximately 0.33 degrees.

2.3.3 Unbalanced Polyampholytes

Figures 2-8 shows the squared radius of gyration of polyampholyte polymers with varying charge offsets as a function of temperature. In agreement with previous

studies[Kan92] and intuition increasing charge offset results in increasing swelling as the temperature is lowered. It must be realized, however, that these simulations only represent the effects of bare unshielded charges.

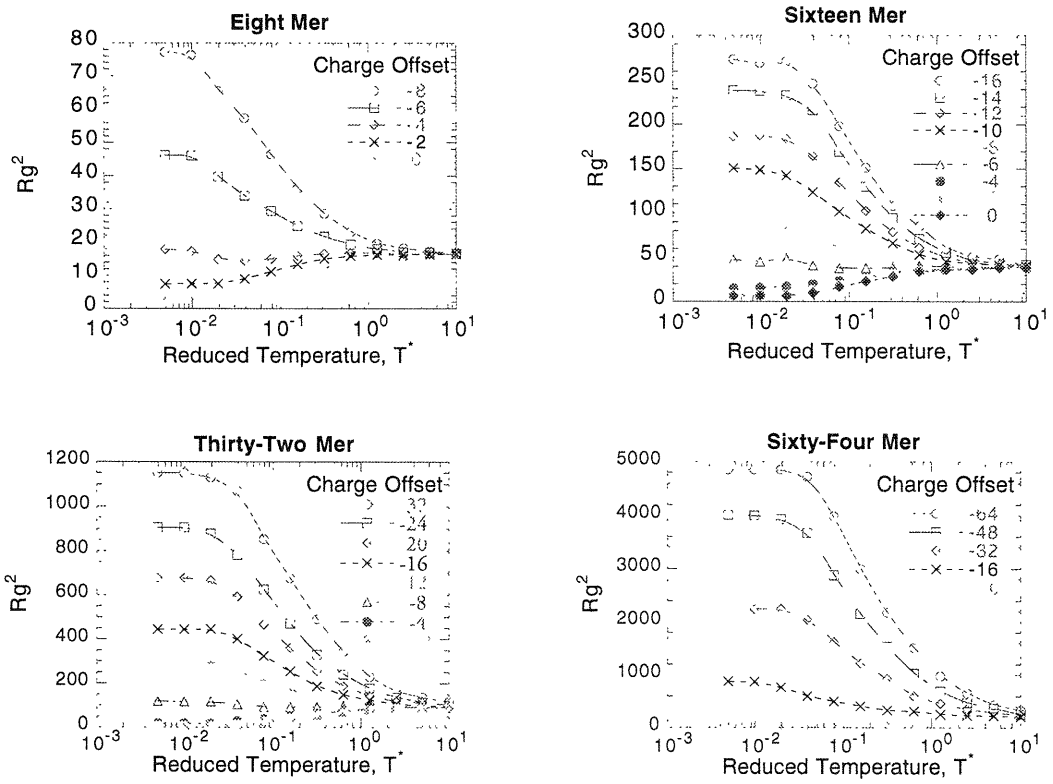

Figure 2-8: Charged polyampholyte squared radius of gyration versus reduced temperature. Increasing charge offsets result in progressively more swollen polymers.

Figure 2-9 shows the low temperature behavior of the squared radius of gyration of polyampholytes with different charge offsets and lengths. One notes that a critical charge offset is required for the polyampholyte to begin swelling at low temperatures and that this critical charge offset increases with the length of the polyampholyte chain.

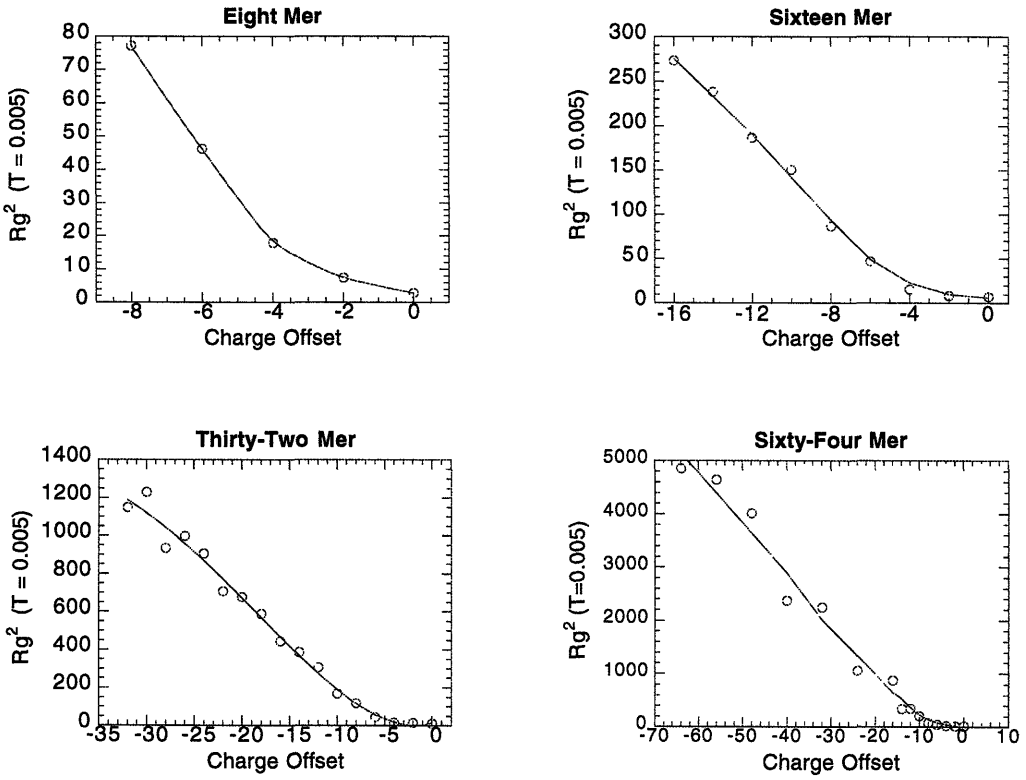

Figure 2-9: Low temperature squared radius of gyration versus polyampholyte charge offset. In agreement with previous studies, as the polymer length increases a greater critical charge offset is required to cause swelling.

2.3.4 The Role of Counter Ions

The omission of counter ions in charged polyampholytes is a serious limitation of this model. Mobile ions can be included in both Monte Carlo and Molecular Dynamics simulations using periodic boundary conditions[Lee80]. However, the computational intensity required to include all but very small numbers of charged particles make the inclusion of counter ions very demanding.

In an aqueous solutions the exclusion of counter ions becomes even more problematic since hydrogen and hydroxide ions always exist in small concentrations. If a fractional charge offset of $Q = fN$ exists then the potential of a roughly spherical

globule with respect to the surrounding solution will be

$$\phi \approx \frac{Q}{R_g} \sim \frac{fN}{N^{\nu}} = fN^{1-\nu}. \tag{2.8}$$

Equating the electrochemical potential of hydrogen ions inside and outside of the globule one gets

$$\mu^s + kT\ln C^i_{H+} + e\phi = \mu^s + kT\ln C^o_{H+}, \tag{2.9}$$

where μ^s is the reference state chemical potential of hydrogen, e the unit charge, C^i_{H+} the internal concentration of hydrogen ions, and C^o_{H+} the external concentration of hydrogen ions. This implies that

$$\frac{C^i_{H+}}{C^o_{H+}} = e^{-e\phi/kT}. \tag{2.10}$$

At room temperature the potential created by fixed negative charges can lead to much higher internal concentrations of hydrogen ions in the thermodynamic limit. Furthermore, if hydrogen or hydroxide ions are capable of binding and neutralizing charged monomers then the net effective charge can be drastically altered.

The transition from spherical to rod like conformations introduces the additional complication of ion condensation[Oos71]. For a charged rod where the inter ion separation is less than the Bjerrum length condensation effects will occur regardless of how dilute the polymer solution.

In principle, counter ions could be included using a screened interaction potential [DeS93] of the form

$$U(r_{ij}) = \sum_{i<j}^{N} \frac{z_i z_j e^2 e^{-\kappa r_{ij}}}{4\pi\epsilon r_{ij}}, \tag{2.11}$$

where

$$\kappa = \sqrt{\frac{z^2 e^2 n}{\epsilon k T}} \tag{2.12}$$

is the inverse Debye length. Including counter ions in this type of model with a Debye shielding term, however, becomes problematic for a number of reasons. The screened potential is based on the linearized Poisson Boltzmann[Lan58] equation and as a result is only valid at temperatures where the thermal energy is much greater than the Coulombic energy. From all the simulations shown in this study we immediately notice that charge offset effects do not manifest themselves until the reduced temperature is significantly less than one. The Yukawa potential would therefore only be valid for a very restricted range of temperatures in this type of model that is well above the transition temperature.

2.4 Conclusions

The scaling exponent for the radius of gyration in uncharged polymers based on the algorithm used in this study is 0.6 and therefore represents good solvent behavior. The balanced polyampholyte theta temperature was 0.33 degrees. The transition temperature to globular crystalline conformation occurred at approximately 0.04 degrees. A transition from coiled to Debye-Hückel distribution was not found using this algorithm. The electrostatic coupling was 25 at the transition point. Coulombic interactions begin to influence the thermodynamic parameters when the reduced temperature approaches unity.

Chapter 3

Polyelectrolytic Hydrogel Phase Transitions

Abstract

Polyelectrolytes are polyampholytes with all charges of the same sign. In this study the physical properties of acrylamide based polyelectrolytes with varying charge offsets are examined as a function of bath ionic strength and pH. The complications which arise due to the inclusion of thermally sensitive monomers are also illustrated. The non-equilibrium properties of the polyelectrolyte are examined using coupled ion transport models. The effects of bivalent ions, acid dissociation and polyelectrolyte interactions on the equilibrium swelling response as a function of bath electrolyte concentration are presented.

3.1 Introduction

Polyelectrolytic hydrogels are three dimensional cross-linked polymeric networks consisting of charged monomers of only one sign. Competing elastic, solvent and Coulombic forces can result in large reversible swelling transitions in response to changes in ambient ionic strength, pH, temperature, solvent quality, and applied electric fields.[Osa87,Flo53,Gri90] As a result, polyelectrolytic hydrogels have diverse applications in areas such as drug delivery, actuators, medicine and heavy

metal ion extraction.

The kinetic response of polyelectrolytic hydrogels to changes in some control parameter, such as bath ionic strength or pH, is of particular importance from both a practical and a theoretical point of view. The potential use of polyelectrolytic hydrogels as an actuator or drug release system, for example, is dependent on the characteristic response time. In addition, the kinetic response also provides valuable information regarding the transport of various ions through the hydrogel matrix.

Rička and Tanaka[Ric84a,Ric84b] have examined the equilibrium swelling response of polyelectrolytic hydrogels consisting of acrylamide and acrylic acid to changes in bath pH and ionic strength. They found that the swelling dependence of weakly charged polyelectrolytic hydrogels on monovalent bath salt concentration was in agreement with a Donnan model. Additional effects due to multivalent ions were also observed and noted.

In this study the equilibrium and non-equilibrium behavior of an acrylic acid (AAc), acrylamide (AAm) and N-isopropylacrylamide (NIPA) polyelectrolyte copolymer is investigated. Adding NIPA to a copolymer similar to that investigated by Rička et al. includes temperature as an additional control variable. This study therefore investigates the physical properties of various copolymers of AAc, AAm and NIPA as a function of bath electrolyte concentration, pH and temperature.

3.2 Theoretical Model

A description of both the equilibrium and non-equilibrium properties of a polyelectrolytic hydrogel begins with a statement of the system free energy. The use of a free energy in non-equilibrium processes, however, requires careful justification. In equilibrium the chemical potentials of both the solvent and ion species in the different phases must balance. As a result, equilibrium swelling can be treated using a balance of osmotic pressure terms arising from the polymer solvent interaction,

the hydrogel elasticity and the mobile ion pressure. The non-equilibrium response can in principle be derived from a force balance law beginning with the free energy and its relation to the stress tensor. The analytical treatment of the hydrogel non-equilibrium response can be simplified when the response times of the mechanical and ion transport kinetics are much different and a linear constitive law is used.

3.2.1 Free Energy Model

The free energy is assumed to consist of four additive components,

$$\Delta F = \Delta F_M + \Delta F_{el} + \Delta F_{trans} + \Delta F_{Coulombic} , \tag{3.1}$$

where $\Delta F_M, \Delta F_{el}, \Delta F_{trans}$, and $\Delta F_{Coulombic}$ represent the mixing, elastic, translational, and Coulombic contributions to the free energy respectively.

Based on the Flory-Huggins lattice theory,[Flo53] the free energy of mixing between monomer and solvent molecules is

$$\Delta F_M = k_B T \frac{V}{v_{site}} (1-\phi) \left[\ln(1-\phi) + \chi\phi\right], \tag{3.2}$$

where V is the hydrogel volume, v_{site} the lattice site volume, ϕ the polymer volume fraction, χ the polymer solvent interaction parameter, k_B is Boltzmann's constant, and T the absolute temperature.

From the affine network model,[Flo53,Flo79] the elastic contribution to the free energy is

$$\Delta F_{el} = \frac{3k_B T}{2} \frac{V\phi}{N_x v_{site}} \left[\left(\frac{\phi_o}{\phi}\right)^{\frac{2}{3}} - 1 - \frac{1}{3}\ln\left(\frac{\phi_o}{\phi}\right) \right], \tag{3.3}$$

where N_x is the average number of monomers between cross-links. The term $\frac{V\phi}{N_x v_{site}}$ is the effective number of chains in the network while $\frac{\phi_o}{\phi}$ is the swelling ratio.

Hydrogel volumes and polymer volume fractions are related through

$$\frac{V}{V_o} = \frac{\phi_o}{\phi} = \left(\frac{D}{D_o}\right)^3, \tag{3.4}$$

where V_o, D_o and ϕ_o are the hydrogel volume, diameter and polymer volume fraction in the reference state respectively.

The translational component represents the ion mobility contribution to the free energy. For this term we consider the ideal gas contribution,

$$\Delta F_{ideal} = k_B T \sum_i N_i \left\{ \ln\left(\frac{N_i}{N_A V}\right) - 1 \right\}, \tag{3.5}$$

where N_A is Avogadro's number and N_i is the total number of a given mobile ion. The sum is over all mobile ion species such that

$$C_{mobile} \equiv \sum_i \frac{N_i}{N_A V} \tag{3.6}$$

is the total mobile ion concentration. We assume that the excluded volume correction to V in Eq. (3.5) is negligible. The Donnan equilibrium relations with the constraint of local charge neutrality lead to

$$C_{mobile} = 2\sqrt{\left(\frac{N_{f-}}{2N_A V}\right)^2 + C_o^2}\ , \tag{3.7}$$

where N_{f-} is the total number of negative fixed charges and C_o is the sum of all positive ion concentrations in the bath. That is $C_o = C_s + C_{H^+Bath}$ where C_s is the bath salt concentration.

The Coulombic contribution to the free energy is

$$\Delta F_{Coulombic} = \sum_i z_i e N_i \phi_D + \Delta F_{fixed} + \Delta F_{DH}, \tag{3.8}$$

where ϕ_D is the Donnan potential and ΔF_{fixed} represents the contribution due to

the interaction between fixed charge groups and ΔF_{DH} represents the Debye-Hückel correction to the ideal gas assumption. Omitting the Coulombic contribution to the free energy in ionic hydrogels[Ric84a,Tan80] has been the subject of criticism. [Vas86] The Coulombic contribution to the free energy, $\Delta F_{Coulombic}$, corresponds to the free energy of the Coulombic interactions of the network polyion charges and the those of the counter ions and added salt. It is extremely important to realize that $\Delta F_{Coulomb}$ can included a number of effects.

For a weakly charged polyelectrolyte it is customary to include the Debye-Hückel contribution to the free energy as

$$\Delta F_{DH} = -\frac{\kappa^3}{12\pi}, \tag{3.9}$$

where

$$\kappa = \sqrt{\frac{z^2 e^2 n_t}{\epsilon k T}}. \tag{3.10}$$

The term z represents the ion valency, e the unit charge, n_t the number concentration of all mobile ions, ϵ the permittivity, k the Boltzmann constant, and T the absolute temperature. Above concentrations of about 1 mM, however, the Debye-Hückel correction is not valid, in fact it leads to unphysical divergencies in the osmotic pressure. For this very important reason it should not be included in a free energy model for hydrogels with internal ion concentrations of several mM.

3.2.2 Swelling Equilibrium

Balance of solvent chemical potentials is generally expressed as

$$\Delta\Pi_{swelling} = \frac{\mu_s^{gel} - \mu_s^{bath}}{\overline{v}_w} = 0, \tag{3.11}$$

where $\overline{v}_w$ is the solvent molar volume. Equating hydrogel and bath solvent chemical potentials gives us the swelling equilibrium condition

$$-\frac{1}{\overline{v}_{site}}\left[\ln(1-\phi)+\phi+\chi\phi^2\right]+\frac{\phi_o}{N_x\overline{v}_{site}}\left[\frac{1}{2}\left(\frac{\phi}{\phi_o}\right)-\left(\frac{\phi}{\phi_o}\right)^{\frac{1}{3}}\right]+C_{mobile}-2C_o, \quad (3.12)$$

where $\overline{v}_{site} \equiv N_A v_{site}$ represents the molar volume of the lattice sites, ϕ the polymer volume fraction, χ the Flory interaction parameter, N_x the number of monomers between cross-links, ϕ_o the polymer volume fraction in the reference state, C_{mobile} the total mobile ion concentration within the hydrogel, and C_o is half the total concentration of monovalent ions in the external bath.

3.2.3 Dissociation Equilibrium

Acid dissociation is expressed as

$$K_a = \frac{C_{A^-}C_{H^+}}{C_{AH}}, \quad (3.13)$$

where K_a is the acid dissociation constant, C_{A^-} the concentration of dissociated acid groups, C_{H^+} the hydrogen ion concentration and C_{AH} the concentration of undissociated acid groups. For the case of monovalent ions, Eq. 3.13, local electoneutrality and Donnan equilibrium allows us to write a third order polynomial equation in terms of the known bath concentrations and the unknown internal hydrogen ion concentration,

$$C_{H^+}^3 + K_a C_{H^+}^2 - \left(C_{H^+Bath}^2 + \frac{C_A K_a C_{H^+Bath}}{C_o}\right) C_{H^+} - K_a C_{H^+Bath}^2 = 0. \quad (3.14)$$

The term C_{H^+} represents the internal hydrogen ion concentration, C_{H^+Bath} the bath hydrogen ion concentration and C_o the total concentration of positive ions in the bath solution. If we have one monovalent salt with bath concentration C_s then $C_o = C_s + C_{H^+Bath}$. It is important to keep in mind that because Eq. 3.14 is based

on Donnan equilibrium condensation effects[Oos71] and electric field and charge inhomogeneities are being ignored.[Ove56]

3.2.4 Mechanical Response

In non-linear elasticity the fundamental constitutive relation between a spatially dependent free energy, $F(X)$, and the stress tensor is[Mar83]

$$S^{AB}(X) = 2\rho_{Ref}(X)\frac{\partial F(X)}{\partial C_{AB}(X)}, \tag{3.15}$$

where X represents the Lagrangian or body coordinates, $S^{AB}(X)$ is the second Piola Kirchhoff stress tensor, $\rho_{Ref}(X)$ the reference state density, and $C_{AB}(X)$ the right Cauchy Green strain tensor. In principle, one could start from the free energy defined by Eq. 3.1. However, linearization under the assumption of small displacements and negligible inertial contributions leads to a simple fundamental equation of motion[Tan73]

$$f\frac{\partial u}{\partial t} = \nabla \cdot \boldsymbol{\sigma}, \tag{3.16}$$

where f represents the friction between the network and the solvent, u is the displacement of a point in the network from its equilibrium location and σ is the stress tensor.

If the stress tensor is of the form

$$\sigma_{ij} = K\nabla \cdot u\delta_{ik} + 2\mu\left(u_{ik} - \frac{1}{3}\nabla \cdot u\delta_{ik}\right) \tag{3.17}$$

where

$$u_{ij} = \frac{1}{2}\left(\frac{\partial u_i}{\partial x_i} + \frac{\partial u_j}{\partial x_j}\right), \tag{3.18}$$

and K is the bulk modulus, μ is the shear modulus and δ_{ij} the Kronecker delta then

$$\frac{\partial \boldsymbol{u}}{\partial t} = \frac{K+\frac{4}{3}\mu}{f}\boldsymbol{\nabla}(\nabla \cdot \boldsymbol{u}) + \frac{\mu}{f}\nabla^2 \boldsymbol{u}. \tag{3.19}$$

In the case of an infinite cylinder radial deformation[Can87] equation 3.19 becomes in the limit $\frac{\mu}{K+\frac{4}{3}\mu} \ll 1$

$$\frac{\partial u_r}{\partial t} = D_c\left[-\frac{1}{r^2}u_r + \frac{1}{r}\frac{\partial u_r}{r} + \frac{\partial^2 u_r}{\partial r^2}\right], \tag{3.20}$$

where $D_c = \frac{K+\frac{4}{3}\mu}{f}$ is collective diffusion coefficient and $u(0,t) = 0$ for all t. The boundary condition on the surface of the hydrogel can be expressed as

$$\sigma_{rr} = (1+\frac{4}{3}\mu)\left[-\frac{\partial u_r}{\partial r} + (1-\frac{2\mu}{(1+\frac{4}{3}\mu)})\frac{1}{r}u_r^2\right] = 0 \quad \text{for} \quad r = a, \tag{3.21}$$

where a is the final equilibrium radius.

An approximate solution to equations 3.19 through 3.21, valid in the limit $\frac{t}{\tau_1} \geq 0.3$, is given by

$$u_r(r,t) = e^{-(\frac{t}{\tau_1}+0.3686)}, \tag{3.22}$$

where

$$\tau_1 = \frac{a^2}{\lambda_1^2 D_c} \tag{3.23}$$

and $\lambda_1 = 2.405$ is the first zero of the Bessel function $J_o(\lambda)$. Based on both light scattering and swelling measurements[Tan73,Can87] of AAm and NIPA, $D_c \approx 7 \times 10^{-11}$ cm^2/sec. For hydrogels with diameters on the order of 200 μm the estimated time constant, τ_1, is therefore approximately 98 seconds.

3.2.5 Ion Transport

For a non-deformable hydrogel of infinite length the ion transport problem can be modeled in cylindrical coordinates. The hydrogel contains carboxyl groups and is immersed in a bath containing NaCl, or $CuCl_2$, and H+ ions. The ionization of the carboxyl groups varies over the bath pH and salt concentration range.

Transport Equations

Coupled ion diffusion within a charged hydrogel is described by considering the solution to the ion flux, continuity and electric field equations,

$$\boldsymbol{\Gamma}_{\pm} = -D_{\pm}\boldsymbol{\nabla}C_{\pm} \pm u_{\pm}C_{\pm}\boldsymbol{E} + C_{\pm}v_f, \tag{3.24}$$

$$\frac{DC_{\pm}}{Dt} = -\boldsymbol{\nabla}\cdot\boldsymbol{\Gamma}_{\pm}, \text{ and} \tag{3.25}$$

$$\boldsymbol{\nabla}\cdot\epsilon\boldsymbol{E} = \rho + z_{+}FC_{+} - z_{-}FC_{-}, \tag{3.26}$$

where $\boldsymbol{\Gamma}_{\pm}$ is the ion flux, $D_{\pm}$ the ion diffusion coefficient, $C_{\pm}$ the ion concentration, $u_{\pm}$ the ion mobility, $\boldsymbol{E}$ the electric field, v_f the fluid velocity with respect to the hydrogel body, ρ the hydrogel charge density, ϵ the permittivity, z the ion valence, and F the Faraday constant. The solution to Eqs. 3.24, 3.25 and 3.26 is the ambipolar diffusion equation

$$\frac{DC_{\pm}}{Dt} + \frac{DC_{B\pm}}{Dt} = D_a\boldsymbol{\nabla}^2C_{\pm}, \tag{3.27}$$

where

$$D_a = \frac{D_{+}D_{-}(C_{+}+C_{-})}{D_{+}C_{+}+D_{-}C_{-}} \tag{3.28}$$

and $C_{B\pm}$ represents the amount of bound ions within the hydrogel. For a deformable hydrogel the convective derivative is with respect to a Lagrangian coordinate system fixed to the hydrogel. Note that a careful distinction between the movement of the

hydrogel and the fluid within the hydrogel is necessary in this case. When no hydrogel expansion or collapse occurs the convective derivative becomes a partial derivative.

Diffusion Reaction

The space time dependence of the hydrogel sodium and chloride ion concentrations, C_{Na} and C_{Cl}, are described by the continuity equation

$$\frac{DC_{\pm}}{Dt} = -\nabla \cdot [-D_{\pm}\nabla C_{\pm} + C_{\pm}v_f]. \tag{3.29}$$

The convective term, v_f, represents the ion fluxes due to fluid velocities with respect to the hydrogel body coordinates and is included for completeness. Proton continuity inside the hydrogel is described by

$$\frac{DC_{H^+}}{Dt} + \frac{DC_{AH}}{Dt} = -\nabla \cdot [-D_{H^+}\nabla C_{H^+} + C_{H^+}v_f], \tag{3.30}$$

where C_{AH} is the total concentration of unionized acidic monomeric sites.

The effect of hydrogen ion binding to carboxylate groups is to slow the diffusion process. This can be shown by deriving an effective diffusion coefficient which includes binding reactions. To include this binding process we use a first order bimolecular reaction equation

$$AH \rightleftharpoons A^- + H^+, \tag{3.31}$$

where

$$K_{eq} = \frac{C_{A^-}C_{H^+}}{C_{AH}}. \tag{3.32}$$

Assuming instantaneous reaction rates relative to the diffusion times allows us to decouple Eq. 3.31 from Eq. 3.30 and write an effective diffusion equation of the

form

$$\frac{DC_{H^+}}{Dt} = D_{eff}\nabla^2 C_{H^+}, \tag{3.33}$$

where

$$D_{eff} = \left\{ \frac{D_{H^+}}{1 + \frac{C_T K_{eq}}{(K_{eq}+C_{H^+})^2}} \right\}, \tag{3.34}$$

and C_T is the total concentration of acidic monomeric groups. We notice that for perturbations from equilibria with a large number of free binding sites the effective diffusion coefficient can be much lower than free diffusion coefficient.

3.2.6 Cylindrical Hydrogel Solution

The equilibration time constant for each mode is

$$\tau_n = \frac{1}{k_n^2 D} \approx \frac{R_o^2}{(n-\frac{1}{4})\pi^2 D}. \tag{3.35}$$

The normalized concentration profile is

$$\frac{C - C_1}{C_o - C_1} = 1 - \frac{2}{R_o}\sum_{n=1}^{\infty} \frac{e^{-Dk_n^2 t} J_0(rk_n)}{k_n J_1(k_n R_o)} \tag{3.36}$$

and the normalized total amount of absorbed or released ions is

$$\frac{M(t)}{M(t=\infty)} = 1 - \sum_{n=1}^{\infty} \frac{4}{R_o^2 k_n^2} e^{-Dk_n^2 t}. \tag{3.37}$$

In aqueous solution the free ion diffusion coefficients are $D_{Na^+} = 1.33 \times 10^{-5}$ cm^2/sec, $D_{Cl^-} = 2.03 \times 10^{-5}$ cm^2/sec, and $D_{K^+} = 1.96 \times 10^{-5}$ cm^2/sec. The corresponding ion mobilities are $u_{Na^+} = 5.19 \times 10^{-4}$ cm^2/V sec, $u_{Cl^-} = 7.91 \times 10^{-4}$ cm^2/V sec, and $u_{K^+} = 7.62 \times 10^{-4}$ cm^2/V sec. Hence, the ambipolar diffusion

constant is $D = 8.035 \times 10^{-6}$ cm^2/sec. Using these values the time constants for the first mode for a 500 μm and 100 μm radial hydrogel is $\tau_1 = 42$ seconds and 1.7 seconds respectively. With inclusion of binding and assuming the acid dissociation constant is the same as the free monomer dissociation constant the hydrogen ion diffusion time can be reduced by three orders of magnitude for some of the hydrogels in this study.

3.3 Experimental Methods and Procedure

Hydrogels were prepared by free radical copolymerization of N-isopropylacrylamide (NIPA), acrylamide (AAm), sodium acrylate (NaAAc) and N,N′-methylene-bis-acrylamide (BIS) in distilled deionized water at 20 ^{o}C. N-isopropylacrylamide was purified by recrystalization and AAc by distillation. The total monomer concentration was 700 mM and the BIS concentration was 8.6 mM in all samples. The concentrations of sodium acrylate and acrylamide were equal and varied between 0 and 256 mM. Gelation was initiated with 1.76 mM ammonium persulfate (APS) and accelerated using 1.58 mM N,N′,N,N′-tetramethylethylenediamine (TEMED). The hydrogels were cast in test tubes containing 200 μm inner diameter micropipettes.

After gelation the hydrogels were removed from their pipettes and washed continuously with distilled deionized water for several days. The hydrogel diameters were monitored using a microscope equipped with a charged coupled device camera. The temperature was controlled within 0.04 ^{o}C using a Lauda temperature controller. Continuous washing with different bath salt concentrations and pH values were carried out and the kinetic response was monitored in order to ensure that equilibrium had been reached.

3.4 Results and Discussion

The equilibrium swelling diameters as a function of monovalent bath salt concentration are presented in Fig. 3-1. The lowest swelling curve is that of pure NIPA while the successively higher curves represent hydrogels with net charge offsets of -2, -4, -8, -16, -32, -64, -128, and -256 mM respectively. With increasing concentrations of acrylic acid polyelectrolyte behavior is observed. Pure NIPA begins to collapse at about 0.1 M. Since NIPA is a neutral monomer the collapse at high sodium chloride concentrations appears to be a solvent quality mediated effect or some other form of ionic interaction with the neutral monomers. Normally it is only the contributions ΔF_{trans} and $\Delta F_{Coulombic}$ to the total free energy that are changed when a low molecular weight salt is added. In the case of NIPA, however, it appears that ΔF_M and possibly ΔF_{el} are being affected at high salt concentrations.

Figure 3-2 shows the simulated equilibrium hydrogel parameters as a function of bath salt concentration for a hydrogel with 128 mM charge offset. Although this simulation predicts the same qualitative swelling pattern as the actual data, the simulated peak swelling is significantly higher. Based on this simulation, however, it is clear that at low bath salt concentrations the hydrogel collapses as a result of the low internal pH and hydrogen ion association. With increasing bath salt concentration the hydrogel initially swells as the internal pH rises from sodium ion exchange with hydrogen ions. Further increases in bath salt concentration causes the hydrogel to collapse due to the loss of the osmotic pressure gradient and electrostatic shielding.

Figure 3-3 shows the polyion separation and internal Debye length as a function of bath salt concentration if one were to assume a uniform polyion distribution. Although the concept of a Debye length is questionable at ion concentrations above 1 mM, this simulation clearly shows that at low ionic strengths the Debye length is comparable to the polyion spacing. Long Debye lengths with respect to the polyion

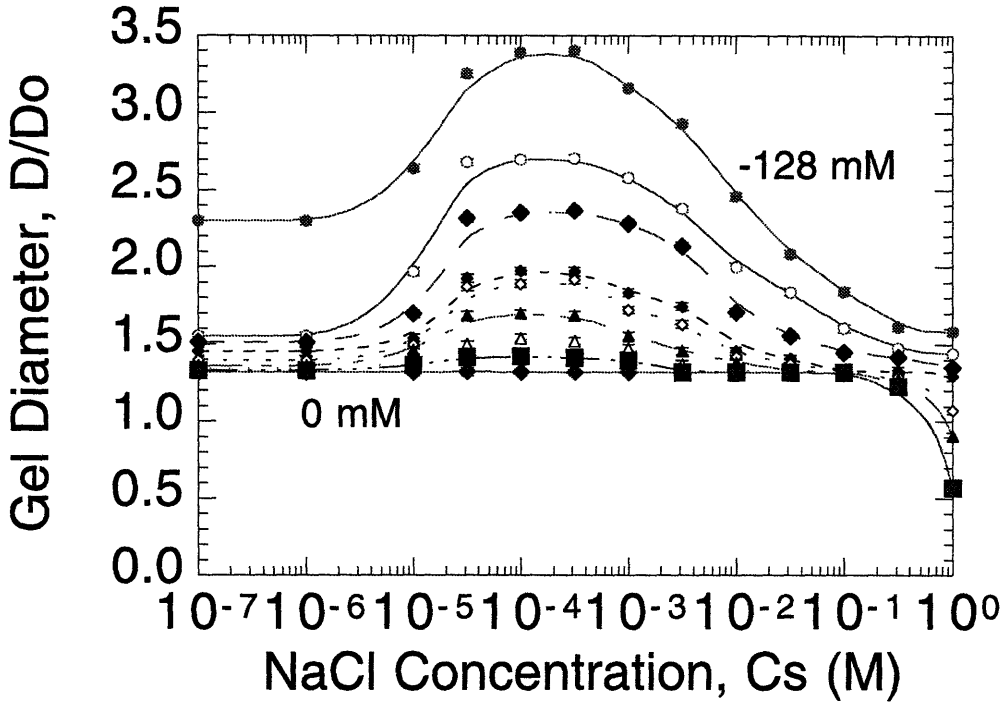

Figure 3-1: Polyelectrolyte swelling equilibria versus monovalent bath salt concentration. Both solvent effects and polyelectrolyte behavior are evident in the swelling dependence versus bath sodium chloride concentration at 25°C. The lowest swelling curve represent pure NIPA while curves with increasing swelling diameters are those of AAm/AAc concentrations of 2, 4, 8, 16, 32, 64, 128 and 256 mM respectively.

charge spacing implies a uniform internal potential and hence there is some justification for using a Donnan potential to describe this system. Based on a Donnan model the mobile ion contribution gives a Van-Hoff contribution to the osmotic pressure. If the polyions are fixed to the polymer backbone in such a way that they can generate an internal stress through mutual electrostatic interactions, however,then electrostatic component to the free energy should be considered. This leads to the conclusion that in some cases the point at which the Donnan model becomes applicable, that is, at large Debye lengths with respect to polyion separation, an additional osmotic term due to ionic interactions must be included. At very high

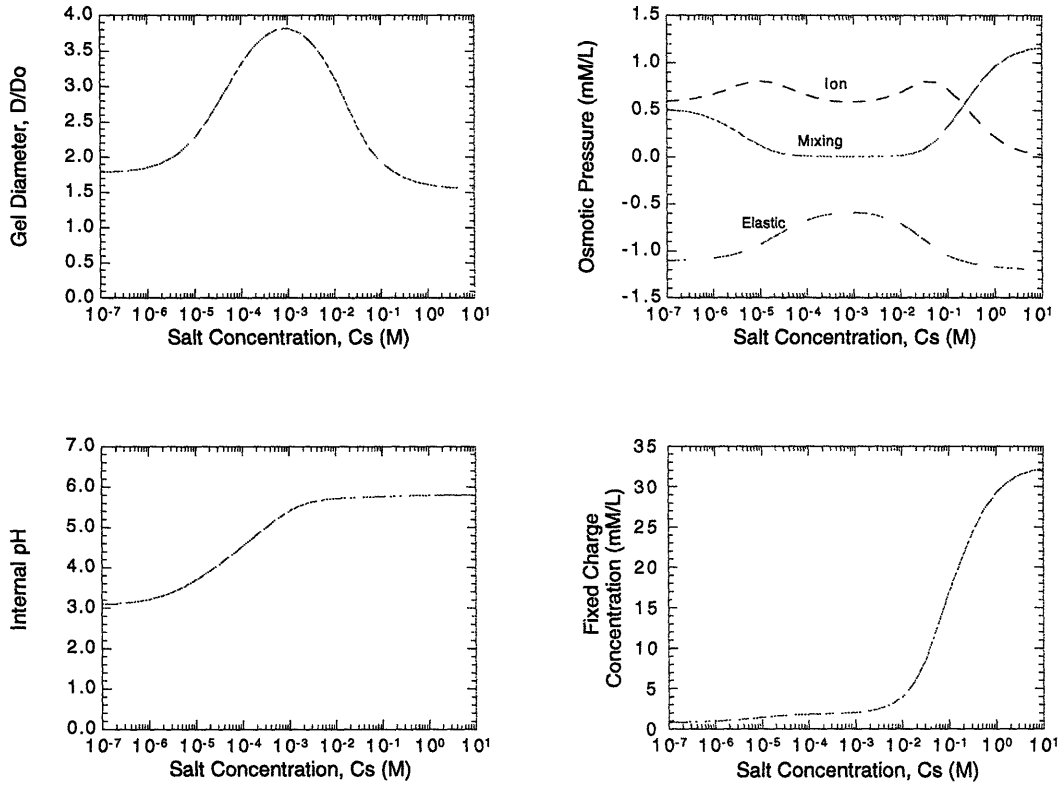

Figure 3-2: Simulated equilibrium swelling parameters for 128 mM AAc hydrogel as a function of bath salt concentration. At low bath ionic strength the internal pH can drop to relatively low values with respect to the bath pH. Notice also that the fixed charge density peaks at high bath salt concentrations.

bath salt concentrations the Debye length becomes shorter than the average interion separation making the uniform Donnan potential assumption invalid.

The distribution and mobility of polyions in the hydrogel matrix is an important consideration when evaluating Debye length and osmotic terms. If the polyions are uniformly distributed over a given hydrogel volume then electrostatic interactions exist between point charges. The fact that polyions are restricted to the linear chain alters this situation. In this case the persistence length of the chain as well as the linear charge density are important variables. An estimate of the Debye length can be made in this case by considering the charge distribution surrounding a uniformly

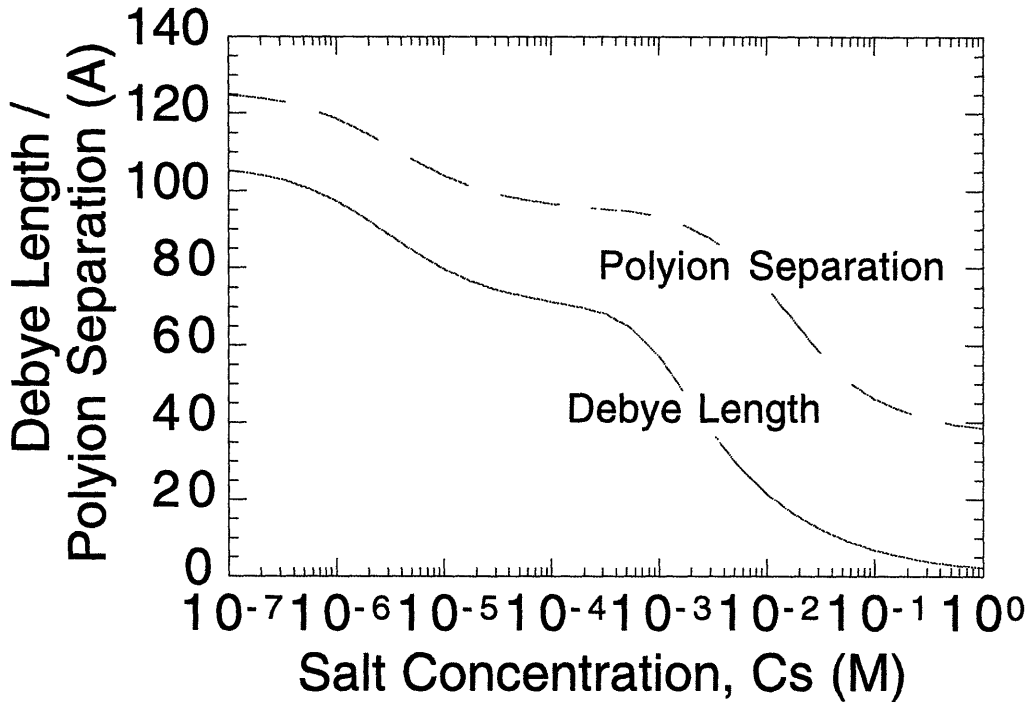

Figure 3-3: Debye length and interion spacing assuming a uniform ion distribution. Although the interion separation becomes greater at lower ionic strengths, in units of Debye lengths it in fact becomes shorter corresponding to greater unshielded electrostatic interactions.

charged rod.

Figure 3-4 shows that pH swelling dependence of hydrogels consisting of 444 mM NIPA, 128 mM AAm and 128 mM AAc at various bath salt concentrations. It is clear from this data that hydrogen ion dissociation equilibrium plays an important role even at high bath salt concentrations. At low pH values the solvent effect becomes evident at high bath salt concentrations. With increasing pH the hydrogels are increasingly ionized and as a result swell.

Figures 3-5, 3-6 and 3-7 show the kinetic response to changes in bath salt concentration at pH 4.2, 5.8 and 8.0 respectively. At pH 5.8 a biphasic swelling response is observed. At pH 4.3 and 8.0 the kinetic response is dominated by the

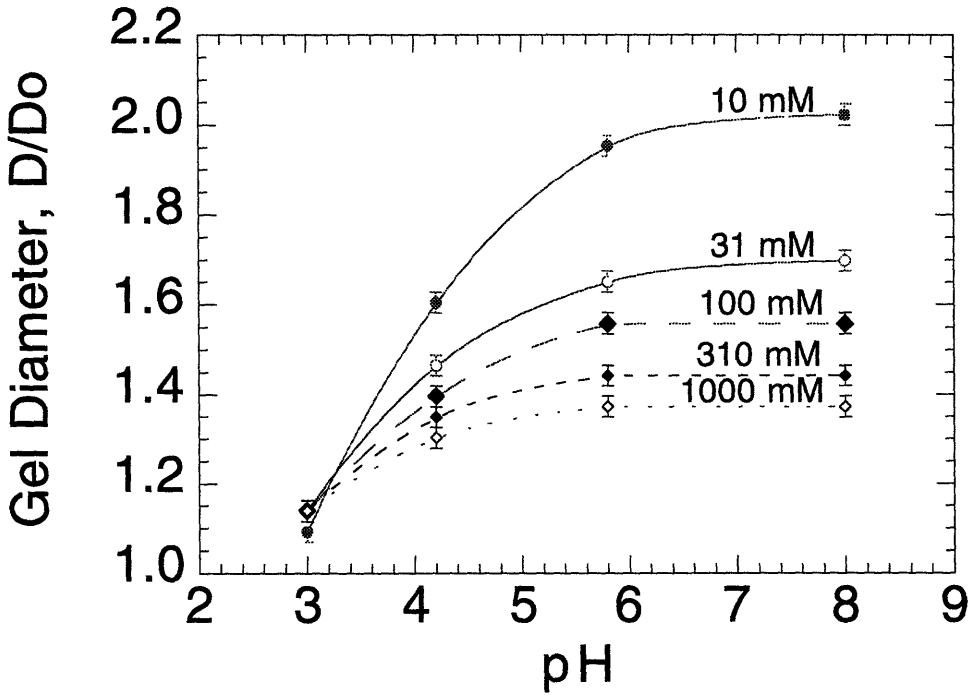

Figure 3-4: Equilibrium swelling of 128 mM AAc as a function of pH at 25 °C. Hydrogen ion dissociation equilibria plays an important role even at high bath salt concentrations.

monotonic poroelastic response.

Since hydrogen ions can bind to carboxylate groups in the hydrogel matrix the diffusion coefficient depends on the local charge density. The charge density in turn depends on the internal pH. Since the local charge density leads to counter ion osmotic pressure, or equivalently to local charge repulsion, the hydrogel elasticity and or the solvent interaction also contribute. A greater charge density will lead to greater internal pressure and tend to swell the hydrogel and thereby reduce the charge density. For hydrogels with small elastic or bulk moduli the fixed charge density can remain constant over a significant range of the external bath salt and pH range. The interplay between solvent and elastic effects with the charge density is an important contributing factor to the rate at which hydrogen ions are transported

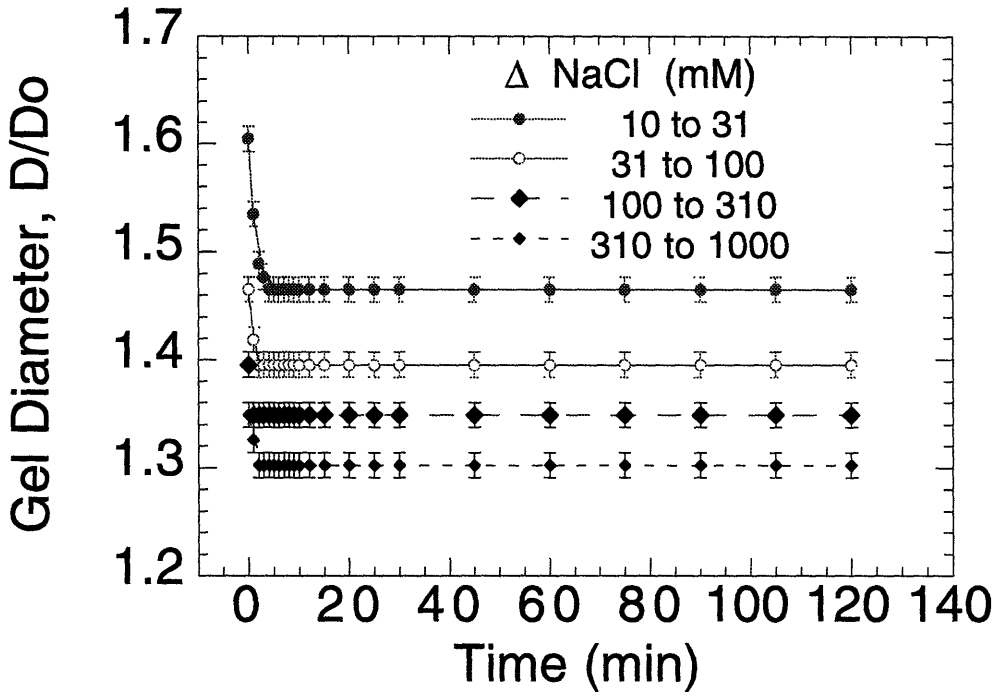

Figure 3-5: Kinetic response to changes in bath salt concentration at pH 4.1 and 25 °C.

over a significant range of the external bath pH and ionic strength.

The hydrogen ion transport time constant is plotted in Fig. 3-8. We notice that for a bath pH of 5.8, no added acid or base, that the internal hydrogen ion concentration monotonically increases with the bath salt concentration. As a result, the corresponding hydrogen ion transport time constant shows a similar increase. The actual charge concentration, however, also influences this swelling behavior since it varies with bath salt concentration. Once the majority of the hydrogen ions have been replaced with sodium ions and the hydrogel collapses due to the reduction in osmotic pressure at high salt concentrations the local charge density reaches a maximum value. At this point the transit time for hydrogen ions will be slowest due to the large density of dissociated acid groups within the hydrogel.

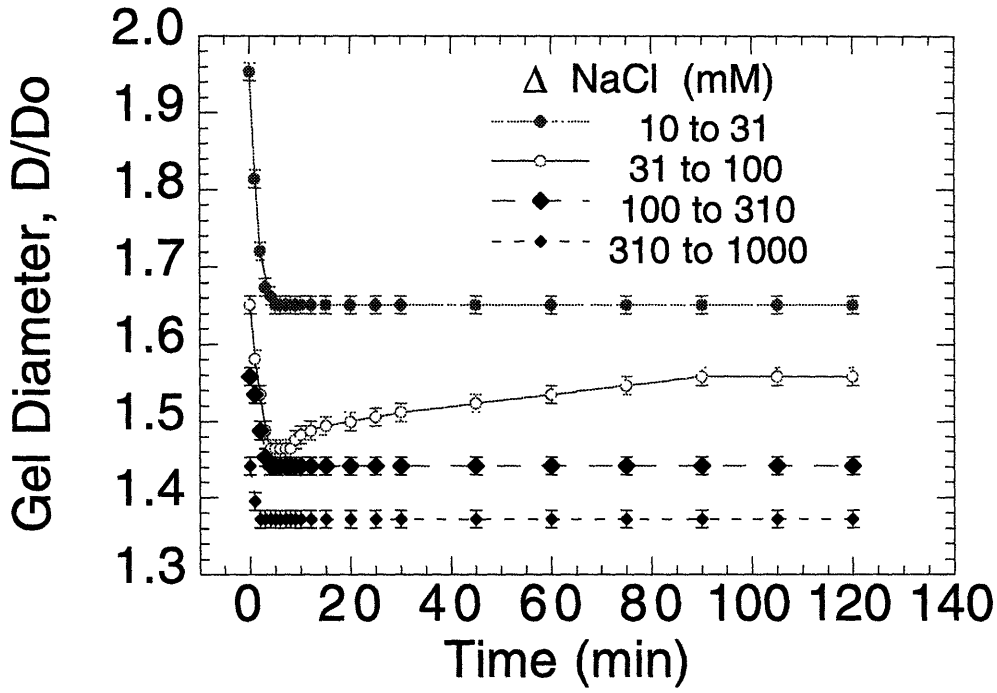

Figure 3-6: Kinetic response to changes in bath salt concentration at pH 5.8 and 25 °C.

Based on ion transport alone the rate limiting swelling response due to hydrogen ion transport becomes less important at higher bath salt concentration in response to changes in salt concentration. This is due to fact that the transport of hydrogen ions become less relevant. At high salt concentrations the internal pH values do not reach low enough values to alter the degree of hydrogen ion association and as a result will not effect swelling. One would predict that hydrogen ion exchange for sodium may take place but not influence the equilibrium swelling. This effect can not be measured from swelling diameters alone. The role of hydrogen ion exchange becomes important in concentration regimes where the internal hydrogen ion concentration can influence the degree of ion association. In this concentration regime it becomes important to consider the ambipolar diffusion coefficient in order to estimate the swelling equilibrium time where this form of ion transport is rate

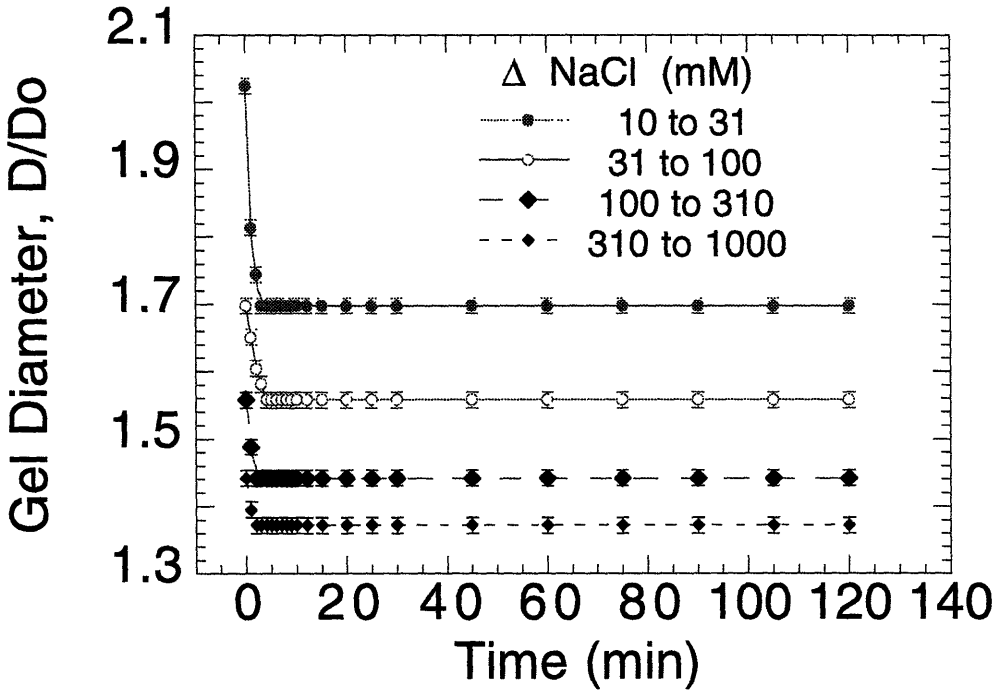

Figure 3-7: Kinetic response to changes in bath salt concentration at pH 8.0 and 25 °C.

limiting.

The equilibrium swelling diameters as a function of bath $CuCl_2$ concentration are presented in Fig. 3-9. The lowest swelling curve is that of pure NIPA while the successively higher curves represent hydrogels with net charge offsets of -2, -4, -8, -16, -32, -64, -128, and -256 mM in their reference states respectively. Figure 3-10 shows the swelling dependence of a hydrogel consisting of 444 mM NIPA, 128 mM AAc and 128 mM AAm as a function of $CuCl_2$ wash concentration at 35 and 40 °C. In this case the polyelectrolyte swelling observed for monovalent ions is greatly reduced. With increasing $CuCl_2$ concentration a much greater collapse transition is observed up to 10 mM. Further increase in $CuCl_2$ concentration results in a transient increase in swelling followed by a collapse transition. Condensation effects, solvent quality changes, and cross-linking effects may be taking part in this complicated

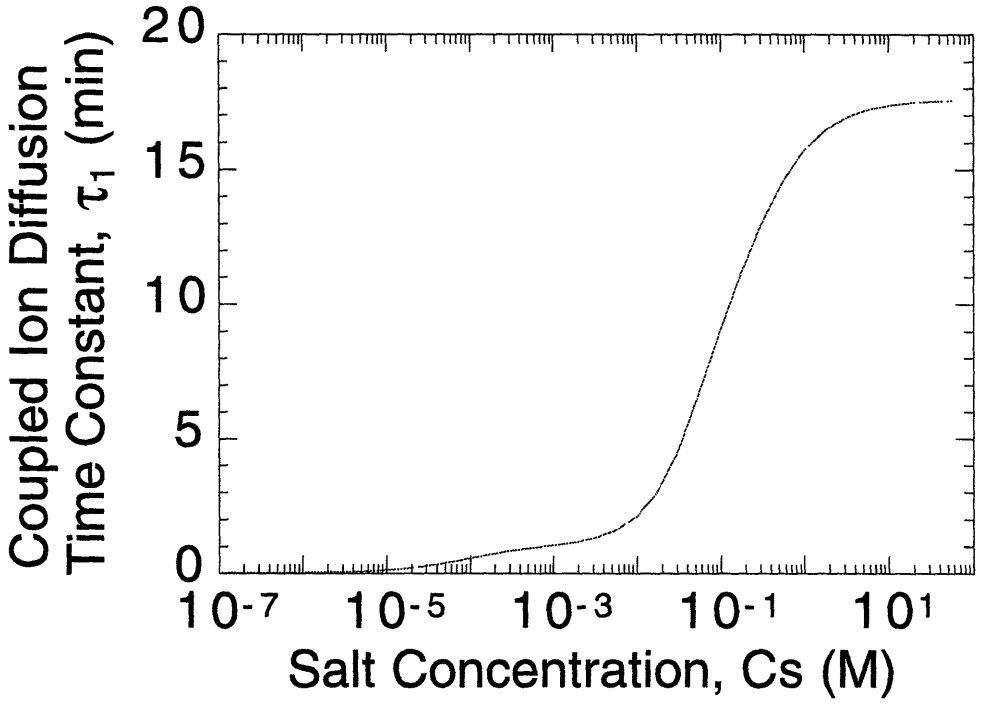

Figure 3-8: Hydrogen ion equilibration time constant as a function of bath salt concentration.

swelling behavior.

Figure 3-10 shows the swelling dependence of a hydrogel consisting of 444 mM NIPA, 128 mM AAc and 128 mM AAm as a function of temperature at different $CuCl_2$ wash concentrations. First order phase transitions are not observed. The acrlyamide effectively prevents discontinuities in the phase behavior normally observed for NIPA and AAc.[Hir87]

3.5 Conclusions

The equilibrium swelling response of an acrylamide, acrylic acid and NIPA copolymer as a function of bath salt concentration can be divided into three regimes. At

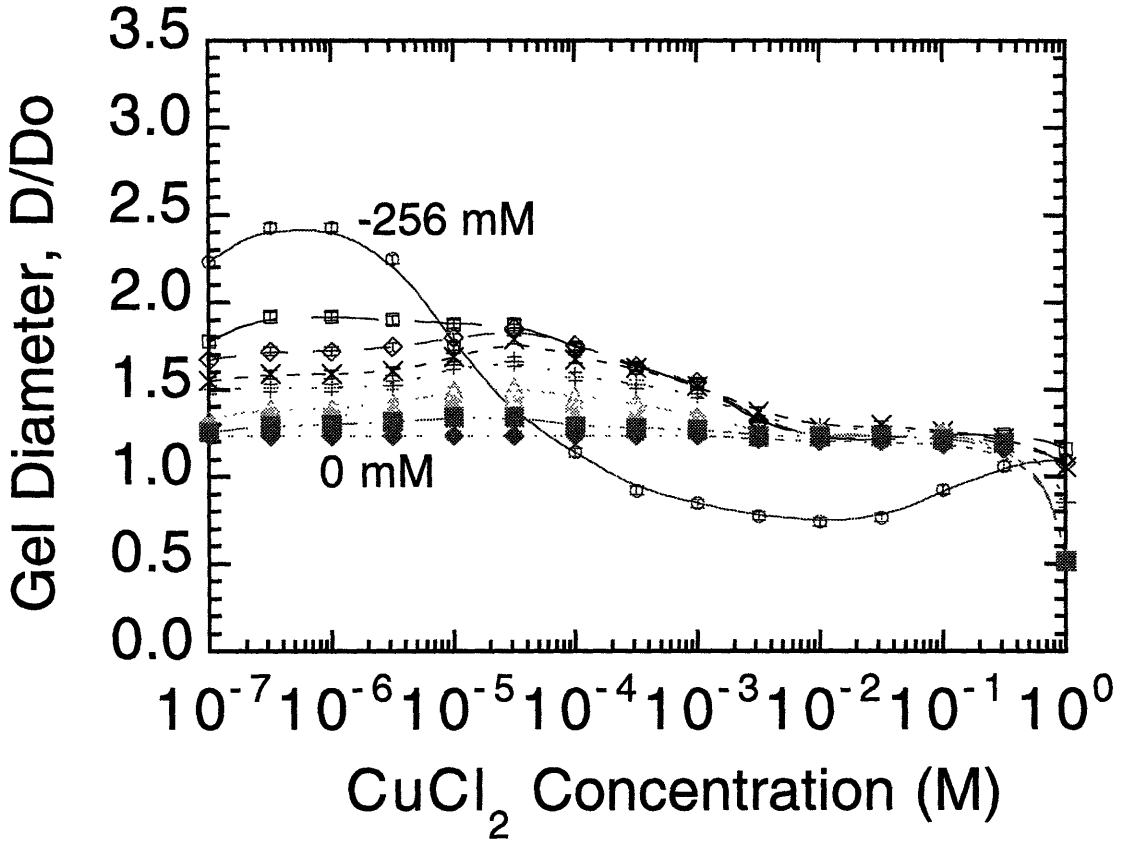

Figure 3-9: Polyelectrolyte swelling versus copper chloride concentration at 25 °C. Washing with bivalent ions results in a complicated swelling pattern which involves more than just Donnan partitioning.

low ionic strengths ion dissociation equilibrium governs the swelling response in charged copolymer hydrogels. At intermediate ion strengths polyelectrolyte effects become important. At very high ionic strengths the effect of ions on the neutral NIPA components becomes important. It is important to make a careful distinction between hydrogel collapse due to polyelectrolyte effects and those due to ionic effects on the neutral monomer components.

We observe that the kinetics of the copolymer hydrogel are dominated by diffusion reaction kinetics at low bath ionic strengths and low pH values. At high pH values and ionic strengths the mechanical response of the hydrogel is rate limiting in the kinetic response. Bivalent ions produce a more complicated swelling pattern

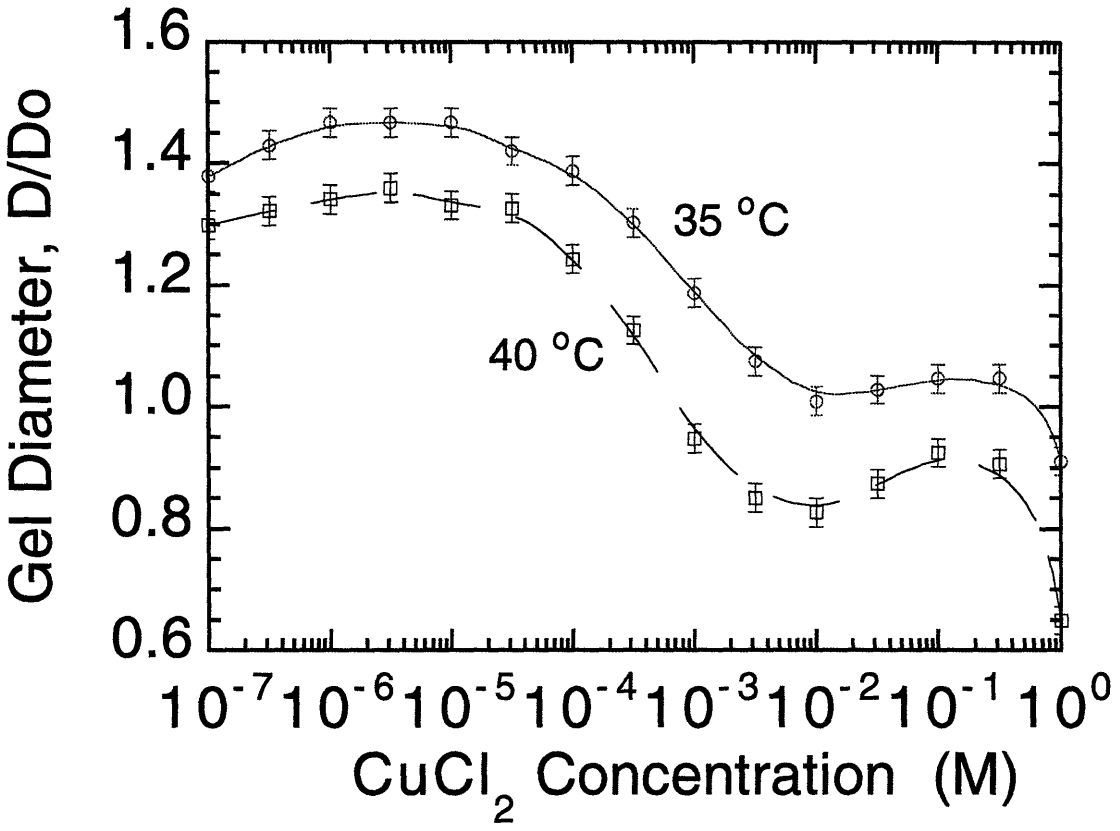

Figure 3-10: Polyelectrolyte swelling versus copper chloride concentration at 35 and 40 °C. Increasing the temperature results in smaller swelling equilibrium values due to the thermally sensitive NIPA component.

as a function of bath ionic strength.

3.6 Appendix A: Derivation of C_{mobile}

For the general case where there are N_{f+} positive ionized charge groups and N_{f-} negative ionized charge groups and only monovalent mobile ions local charge electroneutrality gives us

$$\frac{N_{f+} - N_{f-}}{N_A V} + C_+ = C_-, \tag{3.38}$$

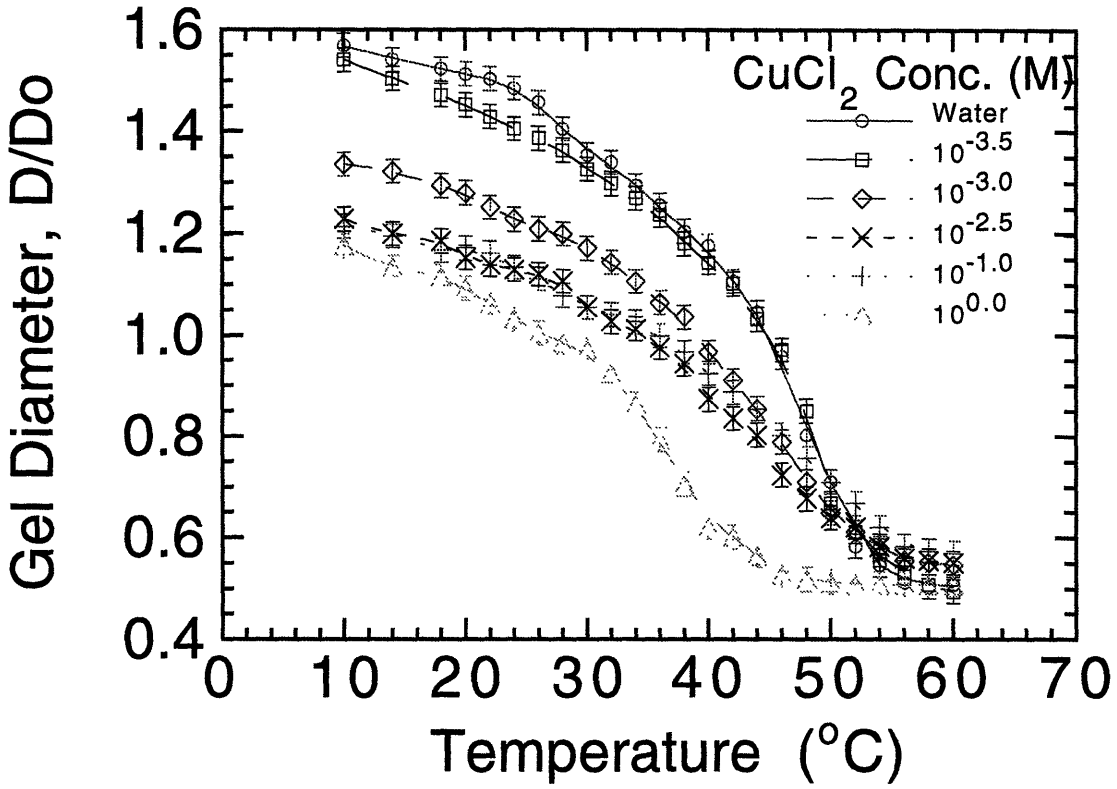

Figure 3-11: Polyelectrolyte swelling versus temperature and copper chloride concentration. Over a wide range of temperatures and copper chloride concentrations only continuous second order phase transitions are observed.

where C_+ and C_- denote the total internal concentration of mobile positive and negative ions respectively. From Donnan equilibrium

$$C_+C_- = C_o^2, \tag{3.39}$$

where $C_o = C_{Na^+Bath} + C_{H^+Bath} = C_s + C_{H^+Bath}$. Combining Eqs. 3.38 and 3.39 yields

$$\begin{aligned} \frac{N_{f+} - N_{f-}}{N_A V} + C_+ &= \frac{C_o^2}{C_+} \\ \Rightarrow C_+^2 + \left(\frac{N_{f+} - N_{f-}}{N_A V}\right) C_+ &- C_o^2 = 0. \end{aligned} \tag{3.40}$$

For physically meaningful concentrations we take the positive root

$$C_+ = -\frac{1}{2}\left(\frac{N_{f+} - N_{f-}}{N_A V}\right) + \frac{1}{2}\left\{\left(\frac{N_{f+} - N_{f-}}{N_A V}\right)^2 + 4C_o^2\right\}^{\frac{1}{2}}. \tag{3.41}$$

Therefore

$$C_{mobile} = C_+ + C_- = 2C_+ + \frac{N_{f+} - N_{f-}}{N_A V} \tag{3.42}$$

or

$$C_{mobile} = 2\left\{\left(\frac{N_{f+} - N_{f-}}{2N_A V}\right)^2 + C_o^2\right\}^{\frac{1}{2}}. \tag{3.43}$$

In the case where only negative polyions exist

$$C_{mobile} = 2\left\{\left(\frac{N_{f-}}{2N_A V}\right)^2 + C_o^2\right\}^{\frac{1}{2}}. \tag{3.44}$$

3.7 Appendix B: Acid and Base Dissociation

Polyelectrolytes, by definition, contain polyions of one charge type. Polyelectrolytes with negative polyions require consideration of the possible influence of acid dissociation on the equilibrium swelling. Similarly, the effects of base dissociation must be considered in polyelectrolytes with positive polyions. The purpose of this appendix is to derive polynomial expressions in terms of the unknown internal hydrogen ion concentration for polyelectrolytes with one type of dissociable fixed charge group in terms of the known monovalent bath ion concentrations. Coupling these polynomial expressions with osmotic swelling relations allows the equilibrium swelling to be determined.

3.7.1 Dissociation Equilibrium With Only Acid Groups

Acid Dissociation

Acid dissociation equilibrium is described by

$$K_a = \frac{C_{A^-} C_{H^+}}{C_{AH}} = \frac{C_{A^-} C_{A^+}}{C_A - C_{A^-}}, \tag{3.45}$$

where K_a is the acid dissociation constant, C_{A^-} the ionized acid group concentration, C_{H^+} the hydrogen ion concentration, C_{AH} the unionized acid group concentration, and C_A the concentration of unionized and ionized acid groups. Rearranging 3.45 gives us

$$C_{A^-} = \frac{C_A K_a}{K_a + C_{H^+}}. \tag{3.46}$$

Thus, for acidic monomers the degree of ionization can be defined as

$$\alpha_a = \frac{K_a}{K_a + C_{H^+}}. \tag{3.47}$$

Local Charge Electroneutrality

Local charge electroneutrality for monovalent ions can be expressed as

$$C_{A^-} = \sum_i z_i C_i, \tag{3.48}$$

where z_i and C_i are the valence and internal concentration of particle i. If all the mobile particles are monovalent or neutral and C_+ and C_- represent the total concentration of positive and negative particles respectively then

$$C_{A^-} = C_+ - C_-, \tag{3.49}$$

and

$$\frac{C_A K_a}{K_a + C_{H^+}} = C_+ - C_-. \tag{3.50}$$

Donnan Equilibrium

The Donnan equilibrium conditions can be succinctly stated in terms of the particle electrochemical potentials which are found from the free energy using

$$\mu_i = \frac{\partial F}{\partial N_i}. \tag{3.51}$$

For ideal solutions, equilibration of internal and external chemical potentials implies that

$$\mu_j^s + p^i v_j + RT \ln x_j^i + z_j F \psi^i = \mu_j^s + p^o v_j + RT \ln x_j^o + z_j F \psi^o, \tag{3.52}$$

where the superscripts i and o indicate internal and external values respectively. The partial molar volumes, v_k, are assumed independent of the pressure p. The term μ^s represents the reference state chemical potential, R the Boltzmann's constant multiplied by avogadro's number, T the absolute temperature, x the mol fraction, z the valency, F the Faraday constant, and ψ the potential.

If all ions are monovalent and each has a concentration much less than the solvent then balance of chemical potentials for each charged particle yields

$$C_+ C_- = C_o^2, \tag{3.53}$$

where C_o is the sum of all bath ions of one sign regardless of pH. Combining the above equations gives us

$$\frac{C_A K_a}{K_a + C_{H^+}} = C_+ - \frac{C_o^2}{C_+} = \frac{C_o C_{H^+}}{C_{H^+Bath}} - \frac{C_o C_{H^+Bath}}{C_{H^+}}$$

$$
\begin{aligned}
\Rightarrow C_A K_a C_{H+Bath} C_{H+} &= C_o C_{H+}^2 (K_a + C_{H+}) - C_o C_{H+Bath}^2 (K_a + C_{H+}) \\
\Rightarrow C_A K_a C_{H+Bath} C_{H+} &= C_o K_a C_{H+}^2 + C_o C_{H+}^3 - C_o K_a C_{H+Bath}^2 - C_o C_{H+Bath}^2 C_{H+} \\
\Rightarrow C_o C_{H+}^3 &+ C_o K_a C_{H+}^2 - (C_o C_{H+Bath}^2 + C_A K_a C_{H+Bath}) C_{H+} - C_o K_a C_{H+Bath}^2 = 0.
\end{aligned}
$$

Therefore

$$
C_{H+}^3 + K_a C_{H+}^2 - \left(C_{H+Bath}^2 + \frac{C_A K_a C_{H+Bath}}{C_o} \right) C_{H+} - K_a C_{H+Bath}^2 = 0. \quad (3.54)
$$

Solving for the internal hydrogen ion concentration, C_{H+}, using the polynomial equation 3.54 allows us to solve for the remaining ion species:

$$
\begin{aligned}
C_{A-} &= \frac{C_A K_a}{K_a + C_{H+}}, && (3.55) \\
C_{Na+} &= \frac{C_{Na+Bath} C_{H+}}{C_{H+Bath}}, && (3.56) \\
C_{Cl-} &= \frac{C_{Cl-Bath} C_{H+Bath}}{C_{H+}}, && (3.57) \\
C_{OH-} &= \frac{K_w}{C_{H+}}, && (3.58) \\
C_{CHCO_3^-} &= \frac{C_{CHCO_3^- Bath} C_{H+Bath}}{C_{H+}}. && (3.59)
\end{aligned}
$$

3.7.2 Dissociation Equilibrium With Only Base Groups

Base Dissociation

Similarly to acid dissociation, a corresponding polynomial expression for base dissociation can be derived. Base dissociation equilibrium can be stated as

$$
K_b' = \frac{C_{B+} C_{OH-}}{C_{BOH}}, \quad (3.60)
$$

where K_b' is the base dissociation constant, C_{B+} the ionized base concentration, C_{OH-} the hydrogen ion concentration, and C_B the ionized and unionized base con-

centration. Letting $K_b = K_w/K_b'$ and using $K_w = C_{H^+}C_{OH^-}$ we get

$$K_b = \frac{C_{BOH}C_{H^+}}{C_{B^+}}. \tag{3.61}$$

Rearranging 3.61 gives us

$$C_{B^+} = \frac{C_B C_{H^+}}{K_b + C_{H^+}}. \tag{3.62}$$

Hence, the degree of ionization for basic monomers can be defined as

$$\alpha_b = \frac{C_{H^+}}{K_b + C_{H^+}}. \tag{3.63}$$

Local Charge Electroneutrality

Local charge electroneutrality gives us

$$C_{B^+} = C_- - C_+, \tag{3.64}$$

where C_- and C_+ are the total concentration of mobile positive and negative ions respectively. Using Eq. 3.62 in Eq. 3.64 gives us

$$\frac{C_B C_{H^+}}{K_b + C_{H^+}} = C_- - C_+. \tag{3.65}$$

Donnan Equilibrium

Recall that from Donnan equilibrium

$$C_+C_- = C_o^2, \tag{3.66}$$

where C_o is the sum of all bath ions of one sign regardless of pH. Combining the above equations gives us

$$\begin{aligned}
\frac{C_B C_{H+}}{K_b + C_{H+}} &= \frac{C_o^2}{C_+} - C_+ = \frac{C_o C_{H+Bath}}{C_{H+}} - \frac{C_o C_{H+}}{C_{H+Bath}} \\
\Rightarrow C_B C_{H+}^2 C_{H+Bath} &= C_o C_{H+Bath}^2 (K_b + C_{H+}) - C_o C_{H+}^2 (K_b + C_{H+}) \\
\Rightarrow C_B C_{H+}^2 C_{H+Bath} &= C_o C_{H+Bath}^2 K_b + C_o C_{H+Bath}^2 C_{H+} - C_o C_{H+}^2 K_b - C_o C_{H+}^3 \\
\Rightarrow C_o C_{H+}^3 &+ (C_o K_b + C_B C_{H+Bath}) C_{H+}^2 - C_o C_{H+Bath}^2 C_{H+} - C_o K_b C_{H+Bath}^2 = 0.
\end{aligned}$$

Hence

$$C_{H+}^3 + \left(K_b + \frac{C_B C_{H+Bath}}{C_o}\right) C_{H+Bath}^2 - C_{H+Bath}^2 C_{H+} - K_b C_{H+Bath}^2 = 0. \quad (3.67)$$

Solving for the internal hydrogen ion concentration, C_{H+}, using the polynomial equation 3.67 allows us to solve for the remaining ion species:

$$C_{B+} = \frac{C_B C_{H+}}{K_b + C_{H+}}, \quad (3.68)$$

$$C_{Na+} = \frac{C_{Na+Bath} C_{H+}}{C_{H+}}, \quad (3.69)$$

$$C_{Cl-} = \frac{C_{Cl-Bath} C_{H+Bath}}{C_{H+}}, \quad (3.70)$$

$$C_{OH-} = \frac{K_w}{C_{H+}} \quad \text{and} \quad (3.71)$$

$$C_{CHCO_3^- Bath} = \frac{C_{CHCO_3^-} C_{H+Bath}}{C_{H+}}. \quad (3.72)$$

3.8 Appendix C: Cylindrical Geometric Solutions

If we assume that the hydrogel does not deform during the ion transport process and is infinite in length we can use the cylindrical geometry[Jac75] to simplify the

problem. In cylindrical coordinates Eq. 3.27 becomes

$$\frac{\partial C(r,\phi,z,t)}{\partial t} = D\left(\frac{\partial^2}{\partial r^2} + \frac{1}{r}\frac{\partial}{\partial r} + \frac{1}{r^2}\frac{\partial^2}{\partial \phi^2} + \frac{\partial^2}{\partial z^2}\right) C(r,\phi,z,t). \tag{3.73}$$

Applying separation of variables we assume a solution of the form

$$C(r,\phi,z,t) = T(t)R(r)\Phi(\phi)Z(z). \tag{3.74}$$

This leads to the ordinary differential equations

$$\frac{dT}{dt} + Dk^2T = 0, \tag{3.75}$$

$$\frac{d^2Z}{dz^2} - k^2Z = 0, \tag{3.76}$$

$$\frac{d^2\Phi}{d\phi^2} + k^2\Phi = 0, \tag{3.77}$$

$$\frac{d^2R}{dr^2} + \frac{1}{r}\frac{dR}{dr} + \left(k^2 - \frac{\nu^2}{r^2}\right)R = 0. \tag{3.78}$$

Ignoring the ϕ and z dependence we obtain temporal solutions of the form

$$T_n(t) = C_n e^{-Dk_n^2 t}. \tag{3.79}$$

Using the substitution, $x = kr$, the radial equation can be put in the form

$$\frac{d^2R}{dx^2} + \frac{1}{x}\frac{dR}{dx} + \left(1 - \frac{\nu^2}{x^2}\right)R = 0 \tag{3.80}$$

Equation 3.80 is Bessel's equation of order ν. The lack of ϕ dependence requires only zeroeth order terms to be kept.

We offset the boundary conditions so that the concentration vanishes at $r = Ro$, i.e., $\overline{C}(r = R_o, \phi, z, t \geq 0) = 0$. Similarly, the initial condition becomes $\overline{C}(0 \leq r \leq$

$R_o, \phi, z, t = 0) = C_o$. As a result, k can only take on values

$$k_n = \frac{x_n}{R_o}, \quad \text{n=1,2,3,...} \tag{3.81}$$

where x_n are the roots of $J_0(x_n) = 0$. The general solution has the form

$$\overline{C}(r, \phi, z, t) \quad = \quad \sum_{n=1}^{\infty} A_n J_0(k_n r) e^{-Dk_n^2 t} \quad . \tag{3.82}$$

Since $\overline{C}(r, z, \phi, t)$ is finite at $r = 0$, the initial condition becomes

$$\overline{C}_o = \sum_{n=1}^{\infty} A_n J_0(k_n r), \tag{3.83}$$

where we assume the constant initial concentration can be expanded in a series of Bessel functions of order 0.

3.9 Appendix D: Purification of N-isopropylacrylamide

In a fume hood N-isopropylacrylamide was purified by recrystalization using the following procedure.

- Approximatly 30 g of unpurified NIPA was dissolved in 180 mM of toluene.
- The toluene NIPA solution was filtered using a 25-50 μm glass filter under aspiration.
- The filtered NIPA toluene solution was poured into a 2000 mM beaker and approximately 1500 mM of petroleum ether was added.
- The precipitated NIPA was filtered out using a 25-50 μm glass filter under aspiration.
- The recrystalized NIPA was dried under vacuum with a dry ice and isopropyl alcohol filter trap for 12 hours.

Chapter 4

Polyampholytic Hydrogel Phase Transitions

Abstract

The role of counter ions and ion dissociation in establishing the equilibrium swelling of balanced and unbalanced polyampholytic hydrogels has been investigated experimentally and theoretically. The swelling dependence on both the net charge offset and the external bath salt concentration has been examined using an acrylamide based polyampholytic hydrogel. By careful consideration of the swelling kinetics, this study illustrates the effects of ion dissociation equilibria and counter ion shielding in polyampholytic hydrogels near their balance point where both polyelectrolyte and polyampholyte effects are present. The theory considers a Flory type swelling model where the Coulombic interactions between fixed ions in the hydrogel resemble those of an ionic solid with a Debye screening factor. Theoretical predictions from this model are in qualitative agreement with experimental results.

4.1 Introduction

Polyampholytic hydrogels are cross-linked polymer networks that are made up of both positive and negative monomeric groups with the possible inclusion of neutral monomeric spacers. Balanced polyampholytes have an equal number of positive and negative charges while unbalanced polyampholytes have a charge excess. The long

range Coulombic interactions which determine the physical properties of polyampholytes are a challenge to both theoretical and experimental understanding.

In recent years, considerable effort has been devoted to understanding the single polyampholyte chain in very dilute solutions where counter ions do not screen the Coulombic potential. It has been shown in extensive studies by Kantor and Kardar[Kan92,Kan94,Kan95a,Kan95b] and by Gutin and Shakhnovich[?] and Dobrynin and Rubinstein[Dob95] that polyampholyte chains form a spherical globular structure when the overall net charge does not exceed $q_o\sqrt{N}$. When the net charge exceeds $q_o\sqrt{N}$ the polyampholyte forms an elongated globule. The globule density is determined by the overall attraction and is almost independent of the charge excess while the globule shape is governed primarily by the net charge.

A macroscopic polyampholytic hydrogel, however, is dramatically different. On length scales greater than a Debye length the distribution of charged monomers, counter ions and co-ions maintains almost perfect charge neutrality. This creates a complicated set of interactions within the system. Unlike a plasma or electrolyte, several components contribute to the screening in a different manner. The charged monomers of both signs, counter ions and co-ions all have different amounts of freedom to respond to local electric fields. In addition, acid and base ion dissociation equilibrium can have important effects on the polymer charge density.

Polyampholytes have been the subject of a number of experimental studies. Corpart et al.[Cor93] and Skouri et al.[Sko94] examined the aqueous solution properties of polyampholytes using viscometry and light scattering measurements. Baker et al.[Bak95] later examined balanced polyampholyte hydrogel swelling and proposed a semiquantitative model based on a Flory type theory with Debye-Hückel contributions. These experimental studies are in qualitative agreement with Higgs and Joanny's model.[Hig91] Balanced polyampholytes collapse at low salt concentrations and swell at high salt concentrations. With increasing charge offset, polyelectrolyte behavior is observed and swelling decreases with increasing salt concentration. For

polyampholytes near their balance point, however, both effects can be important over a wide range of bath electrolyte concentrations.[Yu93,Eng95]

In this work the swelling equilibria of polyampholytic hydrogels are examined both experimentally and theoretically. The theory considers a Flory type swelling model for ionic hydrogels where the Coulombic interactions between the hydrogel fixed ions resemble those of an ionic solid with a Debye screening factor. Higgs and Joanny's theory was based on the assumption that all charges, both mobile and polymeric, contribute equally to the screening. One would expect that the polymer chain connectivity and monomer masses will significantly restrict the polyions compared to the mobile counter and co-ions. As a result, this study considers the opposite limit where the monomers are immobile and do not adjust to fluctuating fields or contribute to the screening. By careful consideration of the swelling kinetics, this work illustrates the additional effects of ion dissociation equilibria using acrylamide based polyampholytic hydrogels near their balance point where both polyelectrolyte and polyampholyte effects are present.

4.2 Theoretical Model

Thermodynamic equilibrium is achieved when the chemical potential of each mobile species is equal in every phase. A balance of solvent chemical potentials is a statement of osmotic pressure or swelling equilibrium. Similarly, the ionic equilibrium of mobile species is obtained when the electrochemical potentials within the hydrogel equal that in the external bath. For those species capable of binding to functional groups, the electrochemical potentials in the bound and unbound states must also be equal. The volumetric charge density will therefore be a complicated function of the swelling process and a model which considers both swelling and dissociation equilibrium must be constructed.

4.2.1 Free Energy Model

Four additive contributions to the free energy are assumed,

$$\Delta F = \Delta F_M + \Delta F_{el} + \Delta F_{trans} + \Delta F_{Coulombic} , \tag{4.1}$$

where $\Delta F_M, \Delta F_{el}, \Delta F_{trans}$, and $\Delta F_{Coulombic}$ represent the mixing, elastic, translational, and Coulombic contributions to the free energy respectively.

Based on the Flory-Huggins lattice theory,[Flo53] the free energy of mixing between monomer and solvent molecules is

$$\Delta F_M = k_B T \frac{V}{v_{site}} (1-\phi) \left[\ln(1-\phi) + \chi\phi\right], \tag{4.2}$$

where V is the hydrogel volume, v_{site} the lattice site volume, ϕ the polymer volume fraction, χ the polymer solvent interaction parameter, k_B is Boltzmann's constant, and T the absolute temperature.

From the affine network model,[Flo53,Flo79] the elastic contribution to the free energy is

$$\Delta F_{el} = \frac{3k_B T}{2} \frac{V\phi}{N_x v_{site}} \left[\left(\frac{\phi_o}{\phi}\right)^{\frac{2}{3}} - 1 - \frac{1}{3}\ln\left(\frac{\phi_o}{\phi}\right)\right], \tag{4.3}$$

where N_x is the average number of monomers between cross-links. The term $\frac{V\phi}{N_x v_{site}}$ is the effective number of chains in the network while $\frac{\phi_o}{\phi}$ is the swelling ratio. Hydrogel volumes and polymer volume fractions are related through

$$\frac{V}{V_o} = \frac{\phi_o}{\phi} = \left(\frac{D}{D_o}\right)^3, \tag{4.4}$$

where V_o, D_o and ϕ_o are the hydrogel volume, diameter and polymer volume fraction in the reference state respectively.

The translational component represents the ion mobility contribution to the free

energy. For this term we consider the ideal gas contribution,

$$\Delta F_{ideal} = k_B T \sum_i N_i \left\{ \ln\left(\frac{N_i}{N_A V}\right) - 1 \right\}, \tag{4.5}$$

where N_A is Avogadro's number and N_i is the total number of the ith mobile ion. The sum is over all mobile ion species such that

$$C_{mobile} \equiv \sum_i \frac{N_i}{N_A V} \tag{4.6}$$

is the total mobile ion concentration. We assume that the excluded volume correction to V in Eq. (4.5) is negligible. For monovalent ions the Donnan equilibrium relations with the constraint of local charge neutrality lead to

$$C_{mobile} = 2\sqrt{\left(\frac{N_{f+} - N_{f-}}{2N_A V}\right)^2 + C_o^2}\ , \tag{4.7}$$

where N_{f+} and N_{f-} are the total number of positive and negative fixed charges respectively. If C_s is the concentration of added salt, then $C_o = C_s + C_{H+Bath}$ is the bath concentration of all positive ions.

The Coulombic contribution to the free energy is

$$\Delta F_{Coulombic} = \sum_i z_i e N_i \phi_D + \Delta F_{lattice}, \tag{4.8}$$

where z_i is the valence of the ith ion, e the unit charge, ϕ_D the Donnan potential, and $\Delta F_{lattice}$ represents the contribution due to the interaction between fixed charge groups. The lattice free energy, $\Delta F_{lattice}$, can be evaluated by considering the bound polymer charges as a quasilattice with screened Coulomb interactions. We now describe this term by considering a lattice model where every site is surrounded by z nearest neighbors.

If only nearest-neighbor interactions are considered, the lowest energy configu-

ration of a balanced polyampholyte ($N_{f+} = N_{f-}$) would be obtained when every charge has z oppositely charged neighbors. The configuration energy would then be

$$\Delta F_{lattice} = -\frac{z}{2}(N_{f+} + N_{f-})\frac{e^2}{4\pi\epsilon}\frac{\exp(-\kappa r)}{r}, \tag{4.9}$$

where ϵ is the solvent dielectric permittivity, r the nearest neighbor distance such that

$$r \approx 2\left(\frac{3V}{4\pi(N_{f+} + N_{f-})}\right)^{\frac{1}{3}}, \tag{4.10}$$

and

$$\kappa = \sqrt{\frac{e^2 N_A C_{mobile} 1000}{\epsilon k_B T}} \tag{4.11}$$

is the reciprocal Debye length in the hydrogel. The factor of 1000 is necessary to convert mols per liter to mols per cubic meter.

If some positive fixed charges are replaced by negative charges, the lowest energy would be obtained when every positive charge has the maximum number z of oppositely charged nearest neighbors. This would give zN_{f+} attractive interactions and $(z/2)(N_{f+} + N_{f-}) - zN_{f+}$ repulsive interactions. The system free energy in this case would be

$$\Delta F_{lattice} = \frac{z}{2}N_{fe}\frac{e^2}{4\pi\epsilon}\frac{\exp(-\kappa r)}{r}, \tag{4.12}$$

where $N_{fe} = N_{f+} + N_{f-} - 2|N_{f+} - N_{f-}|$ is the effective number of fixed charges giving rise to attractive interactions. The absolute value permits us to consider both excess positive or negative fixed charge.

The modification of Eq. 4.12 to include long range interactions involves replacing the number of nearest neighbors, z, by a parameter similar to the Madelung constant

of ionic crystals.[Kit86] Retaining the Debye screening term gives us

$$\Delta F_{lattice} = -\frac{A}{2} N_{fe} \frac{e^2}{4\pi\epsilon} \frac{\exp(-\kappa r)}{r}, \tag{4.13}$$

where A must be of the order of unity. [Kit86]

Although it has received serious criticism,[Val89] the screened potential is common in the polyelectrolyte literature. [Nag61,Gro94] The screened potential, however, contains the essentials of the screening effect and is thus expected to be suitable for the study of balanced and slightly unbalanced polyampholytes.

4.2.2 Swelling Equilibrium

Balance of solvent chemical potentials is generally expressed as

$$\Delta\Pi_{swelling} = \frac{\mu_s^{gel} - \mu_s^{bath}}{\overline{v}_w} = 0, \tag{4.14}$$

where $\overline{v}_w$ is the solvent molar volume. Equating hydrogel and bath solvent chemical potentials gives us the swelling equilibrium condition

$$-\frac{1}{\overline{v}_{site}}\left[\ln(1-\phi)+\phi+\chi\phi^2\right] + \frac{\phi_o}{N_x \overline{v}_{site}}\left[\frac{1}{2}\left(\frac{\phi}{\phi_o}\right) - \left(\frac{\phi}{\phi_o}\right)^{\frac{1}{3}}\right] + C_{mobile} - 2C_o$$
$$-\frac{A}{2}\frac{N_{fe}}{N_A V}\frac{e^2}{12\pi\epsilon k_B T}\frac{\exp(-\kappa r)}{r}\left\{1+\kappa r - \frac{3\kappa r}{2}\left[1+\left(\frac{2N_A V C_o}{N_{f+}-N_{f-}}\right)^2\right]^{-1}\right\} = 0, \tag{4.15}$$

where $\overline{v}_{site} \equiv N_A v_{site}$ represents the molar volume of the lattice sites. The terms inside the curly brackets arise from the volume dependence of κ and r.

4.2.3 Dissociation Equilibria

The balance of chemical potentials for internal hydrogen and hydroxide ions in the free and bound states is equivalent to the chemical equilibrium of acidic and basic

monomeric species,

$$K_a = \frac{C_{A^-}\ C_{H^+}}{C_{AH}} \tag{4.16}$$

and

$$K_b = \frac{C_{BOH}\ C_{H^+}}{C_{B^+}}\ . \tag{4.17}$$

The internal parameters K_a and K_b represent the acid and base dissociation constants, C_{A^-} and C_{B^+} the concentration of ionized acid and base groups, C_{AH} and C_{BOH} the concentration of unionized acid and base groups, and C_{H^+} and C_{OH^+} the concentration of hydrogen and hydroxide ions. Localized hydrogen or hydroxide ion binding is an important consideration since it leads to a reduction in local charge repulsion and osmotic pressure in unbalanced polyampholytes.

When CO_2 is dissolved in water there is a chemical interaction. Most of the dissolved CO_2 becomes hydrated, in a way that is not completely understood, and a small fraction of it forms carbonic acid based on the sequence

$$CO_2 + H_2O \rightarrow H_2CO_3 \rightarrow H^+ + HCO_3^-\ . \tag{4.18}$$

The acid dissociation constant is

$$K_c = \frac{C_{H^+}\ C_{HCO_3^-}}{C_{H_2CO_3}}\ . \tag{4.19}$$

The effect of the bicarbonate ion is important because its concentration is 250 times larger than the hydroxide ion if base is not added. In practice, the effect of the bicarbonate ion can be reduced by running the experiment under a nitrogen or argon atmosphere.

Solving for the molar concentration of hydrogen ions, C_{H^+}, inside the hydrogel

gives us the fourth order algebraic equation

$$C_{H^+}^4 + \left(K_a + K_b + \frac{C_B}{1 + C_s/C_{H^+bath}}\right) C_{H^+}^3 + \left(K_a K_b - C_{H^+bath}^2 + \frac{K_a(C_B - C_A)}{1 + C_s/C_{H^+bath}}\right) C_{H^+}^2$$
$$- \left((K_a + K_b) C_{H^+bath}^2 + \frac{K_a K_b C_A}{1 + C_s/C_{H^+bath}}\right) C_{H^+} - K_a K_b C_{H^+bath}^2 = 0 \ , \tag{4.20}$$

where $C_A = C_{AH} + C_{A^-}$ and $C_B = C_{BOH} + C_{B^+}$ represent the total concentration of acidic and basic groups respectively.

4.2.4 Kinetic Response

The non-equilibrium swelling response to changes in bath composition can be influenced by many competing rate processes. The mechanical, or poroelastic, response time[Bio41,Tan79] involves the elastic reconfiguration of the network and the simultaneous fluid flow into or out of the network. The linearized diffusion of ions within the hydrogel matrix has an associated time constant $\tau_d \sim \frac{l^2}{D_i}$, where l represents the hydrogel dimension and D_i the ion diffusion coefficient. If binding interactions take place the ion diffusion time must be modified. The effect of hydrogen ion binding to acidic groups, for example, is to slow the diffusion process.[Nus81] The effective diffusion coefficient in this case can be written as

$$D_{i,eff} = \frac{D_{H^+}}{1 + \frac{C_A K_a}{(K_a + C_{H^+})^2}}, \tag{4.21}$$

where C_A is the total acidic monomer concentration. For small perturbations from equilibrium with a large number of free binding sites the effective diffusion coefficient can be much lower than the free diffusion coefficient. In addition to ion transport, critical point phenomenon can result in very slow kinetics.[Sta71]

4.3 Experimental Methods and Procedure

Copolymer hydrogels of varying proportions of acryl-amido methyl propyl sulfonic acid (AMPS-H) and methacryl-amido propyl trimethyl ammonium chloride (MAPTA-Cl) as negative and positive monomeric species respectively have been synthesized. Two sets of hydrogels were made in this study. In both cases the balance point was determined using a precipitation reaction. Silver AMPS (AMPS-Ag) is initially formed from AMPS-H and Ag_2CO_3 and then mixed with MAPTA-Cl to precipitate the Ag and Cl counter ions. The first set of hydrogels were made at a total concentration of 700 mM and had gelation diameters of 505 μm. In the second set of hydrogels, intended for the kinetic study, the total concentration was 1.4 M and the gelation diameters were 205 μm.

4.3.1 Sample Preparation

The AMPS-MAPTA polyampholyte pregel solution was prepared by initially dissolving 0.2 moles of AMPS-H in 200 mL of H_2O. Throughout the procedure the solution was kept cool using an ice bath in order to avoid polymerization. While stirring the hydrogen AMPS solution 0.1 moles of Ag_2CO_3 was slowly added to produce CO_2 and AMPS-Ag. The solution was then centrifuged at 3000 rpm and filtered with a 0.2 μm filter. After adding MAPTA-Cl the resulting AgCl precipitate was filtered out using a 0.2 μm filter. Small aliquots of the AMPS-MAPTA solution were tested with MAPTA-Cl and AMPS-Ag to ensure the solution had an equal concentration of AMPS and MAPTA monomers. The balanced stock solution was then diluted to the required concentrations.

Hydrogels were made using 8.6 mM N,N'-methylene-bis-acrylamide (cross-linker) and 1.76 mM ammonium persulfate (initiator) at a gelation temperature of 60 °C. Hydrogel samples with a charge offset were made by adding excess AMPS-H or MAPTA-Cl while keeping the total monomer concentration at 700 mM or 1.4 M.

In the first set of hydrogels, made at 700 mM, the AMPS-H solution used to offset the balanced pregel solution was neutralized with an equal molar concentration of NaOH. In the second set of hydrogels, made at 1.4 M, the net charge was offset by -16 mM by adding the appropriate amount of AMPS-H. One sample was neutralized to pH 7 with NaOH and the other was left at $\approx$ pH 2.

4.3.2 Experimental Outline

The hydrogels were removed from their pipettes and placed into individual glass cell holders. The hydrogels were then washed continuously and in parallel from the same stock solution to make quantitative comparisons. The slow kinetic response of these hydrogels make it necessary to consider time as a variable during all measurements. Hydrogel diameter measurements were made using a microscope equipped with a charged coupled device camera. Swelling diameter error estimates were based on the video resolution.

4.4 Results and Discussion

Figure 4-1 shows the initial swelling pattern of hydrogels prepared at pH 2 and pH 7 upon washing with deionized distilled water. The initial transient response of both hydrogels lasts approximately five to ten minutes and appears to be dominated by the matrix poroelastic response. The lower swelling peak value of the hydrogel made at pH 2 may be the result of localized hydrogen ion binding to the AMPS monomers. Since these hydrogels reswell upon washing in a 0.1 mM NaCl bath the slow reptation and loss of charged oligomers cannot be attributed to the slow collapse following the poroelastic response. Reswelling following a salt wash at 0.1 mM is more consistent with an ion exchange mechanism leading to the replacement of hydrogen ions by sodium ions. However, the fact that the hydrogel made at pH 2 with no sodium ions to begin with shows an initial biphasic swelling transient

strongly suggests that more complicated processes besides sodium ion exchange are involved in the initial non-equilibrium response. Furthermore, diameter measurements alone do not represent the non-uniform evolution of the hydrogel density as it swells and collapses.

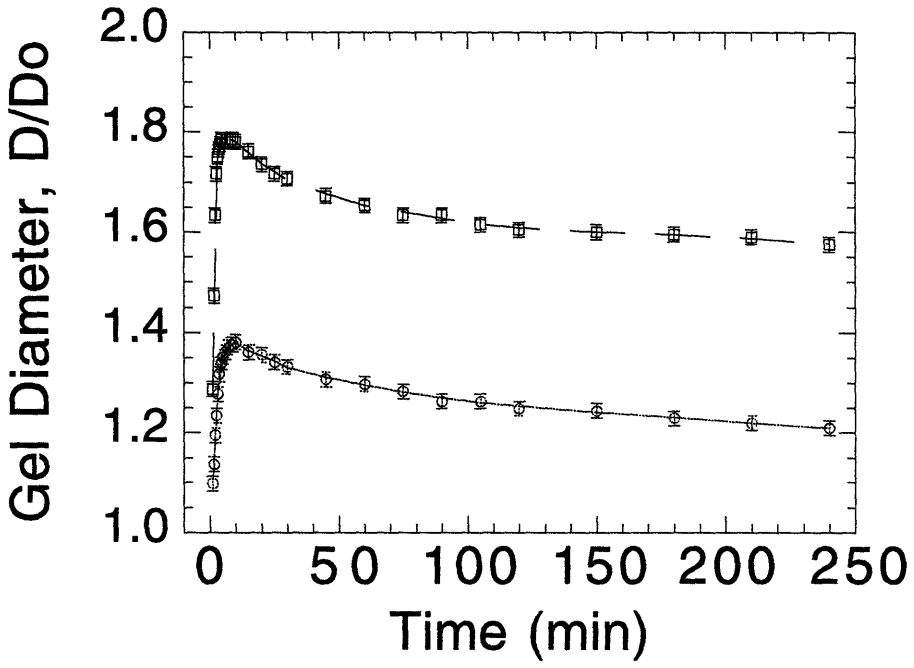

Figure 4-1: Biphasic swelling response of negatively charged polyampholytes when washed with distilled deionized water. Hydrogels made at a low pH (lower solid curve) do not swell to the same initial extent as those made at neutral pH (upper dashed curve).

Figure 4-2 shows the normalized hydrogel diameter as a function of charge offset after twelve hours of washing with distilled deionized water. The positive offset about the balance point in the initial swelling pattern may be attributed to error in the pregelation monomer concentrations or to other physico-chemical differences between monomers. Figure 4-3 shows the flat skewed swelling pattern that resulted after several days of continuous washing.

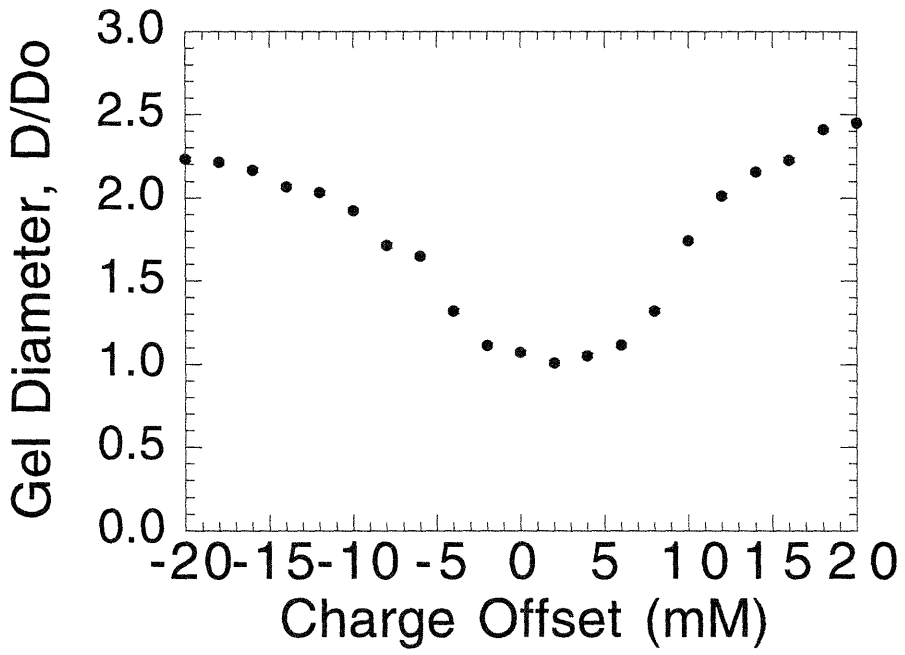

Figure 4-2: Metastable symmetric swelling distribution of charged polyampholytic hydrogels. Variably charged polyampholytic hydrogels initially swell to a symmetric distribution about the balance point within several hours of washing with distilled deionized water. The actual balance point appears to be at +2 mM due to experimental error or physico-chemical differences between monomers.

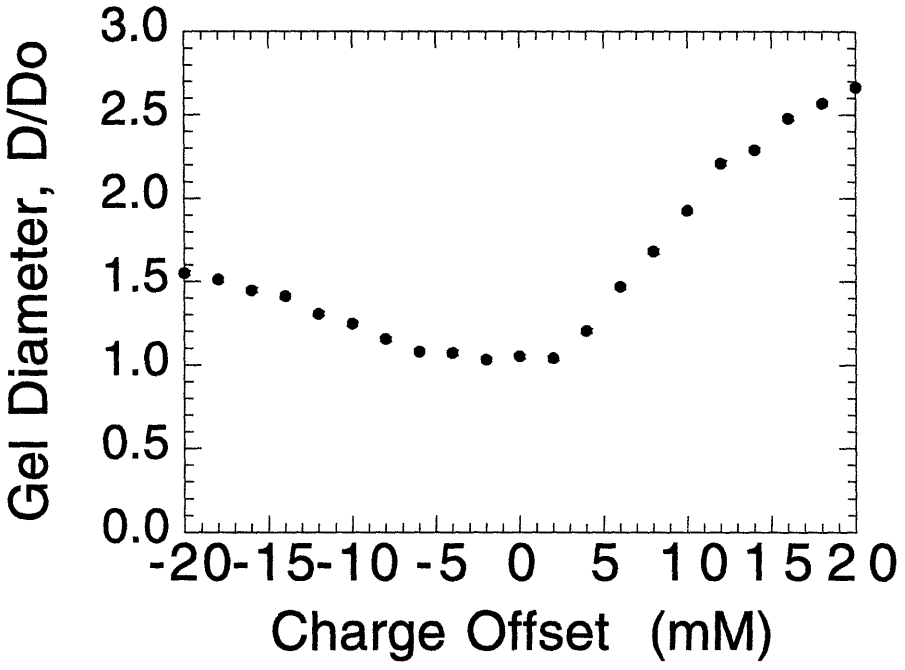

Figure 4-3: Stable equilibrium swelling distribution of charged polyampholytes. Washing variably charged polyampholytic hydrogels over a period of several days with distilled deionized water produces a skewed flattened diameter distribution.

Figures 4-4 and 4-5 show the results of washing negatively and positively charged hydrogels with increasing concentrations of sodium chloride. Polyampholytes near the balance point begin to swell at about 10 mM NaCl. Unbalanced polyampholytes initially swell up to about 0.1 mM. This initial swelling is far more pronounced for hydrogels with a negative charge offset. The discrepancy in the peak values between the positive and negative sets of hydrogels may be partially attributed to the experimental uncertainty in the actual balance point. Above 0.1 mM unbalanced polyampholytic hydrogels show an initial collapse followed by reswelling at 10 mM. The collapse transition between 0.1 and 10 mM represents the screening of the polyelectrolyte contribution while subsequent swelling is due to screening of the polyampholyte effect.

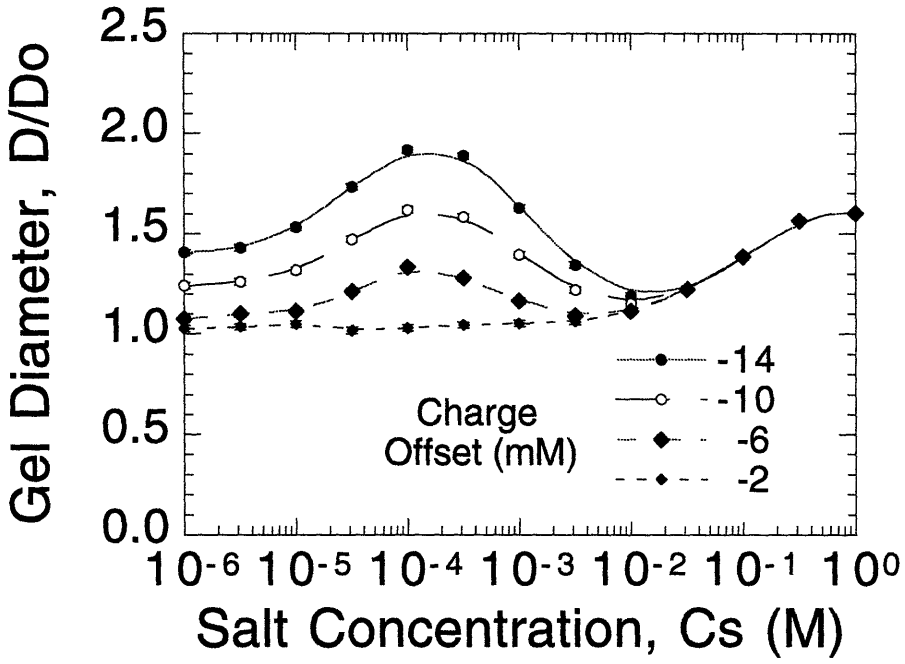

Figure 4-4: Negatively charged polyampholytic hydrogel swelling versus bath salt concentration. Hydrogels with increasing negative charge offsets of -2 (lower), -6, -10, and -14 mM (upper) show the development of three distinct diameter swelling regimes as a function of bath electrolyte concentration. At very low bath salt concentrations the hydrogels collapse. The smooth curves are drawn to guide the eye.

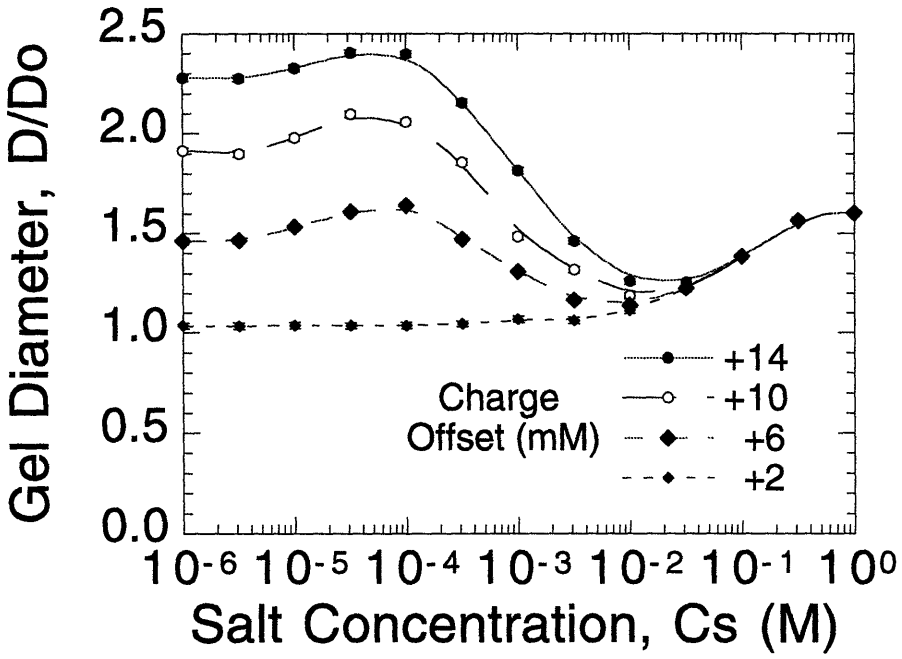

Figure 4-5: Positively charged polyampholytic hydrogel swelling versus bath salt concentration. Hydrogels with positive charge offsets of +2 (lower), +6, +10, and +14 mM (upper) show similar swelling patterns as the negatively charged hydrogels with the exception of the low salt concentration regime. At low salt concentrations some collapsing is observed but not to the same extent as those of the negatively charged hydrogels. The smooth curves are drawn to guide the eye.

During the salt wash experiments the equilibration time for salt concentration changes below 0.1 mM was several hours to days. Much faster equilibration times were observed for changes in bath salt concentrations above 0.1 mM. The slow kinetics at low sodium chloride concentrations may simply be an experimental artifact resulting from diffusion boundary effects at the hydrogel surface or the low sodium chloride availability in the wash. Diffusion reaction kinetics or other forms of slow ion transport that are dominant at low ionic strengths may be involved. Although some caution should be used when extrapolating free monomer pK values to those following gelation, a diffusion reaction mechanism based on the free monomer pK values does not predict the very long observed equilibration times. In addition, one cannot completely rule out the possibility of critical kinetics.

A theoretical interpretation of our experimental results requires parameter estimates for $\phi_o, N_x, \chi, \overline{v}_{site}$ and A. Although these parameters are not known precisely, the range of realistic values is well defined for all of them. These parameters can therefore be estimated from the hydrogel preparation conditions, the observed swelling ratios under limiting conditions and from published values. The swelling ratio is then calculated as a function of bath electrolyte concentration.

Based on the pregel monomer concentrations, $C_{Ao} + C_{Bo} = 700$ mM, and the estimated monomer molar volume, 0.2 M^{-1}, the reference state polymer volume fraction is approximately $\phi_o = 0.7\ M \times 0.2\ M^{-1} = 0.14$. If all of the cross-linker molecules were incorporated into the hydrogel the number of monomers between cross-links, N_x, would be $N_x > 700\ mM/(2 \times 8.6\ mM) \approx 40$. Not all the cross-linker molecules, however, lead to effective cross-links and some are not incorporated into the polymer network. As a result, a much higher value of N_x can be anticipated.

In this experiment, the copolymer charged monomers have a high affinity for the solvent water molecules.[Bak95] The hydrophilic properties of fixed charge groups in ion-exchange materials are well documented.[Hel62,Sim91] Since the Flory interaction parameter,χ, is less than 0.5 for good solvents[Hil60] our value of χ should fall in this range.

The molar value of the lattice sites in the Flory-Huggins theory can be considered an effective value ranging between that of the solvent molecules, $\overline{v}_w \approx 0.018\ M^{-1}$, and that of the monomers, $\overline{v}_m \approx 0.2\ M^{-1}$. In addition, the Coulombic free energy constant, A, should be of the order of unity. In the case of perfectly ordered ionic crystals,[Kit86] this constant has a value close to 1.5. Since the charge distribution in polyampholytes is much more disordered, a smaller value of A should be expected.

The actual values used in the calculations presented below are: $\phi_o = 0.14, N_x = 300, \chi = 0.3, \overline{v}_{site} = 0.2\ M^{-1}$, and $A = 0.4$. Figure 4-6 shows the swelling behavior predicted by our theory for a balanced polyampholyte (lower curve) and an unbalanced polyampholyte with a charge offset of 14 mM (in the reference state) of

either AMPS-Na (lower curve) or MAPTA-Cl (upper curve). The pK values used in Fig. 4-6 are $pK_a = 1.5$ and $pK_b = 2.5$. The pK_a was estimated from direct measurements of free monomer solutions of AMPS-H while the pK_b was chosen to account for the observed swelling behavior.

As we proceed from concentrated to dilute electrolyte concentrations, the different contributions to the hydrogel osmotic pressure vary. For $C_s \approx 1$ M, the Coulombic interactions between fixed ions are effectively screened and the ideal contribution to the hydrogel osmotic pressure balances the bath osmotic pressure. As a result, the equilibrium swelling is determined only by the hydrogel elastic and solvent properties and hence values of ϕ_o, N_x, and χ.

Decreasing C_s from 1 M to 10 mM results in the collapse of the hydrogel due to increasing fixed charge Coulombic interactions. When C_s reaches 10 mM the mobile ions within the hydrogel can no longer screen the fixed charges. Balanced polyampholytes, therefore, remain collapsed when the bath salt concentration is further reduced below 10 mM. Unbalanced polyampholytes, however, begin to swell due to the increasing counter ion ideal gas pressure. In unbalanced polyampholytes the combination of these two effects produces a clear minimum at $C_s \approx 20$ mM.

As C_s is reduced from 10 mM unbalanced polyampholytes continue to swell until C_s reaches ≈ 0.1 mM. Figure 4-6 shows that different swelling patterns are observed between unbalanced polyampholytes with excess acidic and excess basic groups when C_s is reduced below 0.1 mM. For polyampholytes with excess sulfonic acid groups the internal concentrations of the mobile positive ions, sodium and hydrogen, are higher than that of the bath. As a result, the internal pH is smaller than the bath pH ≈ 5.8.

At $C_s \approx 0.1$ mM, the actual fixed charge concentration can be estimated as 14 mM/$2.1^3 \approx 1.5$ mM. Based on Donnan equilibrium, the internal and external pH differ by log(1.5 mM/0.1 mM) ≈ 1.2 pH units. Although this internal pH is not low enough to affect the sulfonic acid dissociation equilibrium, the situation changes for

lower electrolyte concentrations. When $C_s \approx 0.01$ mM, for example, the internal pH is 5.8 - log (1.5 mM/0.01 mM) ≈ 3.6. The sulfonic acid ionization degree in this case is $\alpha_a = 1/(1+C_{H^+}/K_a) \approx 0.9925$. As a result, 0.75% of the 357 mM of sulfonic groups, or 3 mM, are not dissociated. The net charge concentration decreases from 14 mM to 11 mM and the hydrogel collapses. These concentrations are given as their equivalent in the reference state for the sake of clarity.

The swelling ratio, D/D_o, continues decreasing from 10 μM to 1 μM and reaches a constant value of approximately 1.2 at 1μM. When $C_s \rightarrow 0$ local electroneutrality yields $C_{A^-} = C_{H^+} + C_{B^+}$ and the fixed charge concentration is compensated by hydrogen ions. Assuming the base groups are completely dissociated and the acid dissociation is described by Eq. 4.16, or the appropriate limit of Eq. 4.20, the minimum internal pH is 2.96. This corresponds to an actual fixed charge concentration of only 1.11 mM and an acid group ionization degree of $\alpha_a \approx 0.966$. Hence, when C_s decreases below the bath hydrogen ion concentration, 1.6 μM, all the contributions to the hydrogel osmotic pressure reach a constant value and are dominated by the mixing and Coulombic terms.

The upper curve of Fig. 4-6 shows that the polyampholyte swelling with excess base groups is essentially the same as the acidic polyampholyte except at low bath ionic strengths. As $C_s \rightarrow 0$ the basic polyampholyte fixed charges are now compensated with bicarbonate ions. In this case, local electroneutrality, $C_{A^-} + C_{HCO_3^-} = C_{B^+}$, leads to a limiting internal pH value of 8.72, a fixed charge concentration of 1.26 mM and a basic group ionization degree of $\alpha_b \approx 0.988$. The higher ionization degree and fixed charge concentration explains why this hydrogel is more swollen than that with excess acidic groups.

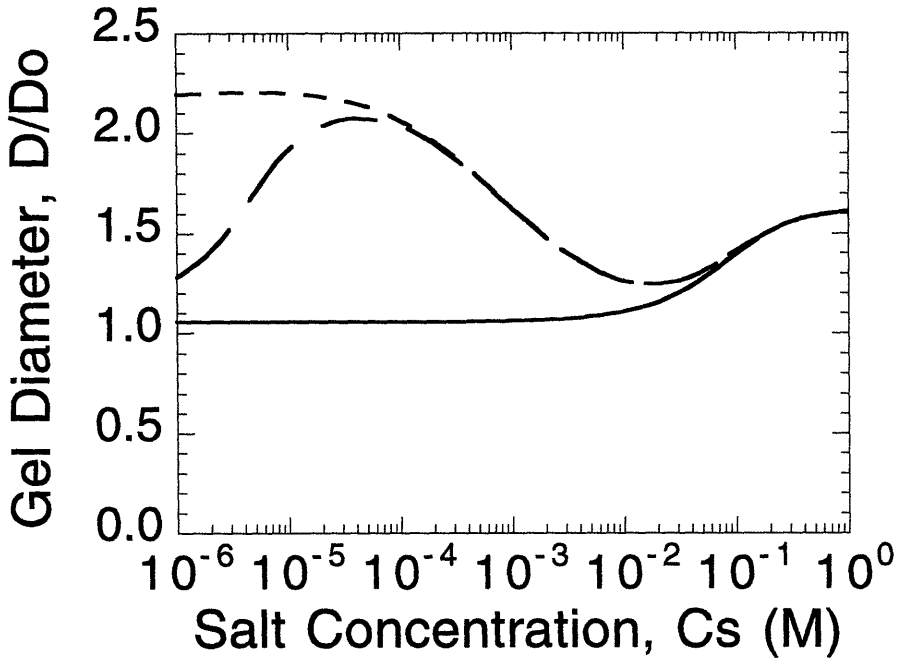

Figure 4-6: Theoretical predictions for polyampholytic hydrogel swelling versus bath salt concentration. Theoretical predictions for charge offsets of 0 (lower solid), -14 (middle dashed), and +14 mM (upper dashed), have the same qualitative shape as those shown in Figs. 4-4 and 4-5.

The lower skewed curve in Fig. 4-7 shows the predicted swelling ratio as a function of net fixed charge concentration when the polyampholyte hydrogel is immersed in distilled water. If complete ionization is assumed, theory predicts the upper symmetrical distribution shown in Fig. 4-7. Asymmetry results when acid and base dissociation equilibria are included. The observed asymmetry can be attributed to the differences in monomer pK values with respect to the slightly acidic external pH. Since (5.8 - 1.5) < (11.5 - 5.8) the acid group ion association is greater despite the very low pK_a.

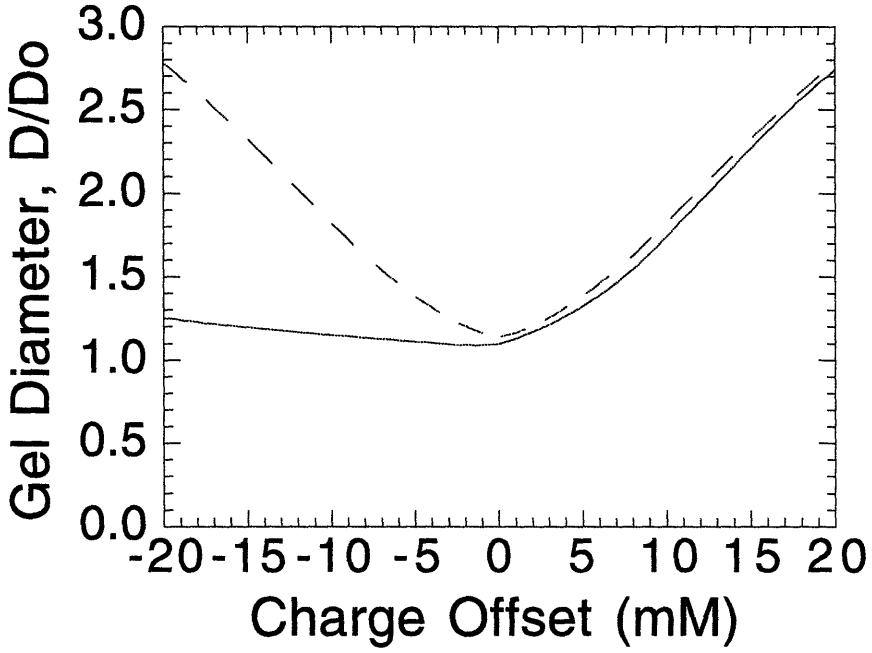

Figure 4-7: Theoretical predictions of asymmetric swelling dependence. Theoretical predictions show the development of asymmetric swelling when dissociation equilibria are included in agreement with the data shown in Figs. 4-2 and 4-3.

Figure 4-8 shows the theoretical predictions for the swelling ratio when complete ionization of both acid and base groups is assumed over the whole electrolyte concentration range. The hydrogel parameters used are the same as those for Fig. 4-6, with net fixed charge concentrations of $\mid C_{Bo} - C_{Ao} \mid = 0$, 10, 20, 30, and 40 mM. Experimentally, the assumption of complete ionization may correspond to measurements carried out at relatively short times, exceeding the poroelastic response time, when electrochemical equilibrium of hydrogen and hydroxide ions between the bath and the free and bound states within the hydrogel have not been attained.

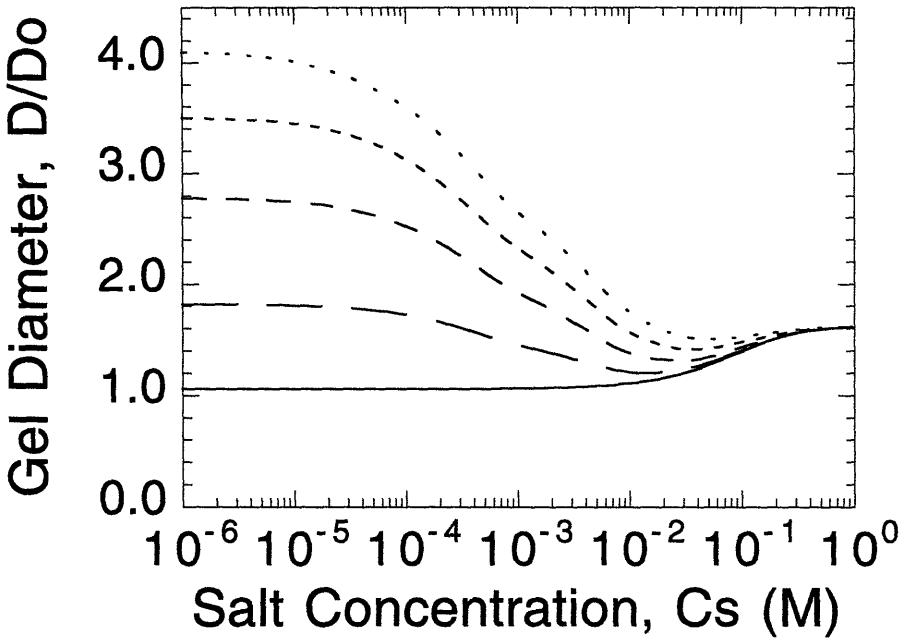

Figure 4-8: Theoretical prediction of acid and base dissociation effects on polyampholyte swelling equilibrium at low ionic strengths. If the acid and base dissociation equilibria are ignored then theory predicts no collapse transition will occur at low ionic strengths. The curves correspond to charge offsets of 0 (lower curve), 10, 20, 30, and 40 mM (upper curve).

Despite the qualitative agreement with experiment, this model has a number of limitations. Experimental studies,[Cor93,Liu95] for example, have shown that hydrogel swelling is influenced by the nature of the counter ion species and may be related to a specific counter ion condensation phenomenon. The only counter ion characteristic allowed in this model is the counter ion charge number which enters the ideal and Coulombic terms. Contrary to experiment, the model in its present form, cannot differentiate between lithium and sodium ions.

Recent experimental results[Bak95] have also shown that specific interactions between the mobile ions and the neutral polymer network lead to an increase in the swelling ratio with increasing C_s. The model assumes, however, that this increase is due exclusively to the screening of the attractive interactions between fixed charges. Furthermore, it is well known that the screened Coulomb potential, and the ideal

contribution to the hydrogel free energy are not valid at high concentrations. This implies that a significant range of our experimental concentrations may be well beyond the limit of our theory.[Hil60,McQ76]

The use of a thermally smeared out quasilattice model for the Coulombic interactions between fixed charges in the random copolymer, instead of the Debye-Hückel theory, may be justified for the case of collapsed balanced polyampholytes. For highly swollen slightly unbalanced hydrogels, where the model can be questioned, the Coulombic term becomes less important. Since the quasilattice model temperature dependence is different from the Debye-Hückel theory an experimental study of balanced polyampholyte swelling at different temperatures could be useful to establish the conditions for the validity of each model.

4.5 Conclusions

The combination of equilibrium and kinetic measurements in this study underscore the importance of counter ions in establishing equilibrium in polyampholyte hydrogels. Despite the very low pK_a of AMPS-H, the flattening of the swelling distribution shown in Fig. 4-3 appears to be the result of hydrogen ion association to AMPS. Without added base the concentration of free bicarbonate ions is approximately 250 times the hydroxide ion concentration. As a result, most MAPTA monomers remain in their ionized state and hydrogels containing excess MAPTA are more swollen at low ionic strengths. This suggests that in practice, dissociation equilibria dominate polyampholytic equilibrium swelling at low ionic strengths.

This study has shown that an extension of the Flory-Huggins theory incorporating a quasi-lattice screened Coulombic term for the hydrogel fixed charge groups can explain the observed trends for balanced and slightly unbalanced polyampholytic hydrogels. Although a high degree of parameter uncertainty exists in this simplified model, satisfactory agreement between theory and experiment has been obtained.

In particular, the polyampholyte effect is predicted to be effective within a certain range of concentrations and negligible when $C_s \geq \mid C_{B+} - C_{A-} \mid$, in qualitative agreement with Higgs and Joanny's scaling theory. In our model the Debye screening length $1/\kappa$ decreases with increasing C_s until it eventually reaches values smaller than the average distance r between fixed charges. As a result, the screening factor suppresses attractive electrostatic interactions between unlike fixed charges and the hydrogel swells.

4.6 Appendix A: Combined Acid and Base Dissociation Equilibrium

Since polyampholytes contain both positive and negative polyions, it is necessary to consider the role of both acid and base dissociation on the equilibrium swelling of these materials. The purpose of this appendix is, therefore, to derive a polynomial expression (Eq.4.20) in terms of the unknown internal hydrogen ion concentration and the known monovalent bath ion concentrations. This polynomial can be coupled with osmotic terms to evaluate equilibrium swelling ratios.

4.6.1 Dissociation Equilibria

The balance of chemical potentials for internal hydrogen and hydroxide ions in the free and bound states is equivalent to the chemical equilibria for the acidic and basic monomeric species,

$$K_a = \frac{C_{A-}\, C_{H+}}{C_{AH}} \tag{4.22}$$

and

$$K_b = \frac{C_{BOH}\, C_{H+}}{C_{B+}} \,. \tag{4.23}$$

The internal parameters K_a and K_b represent the acid and base dissociation constants, C_{A^-} and C_{B^+} the concentration of ionized acid and base groups, C_{AH} and C_{BOH} the concentration of unionized acid and base groups, and C_{H^+} and C_{OH^+} the concentration of hydrogen and hydroxide ions.

Rearranging Eqs. 4.22 and 4.23 gives

$$C_{A^-} = \frac{C_A K_a}{K_a + C_{H^+}}. \tag{4.24}$$

and

$$C_{B^+} = \frac{C_B C_{H^+}}{K_b + C_{H^+}}. \tag{4.25}$$

4.6.2 Local Charge Electroneutrality

Local charge electroneutrality for monovalent ions gives us

$$C_{A^-} + C_- = C_{B^+} + C_+, \tag{4.26}$$

where C_- and C_+ are the total concentration of mobile positive and negative ions respectively. Using Eqs. 4.24 and 4.25 in Eq. 4.26 yields

$$\frac{AK_a}{(K_a + C_{H^+})} + C_- = \frac{C_B C_{H^+}}{K_b + C_{H^+}} + C_+. \tag{4.27}$$

4.6.3 Donnan Equilibrium

From Donnan equilibrium

$$C_+ C_- = C_o^2, \tag{4.28}$$

$$\tag{4.29}$$

where C_o is the sum of all bath ions of one sign regardless of pH. If C_s represents the concentration of added salt then $C_o = C_s + C_{H^+Bath}$.

Substituting Eq. 4.29 into Eq. 4.26 gives us

$$\begin{aligned}
\frac{C_A K_a}{(K_a + C_{H^+})} + \frac{C_o^2}{C_+} &= \frac{C_B C_{H^+}}{(K_b + C_{H^+})} + C_+ \\
\Rightarrow \frac{C_A K_a}{(K_a + C_{H^+})} + \frac{C_o C_{H^+Bath}}{C_{H^+}} &= \frac{C_B C_{H^+}}{(K_b + C_{H^+})} + \frac{C_o C_{H^+}}{C_{H^+Bath}} \\
\Rightarrow C_A K_a C_{H^+}(K_b + C_{H^+}) C_{H^+Bath} &+ C_o C_{H^+Bath}^2 (K_a + C_{H^+})(K_b + C_{H^+}) \\
= C_B C_{H^+}^2 (K_a + C_{H^+}) C_{H^+Bath} &+ C_o C_{H^+}^2 (K_a + C_{H^+})(K_b + C_{H^+}) \\
\Rightarrow C_A K_a K_b C_{H^+} C_{H^+Bath} + C_A K_a C_{H^+Bath} C_{H^+} &+ (C_o C_{H^+Bath} K_a + C_o C_{H^+Bath}^2 C_{H^+})(K_b + C_{H^+}) \\
= C_B K_a C_{H^+Bath} C_{H^+}^2 + C_B C_{H^+Bath} C_{H^+}^3 &+ (C_o K_a C_{H^+} + C_o C_{H^+}^3)(K_b + C_{H^+}) \\
\Rightarrow C_A K_a K_b C_{H^+Bath} C_{H^+} + C_A K_a C_{H^+Bath} C_{H^+} &+ C_o C_{H^+Bath} K_a K_b + C_o K_b C_{H^+Bath}^2 C_{H^+} \\
+ C_o K_a C_{H^+Bath}^2 C_{H^+} + C_o C_{H^+Bath}^2 C_{H^+}^2 &= C_B K_a C_{H^+Bath} C_{H^+}^2 + C_B C_{H^+Bath} C_{H^+}^3 \\
+ C_o K_a K_b C_{H^+}^2 + C_o K_b C_{H^+}^3 &+ C_o K_a C_{H^+}^3 + C_o C_{H^+}^4 \\
\Rightarrow C_o C_{H^+}^4 + (C_o K_a + C_o K_b + C_B C_{H^+Bath}) C_{H^+}^3 &+ (C_o K_a K_b + C_B K_a C_{H^+Bath} - C_o C_{H^+}^2 \\
- C_A K_a C_{H^+Bath}) C_{H^+}^2 - (C_o K_a C_{H^+Bath}^2 &+ C_o K_b C_{H^+Bath}^2 + C_A K_a K_b C_{H^+Bath}) C_{H^+} \\
- C_o C_{H^+Bath}^2 K_a K_b = 0.
\end{aligned}$$

This gives us

$$\begin{aligned}
&C_{H^+}^4 + \left(K_a + K_b + \frac{C_B C_{H^+Bath}}{C_o}\right) C_{H^+}^3 \\
&+ \left(K_a K_b - C_{H^+bath}^2 + \frac{K_a (C_B - C_A) C_{H^+Bath}}{C_o}\right) C_{H^+}^2 \\
&- \left((K_a + K_b) C_{H^+bath}^2 + \frac{K_a K_b C_A C_{H^+Bath}}{C_o}\right) C_{H^+} - K_a K_b C_{H^+bath}^2 = 0. \quad (4.30)
\end{aligned}$$

Since $C_o = C_s + C_{H^+bath}$ this becomes the fourth order algebraic equation

$$C_{H^+}^4 + \left(K_a + K_b + \frac{C_B}{1 + C_s/C_{H^+bath}}\right) C_{H^+}^3 + \left(K_a K_b - C_{H^+bath}^2 + \frac{K_a (C_B - C_A)}{1 + C_s/C_{H^+bath}}\right) C_{H^+}^2$$

$$-\left((K_a+K_b)C_{H^+bath}^2+\frac{K_aK_bC_A}{1+C_s/C_{H^+bath}}\right)C_{H^+} \quad - \quad K_aK_bC_{H^+bath}^2=0\ , \tag{4.31}$$

where $C_A = C_{AH} + C_{A^-}$ and $C_B = C_{BOH} + C_{B^+}$ represent the total concentration of acidic and basic groups respectively.

4.7 Appendix B: Lattice Osmotic Pressure

The lattice free energy is

$$\Delta F_{lattice} = -\frac{A}{2}N_{fe}\frac{e^2}{4\pi\epsilon}\frac{\exp(-\kappa r)}{r}, \tag{4.32}$$

where

$$r = 2\left(\frac{3V}{4\pi(N_{f^+}+N_{f^-})}\right)^{\frac{1}{3}} = aV^{\frac{1}{3}}, \tag{4.33}$$

$$\kappa = \sqrt{\frac{e^2N_AC_{mobile}}{\epsilon k_BT}} = bC_{mobile}^{\frac{1}{2}} \tag{4.34}$$

and

$$C_{mobile} = 2\sqrt{\left(\frac{N_{f^+}-N_{f^-}}{2N_AV}\right)^2+C_o^2}\ , \tag{4.35}$$

By definition

$$\Pi_{lattice} \quad = \quad -\frac{1}{N_Ak_BT}\frac{\partial F_{lattice}}{\partial V}. \tag{4.36}$$

Therefore

$$\Pi_{lattice} \quad = \quad \frac{A}{2}\frac{N_{fe}}{N_A}\frac{e^2}{4\pi\epsilon k_BT}\frac{\partial}{\partial V}\left(\frac{\exp(-\kappa r)}{r}\right)$$

$$
\begin{aligned}
&= \frac{A}{2}\frac{N_{fe}}{N_A}\frac{e^2}{4\pi\epsilon k_B T}\left\{\frac{-1}{3aV^{\frac{4}{3}}}\exp(-\kappa r)+\frac{\exp(-\kappa r)}{r}\left(-r\frac{\partial\kappa}{\partial V}-\kappa\frac{\partial r}{\partial V}\right)\right\}\\
&= -\frac{A}{2}\frac{N_{fe}}{N_A}\frac{e^2}{4\pi\epsilon k_B T}\frac{\exp(-\kappa r)}{r}\left\{\frac{1}{3V}+\frac{\kappa r}{3V}+r\frac{\partial\kappa}{\partial V}\right\}\\
&= -\frac{A}{2}\frac{N_{fe}}{N_A 3V}\frac{e^2}{4\pi\epsilon k_B T}\frac{\exp(-\kappa r)}{r}\left\{1+\kappa r+3Vr\frac{\partial\kappa}{\partial V}\right\} \qquad (4.37)
\end{aligned}
$$

but

$$
\frac{\partial\kappa}{\partial V} = b\frac{\partial C_{mobile}^{\frac{1}{2}}}{\partial V} = b\frac{1}{2}C_{mobile}^{-\frac{1}{2}}\frac{\partial C_{mobile}}{\partial V} \qquad (4.38)
$$

and

$$
\begin{aligned}
\frac{\partial C_{mobile}}{\partial V} &= \left(\left\{\frac{N_{f+}-N_{f-}}{2N_A V}\right\}^2+C_o\right)^{-\frac{1}{2}}2\left(\frac{N_{f+}-N_{f-}}{2N_A V}\right)(-1)\left(\frac{N_{f+}-N_{f-}}{2N_A}\right)\frac{1}{V^2}\\
&= -\frac{4}{C_{mobile}}\frac{1}{V}\left(\frac{N_{f+}-N_-}{2N_A V}\right)^2. \qquad (4.39)
\end{aligned}
$$

Therefore

$$
\begin{aligned}
3Vr\frac{\partial\kappa}{\partial V} &= 3Vrb\frac{1}{2}C_{mobile}^{-\frac{1}{2}}(-4)C_{mobile}^{-1}\frac{1}{V}\left(\frac{N_{f+}-N_{f-}}{2N_A V}\right)^2\\
&= \frac{3}{2}r(-4)\kappa C_{mobile}^{-2}\left(\frac{N_{f+}-N_{f-}}{2N_A V}\right)^2\\
&= -\frac{3}{2}\kappa r\left\{\left(\frac{N_{f+}-N_{f-}}{2N_A V}+C_o^2\right)^2\right\}^{-1}\left(\frac{N_{f+}-N_{f-}}{2N_A V}\right)^2\\
&= -\frac{3}{2}\kappa r\left\{1+\left(\frac{2N_A VC_o}{N_{f+}-N_{f-}}\right)\right\}^{-1}. \qquad (4.40)
\end{aligned}
$$

Hence

$$
\Pi_{lattice} = -\frac{A}{2}\frac{N_{fe}}{N_A V}\frac{e^2}{12\pi\epsilon k_B T}\frac{\exp(-\kappa r)}{r}\left\{1+\kappa r-\frac{3}{2}\kappa r\left(1+\left\{\frac{2N_A VC_o}{N_{f+}-N_{f-}}\right\}^2\right)^{-1}\right\}. \qquad (4.41)
$$

Chapter 5

Charge Dilution in Polyampholytic Hydrogel Phase Transitions

Abstract

This study investigates the effects of charge dilution on balanced and unbalanced polyampholytic hydrogel swelling transitions as a function of bath electrolyte concentration. Using varying concentrations of neutral monomers in acrylamide based polyampholytic hydrogels, the results of this work illustrate the competing effects of ion dissociation, polyelectrolyte repulsion, polyampholyte attraction and solvent interactions. Extremely long transient swelling responses have been observed at low ionic strengths and have been considered in obtaining accurate equilibrium measurements. The equilibrium swelling is modeled using a modified Flory-Huggins lattice model. The validity of Flory-Huggins and Debye-Hückel based models for this type of polymeric system is critically examined.

5.1 Introduction

Polyampholytic hydrogels consist of positive, negative and even neutral monomeric species which are polymerized and cross-linked into a three dimensional network. Due to their many potential applications in the field of biotechnology and medicine,

polyampholytes have received increasing interest from experimentalists. [Yu93,Cor93,Sko94,Bak95] Polyampholytes have also been the subject of many theoretical studies since they provide a model for studying the long range interactions found in proteins and other forms of soft condensed matter. [Hig91,Whi93,Kan95b,Gut95] Despite their enormous technological and scientific importance, polyampholytes remain a challenge to both the experimentalist and theorist.

Most physico-chemical applications of polyampholytes concern their swelling behavior when immersed in an electrolyte bath. The electrostatic interactions between polymeric and mobile charges which determine the hydrogel swelling equilibrium are still not very well understood. Recent experimental studies[Yu93,Eng95,Eng96] have shown that, depending on the magnitude of the net polymer charge and bath ionic strength, the swelling properties can be dominated by acid and base dissociation, electrostatic repulsion and electrostatic attraction.

Alterations in the fixed polymeric charge density can be brought about by adding neutral monomers to the network, changing the solvent quality, elasticicity, bath salt concentration and pH, and even through the application of electric fields and external pressures. The internal forces which determine swelling equilibrium, however, do not normally act independently of each other. By adding neutral monomers to a hydrogel network, for example, the elasticity, solvent interactions and local ion concentrations are altered. This in turn can have important effects on the degree of dissociation in hydrogels containing dissociable monomeric groups. In polyampholytes charge dilution brought about by the addition of neutral monomers will have additional effects on the attractive interactions between positive and negative charges.

The objective of this study is to present experimental results and analytical arguments that describe the concentration dependence of competing ionic, solvent and elastic effects. The equilibrium swelling is modeled using a Flory-Huggins

lattice model modified to include multiple solvent and ionic effects. By careful consideration of the experimental constraints, the application of Flory-Huggins and Debye-Hückel based models to this type of polymeric system is critically examined.

5.2 Theoretical Model

In this section we extent the theoretical model of a previous study[Eng96] to include the addition of neutral monomeric species with different solvent interaction properties. Let f_A, f_B and f_N denote the fraction of acidic, basic and neutral monomers. Note that f_A and f_B represent the total concentration of acidic and basic monomers in their ionized and unionized form such that $f_A + f_B + f_N = 1$. If C_M is the total monomer concentration and both acidic and basic monomers are completely ionized, then $(f_A + f_B) \times C_M$ would represent the total charge concentration and $(f_B - f_A)/(f_A + f_B) \times C_M$ the net charge offset. Similarly, the percent charge offset of the charged component would be $|(f_B - f_A)|/(f_A + f_B) \times 100\%$.

The effective Flory-Huggins solvent interaction parameter, χ_t, and the reference state volume fraction, ϕ_{ot}, will also be functions of composition. In practice, the effective Flory-Huggins interaction parameter can be estimated from experimental results. Based on the molecular weights of the monomers used in this study, we would expect that $\phi_{oA} \approx \phi_{oB} \neq \phi_{oN}$, where ϕ_{oi} represents the reference state volume fraction of the pure ith monomeric component.

5.2.1 Swelling Equilibrium

Recall that balance of solvent chemical potentials can be expressed as[Bak95,Eng96]

$$\Delta\Pi_{swelling} = \frac{\mu_w^{gel} - \mu_w^{bath}}{\overline{v}_w} = 0, \tag{5.1}$$

where $\overline{v}_w$ is the solvent molar volume. Equating hydrogel and bath solvent chemical potentials gives us the swelling equilibrium condition

$$-\frac{1}{\overline{v}_{site}}\left[\ln(1-\phi_t)+\phi_t+\chi_t\phi_t^2\right]+\frac{\phi_{ot}}{N_x\overline{v}_{site}}\left[\frac{1}{2}\left(\frac{\phi_t}{\phi_{ot}}\right)-\left(\frac{\phi_t}{\phi_{ot}}\right)^{\frac{1}{3}}\right]+C_{mobile}-2C_o$$
$$-\frac{A}{2}\frac{N_{fe}}{N_AV}\frac{e^2}{12\pi\epsilon k_BT}\frac{\exp(-\kappa r)}{r}\left\{1+\kappa r-\frac{3\kappa r}{2}\left[1+\left(\frac{2N_AVC_o}{N_{f+}-N_{f-}}\right)^2\right]^{-1}\right\}=0. \quad (5.2)$$

The first two terms represent solvent and elastic effects where $\overline{v}_{site} \equiv N_A v_{site}$ is the molar volume of the lattice sites, N_x the number of monomers between cross-links and N_A is Avogadro's number. The terms C_{mobile} and C_o are the internal mobile ion and bath ion concentrations respectively. The last term on the left hand side represents the shielded Coulombic effects due to the fixed polymeric charges. The hydrogel volume is V, A is the Madelung constant, e the electron charge, ϵ the dielectric permittivity, k_B Boltzmann's constant, and T the absolute temperature. The term r represents the interion separation, κ the reciprocal Debye length, N_{fe} is the effective number of fixed charges giving rise to attraction, N_{f+} the number of positive polyions, and N_{f-} the number of negative polyions.

5.2.2 Dissociation Equilibria

Recall that the acid and base dissociation constants, K_a and K_b respectively, are given by the chemical equilibrium formulae

$$K_a = \frac{C_{A^-}\, C_{H^+}}{C_{AH}} \quad (5.3)$$

and

$$K_b = \frac{C_{BOH}\, C_{H^+}}{C_{B^+}}\,. \quad (5.4)$$

The terms C_{A^-} and C_{B^+} represent the concentration of ionized acid and base groups, C_{AH} and C_{BOH} the concentration of unionized acid and base groups, and C_{H^+} and C_{OH^+} the concentration of hydrogen and hydroxide ions. Localized hydrogen or hydroxide ion binding is an important consideration since it leads to a reduction in local charge repulsion and osmotic pressure in unbalanced polyampholytes.

Solving for the molar hydrogen ion concentration, C_{H^+}, inside the hydrogel gives us the fourth order algebraic equation

$$\begin{aligned} C_{H^+}^4 + \left(K_a + K_b + \frac{C_B}{1 + C_s/C_{H^+bath}}\right) C_{H^+}^3 \quad + \quad \left(K_a K_b - C_{H^+bath}^2 + \frac{K_a(C_B - C_A)}{1 + C_s/C_{H^+bath}}\right) C_{H^+}^2 \\ - \left((K_a + K_b) C_{H^+bath}^2 + \frac{K_a K_b C_A}{1 + C_s/C_{H^+bath}}\right) C_{H^+} \quad - \quad K_a K_b C_{H^+bath}^2 = 0 \ , \end{aligned} \tag{5.5}$$

where $C_A = C_{AH} + C_{A^-} = f_A C_M$ and $C_B = C_{BOH} + C_{B^+} = f_B C_M$ represent the total concentration of acidic and basic groups respectively. Solutions to the internal hydrogen ion concentration are obtained by finding the positive root of Eq. 5.5 in the range of physically meaningful values.

5.2.3 Kinetic Response

Changing the relative concentrations of neutral monomers and the net hydrogel charge offset will have a number of complicated effects on the rate of ion transport. In charged hydrogels the ion fluxes of at least two different ionic species are coupled with one another. The coupled, or ambipolar, diffusion coefficient[Hel62] for ion transport through a charged hydrogel is

$$D_{ac} = \frac{D_a D_c (z_a^2 C_a + z_b^2 C_b)}{z^2 C_a D_a + z_c^2 C_c D_c}, \tag{5.6}$$

where D_a is the anion diffusion coefficient, D_c the cation diffusion coefficient, z_a the anion valency, z_c the cation valency, C_a the anion concentration, and C_c the cation concentration. The value of the coupled diffusion coefficient is dependent

on the relative concentrations of the two ions. This relationship leads to minority carrier dominance in highly charged hydrogels. Based on the concept of ambipolar diffusivity, the rate of ion transport will be dominated by the the anion diffusivity in highly negatively charged hydrogels and that of the cation in highly positively charged hydrogels. One would also expect that in polyampholytes both positive and negative charge fluctuations will have a complicated effect on the local ion diffusivity. Under normal experimental conditions, additional complications can arise due to the formation of stagnant or film layers.[Hel62]

The selective binding of ions to monomer sites, such as occurs with acidic or basic groups, can slow the transport process down by several orders of magnitude.[Nus81] In hydrogels with dissociable acid groups the effective diffusivity of hydrogen, for example, becomes

$$D_{i,eff} = \frac{D_{H+}}{1 + \frac{C_A K_a}{(K_a + C_{H+})^2}}, \tag{5.7}$$

where C_A is the total concentration of acid monomers. Other forms of selective ion trapping, such as hopping conduction, can significantly reduce ion transport times.

The mechanical, or poroelastic, response time[Bio41,Tan79] will also contribute to the kinetic response of hydrogel swelling transition. The elastic reconformation and simultaneous fluid flow through the hydrogel will be dependent on the degree of network swelling or porosity. The poroelastic response time is generally greater than that of ion diffusion when binding interactions do not take place.

5.3 Methods and Procedure

Copolymer hydrogels of varying proportions of acryl-amido methyl propyl sulfonic acid (AMPS-H), methacryl-amido propyl trimethyl ammonium chloride (MAPTA-Cl) and dimethyl acrylmide (DMAAm) were synthesized. To estimate the charged monomer balance point and remove impurities from the pregel solution a counter

ion precipitation using the silver salt of AMPS-H was used. Hydrogen AMPS is a strong acid and silver carbonate (Ag_2CO_3) a weak base with a very low solubility product constant, that is,

$$AMPS \cdot H + H_2O \rightleftharpoons AMPS^- + H_3O^+ \qquad (pK_a = 1.5)$$

and

$$Ag_2CO_3 \rightleftharpoons Ag^+ + AgCO_3^- \qquad (K_{sp} = 6.15 \times 10^{-12} \text{ at } 25^oC).$$

Hydrogen AMPS was converted to silver AMPS (AMPS-Ag) using the reaction

$$2AMPS \cdot H + Ag_2CO_3 \rightleftharpoons 2AMPS \cdot Ag + CO_{2(g)} \uparrow + H_2O.$$

By LeChatelier's principle, the conversion of AMPS-H to AMPS-Ag is driven to the right by the removal of CO_2 during the reaction. Since Ag_2CO_3 is a weak base, the pH of the resulting solution was still low (pH 2.1). The final pH of the pregel solution was adjusted to 5.5 by adding NaOH while making measurements with a pH meter. By adding MAPTA-Cl to AMPS-Ag a silver chloride (AgCl) precipitate was produced,

$$AMPS^- \cdot Ag^+ + MAPTA^+ \cdot Cl^- \rightleftharpoons AMPS^- \cdot MAPTA^+ + AgCl_{(s)},$$

where

$$AgCl_{(s)} \rightleftharpoons Ag^+ + Cl^- \qquad (K_{sp} = 1.56 \times 10^{10} \text{ at } 25^oC).$$

The very low K_{sp} of AgCl permits a large fraction of the counter ions to be filtered out and removed. By repeatedly testing the resulting solution with either hydrochloric acid or silver nitrate and adding AMPS-Ag or MAPTA-Cl as required

it is possible to balance the pregel solution. Although the polymerization process may change the relative ratios of positive and negative monomers, the balance point of the pregel solution is more accurately known.

5.3.1 Sample Preparation

The AMPS-MAPTA polyampholyte pregel solution was prepared by initially making a 1.0 molar aqueous solution of AMPS-H at approximately 4 ^oC. While stirring the AMPS-H solution Ag_2CO_3 was slowly added to produce an equivalent concentration of 1.0 AMPS-Ag. The solution was then centrifuged at 3000 rpm and filtered with a 0.2 μm filter. After adding MAPTA-Cl the resulting AgCl precipitate was filtered out using a 0.2 μm filter. Small aliquots of the AMPS-MAPTA solution were tested with MAPTA-Cl and AMPS-Ag in order to ensure the solution had an approximately equal concentration of AMPS and MAPTA monomers.

The hydrogels were cross-linked using 8.6 mM N,N′-methylene-bis-acrylamide (BIS). Polymerization was initiated using 1.76 mM ammonium persulfate (APS) and the gelation temperature was 60 ^{o}C. Hydrogel samples with a net charge offset were made by adding AMPS-Na or MAPTA-Cl while keeping the total monomer concentration at 1.4 M. The AMPS-Na solution used to offset the balanced pregel solution was produced by neutralized AMPS-H with an equal molar concentration of NaOH. The hydrogels were formed in 200 and 500 μm inner diameter micropipettes.

The polyampholyte concentration swelling dependence was examined by adding neutral dimethyl acylamide (DMAAm) monomers to pregel polyampholyte solutions with different net polyion concentrations. In all cases the total concentration of the pregel solution with neutral and charged monomers was 1.4M.

Large volumes of water were used to wash the hydrogels. After reaching equilibrium with a distilled water solvent the hydrogel diameters were measured under a microscope equipped with charge coupled device camera. Further measurements were then made at different salt concentrations. Error estimates were based on the

video camera image resolution.

5.3.2 Experimental Outline

In this study a series of three experiments were performed. In the first set of experiments the kinetic response of polyampholytic hydrogels with different charge offsets were examined. These hydrogels were all cast in 200 μm inner diameter micropipettes. The diameter of hydrogels with different charge offsets were recorded as a function of time upon initially washing. The purpose of this experiment was to determine the required time necessary to reach thermodynamic equilibrium.

In the second set of experiments the swelling dependence of polyampholytic hydrogels made with a total monomer concentration of 1.4 M and different net charge offsets was examined as a function of bath sodium chloride concentration. These hydrogels were cast in 200 μm inner diameter micropipettes. At each bath salt concentration the hydrogel diameters were monitored repeatedly to ensure equilibrium had been reached.

In the third series of experiments the swelling dependence of hydrogels with a total monomer concentration of 1.4 M was examined as function of neutral monomer concentration, charge offset and bath salt concentration. In one experiment, hydrogels with varying concentrations of neutral spacer and net charge offset were washed in a 0.1 mM sodium chloride bath to minimize the effects of acid and base dissociation on the equilibrium swelling. The bath salt concentration swelling dependence was examined using two sets of hydrogels. One was a set of balanced polyampholytes with varying neutral spacer concentrations and the other was a set of polyampholytes with a 1.4% charge offset and varying concentrations of neutral monomers.

5.4 Results and Discussion

Figure 5-1 shows the initial swelling response of negatively and positively charged hydrogels cast in 200 μm pipettes upon washing. Notice that polyampholytic hydrogels near the balance point do not show an initial swelling response and appear to equilibrate very quickly. Any excess mobile ions within the matrix of balanced polyampholytes do not contribute to the initial swelling transient. Osmotic pressure contributions due to the presence of mobile counter ions which balance the excess charge in unbalanced polyampholytes lead to the observed swelling transients. At low ionic strengths the equivalent concept of unshielded electrostatic interactions can also be considered in the explanation of this phenomenon. Hydrogels with increasing charge offset swell to a peak value within a few minutes of washing. From these measurements it is clear that the mechanical, or poroelastic, response time of unbalanced hydrogels is on the order of minutes.

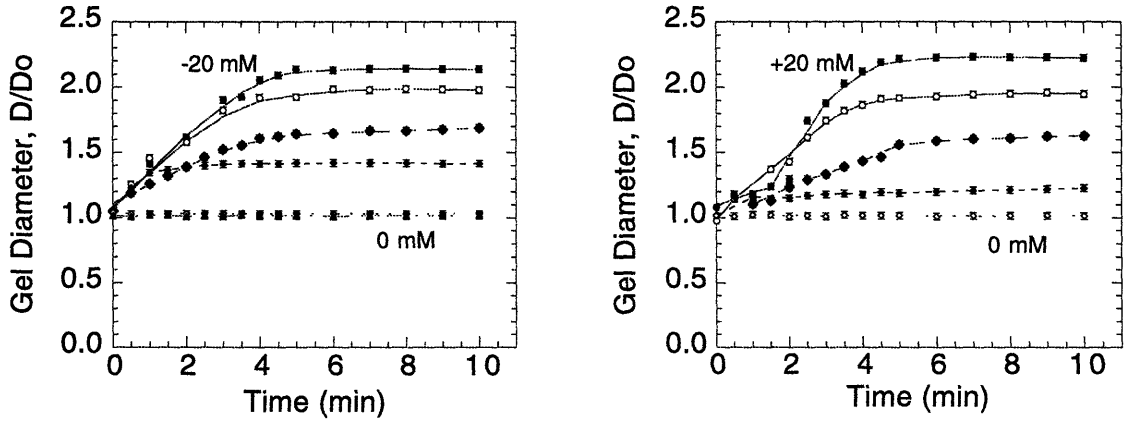

Figure 5-1: Initial poroelastic response of variably charged polyampholytes. Only polyampholytes with a charge offset show an initial swelling transient. This volume transition appears to equilibrate in minutes.

Figure 5-2 shows the initial swelling kinetics on the time span of hours. It is evident from the swelling kinetics of hydrogels with negative charge offsets that on

the time scale of hours equilibrium has not been reached. This slow recollapse is characteristic of ion exchange but may also involve a solvent sorption or desorption process. Over several hours hydrogels with positive charge offsets remain stable. Over a period of several days, however, positively charge hydrogels also collapse but not to the same extent as an equally charged negative hydrogel. In summary, three time scales are important in this study. The shortest time scale for all hydrogels is on the order of minutes and represents the hydrogel poroelastic response. Over a period of several hours, negatively charged hydrogels collapse. On the time scale of weeks positively charged hydrogels also collapse. The very slow collapse of positively charged hydrogels may be the result of competing bicarbonate ion effects.

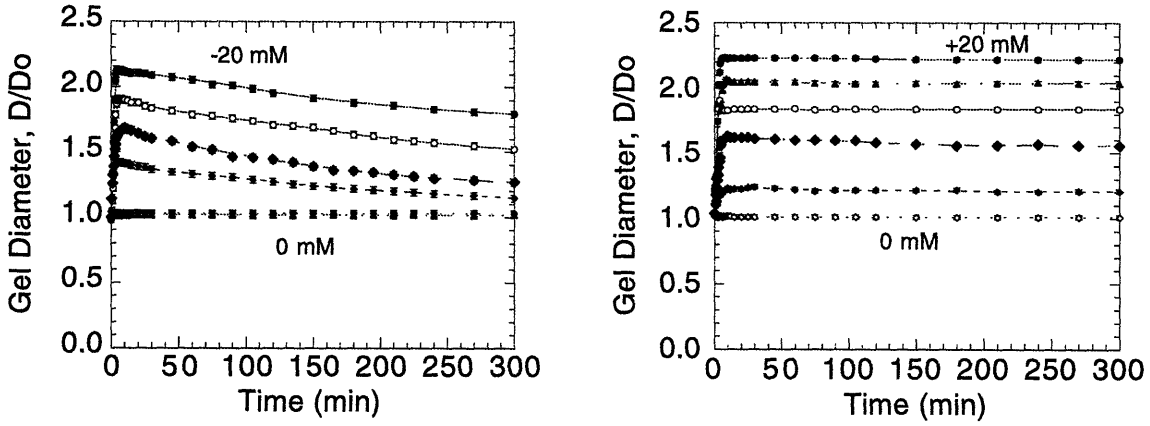

Figure 5-2: Kinetic response of variably charged polyampholytes over five hours. Following the rapid initial swelling transition a slow collapse of negatively charged hydrogels is observed over several hours. Positively charged hydrogels remain swollen over a period of several hours but eventually collapse after several days.

Figure 5-3 shows the equilibrium swelling diameters of polyampholytic hydrogels with total monomer concentrations of 1.4 M and varying negative charge offsets about neutrality. At low ionic strengths the effects of ion dissociation are evident. In fact, negatively charged hydrogels initially swollen with 0.0316 mM NaCl solutions can be forced to recollapse by washing with the same salt solution at pH 4.

This supports the hypothesis that hydrogen ion binding is involved in the collapse transition at low ionic strengths. This effect has been overlooked in previous studies due to the slow kinetics at low ionic strengths.

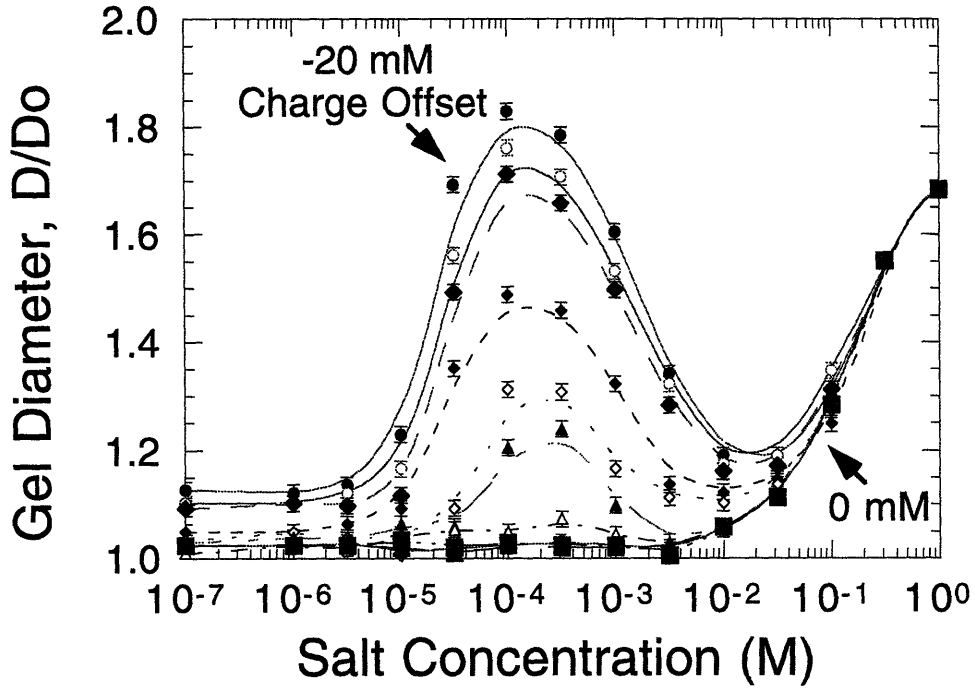

Figure 5-3: Equilibrium swelling of negatively charged polyampholytes versus bath salt concentration. Ion dissociation, polyelectrolyte repulsion and polyampholyte attraction influence the swelling equilibrium.

With increasing charge offset the hydrogel swelling between 0.01 mM and 0.0316 mM bath salt concentrations appears to progress from continuous second order phase behavior to discontinuous first order phase behavior. It is therefore possible that critical point phenomena is contributing to the slow kinetic response of these materials. It is important, however, to a make a very careful distinction between slow kinetics due to critical point behavior and that due to ion transport processes. The retarded kinetics associated with critical point phenomenon is due to the collective behavior of polymeric interactions. Ion transport processes, however, can

lead to retarded kinetics due to much different mechanisms. The swelling transitions observed at low ionic strengths necessary involve the exchange of hydrogen for sodium. Hydrogen ion transport can be retarded by diffusion reaction kinetics, hopping conduction between negative charged sites or for a number of other reasons. Although the very low free monomer pK values in this study are not consistent with long diffusion reactions times, we cannot rule this mechanism out. The fact that the hydrogels with charge offsets swell to metastable states on a much shorter time scale than that required for recollapsing argues against the possibility of critical point phenomenon and is more suggestive of an ion transport mechanism.

It is important to realize that two pK_a values for AMPS-H is necessary to consider in this study. In the pregel solution the pK_a is found using standard titration measurements. Following gelation, however, the pK_a of AMPS-H can be altered significantly due to steric interactions, cooperative behavior or from a number of other effects. In addition, condensation and charge density variations throughout the hydrogel can have an important effect on the binding of hydrogen ions to the $AMPS^-$ monomers. Furthermore, it is very important to realize that the internal hydrogel pH can be much lower than the surrounding bath pH due to Donnan partitioning. The very low pH that can exist within the hydrogel can greatly facilitate the binding of hydrogen ions to this acid even though it has a very low pK_a. The same argument applies to basic MAPTA-OH groups.

Figure 5-4 shows the swelling behavior of polyampholytes with different net charges as a function of neutral monomer concentration. Balanced polyampholytes show a monotonic decrease in swelling as the relative concentration of neutral monomers decreases. A balanced increase in positive and negative polymeric charges, therefore, results in a collapse transition as expected. Slightly unbalanced polyampholytes, however, show an initial decrease in swelling and then an increase as the relative concentration of neutral monomers decreases. This effect is the result of a very subtle competition between solvent, polyampholyte, polyelectrolyte and possi-

bly elastic effects. One may conclude from this data that with a large background of balanced positive and negative charges and a 1.4% charge offset polyampholyte effects are dominant at low relative total charge concentrations and polylectrolyte effects at high total charge concentrations. In drawing these conclusions, however, one must be very careful to consider the possibility that complicated changes in solvent and elasticity as a function of changing monomeric composition can also produce similar effects.

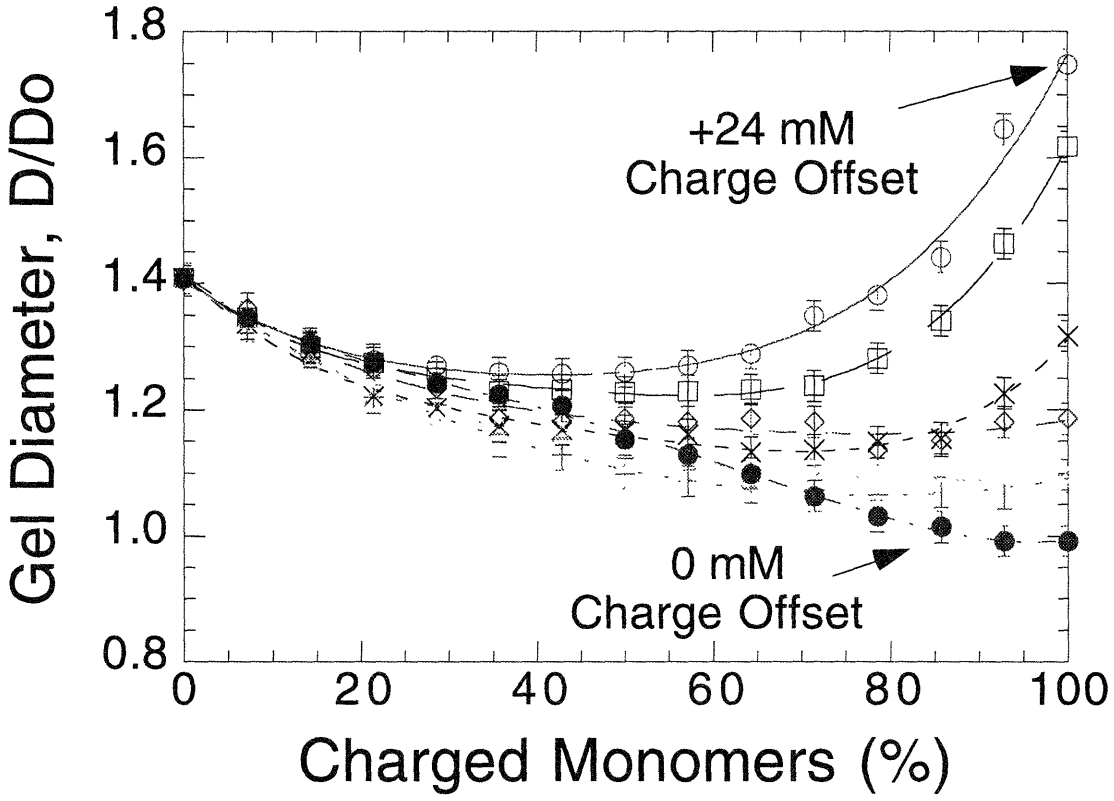

Figure 5-4: Charge dilution swelling equilibria of polyampholytic hydrogels at 0.1 mM NaCl. The swelling ratios of neutral DMAAm and AMPS-MAPTA copolymer hydrogels are plotted as a function of increasing proportions of the AMPS-MAPTA component. The different curves represent different net charge offsets of the AMPS-MAPTA component.

Figure 5-5 shows the effects of bath salt concentration on the swelling equilibrium of balanced polyampholytes with varying concentrations of neutral monomeric spac-

ers. The equilibrium swelling of pure DMAAm does not change over a wide range of bath salt concentrations. With increasing concentrations of balanced charged monomers polyampholyte effects lead to progressively smaller swollen diameters at low bath salt concentrations. At bath salt concentrations comparable to the local charge density the polyampholyte effects are screened and the hydrogels swell. When the polyampholyte effects are completely screened elastic and solvent effects dominate the equilibrium swelling forces. In this case we note that an aqueous solution is a much higher quality solvent for the charged $AMPS^-$ and $MAPTA^+$ monomers than the neutral DMAAm monomers.

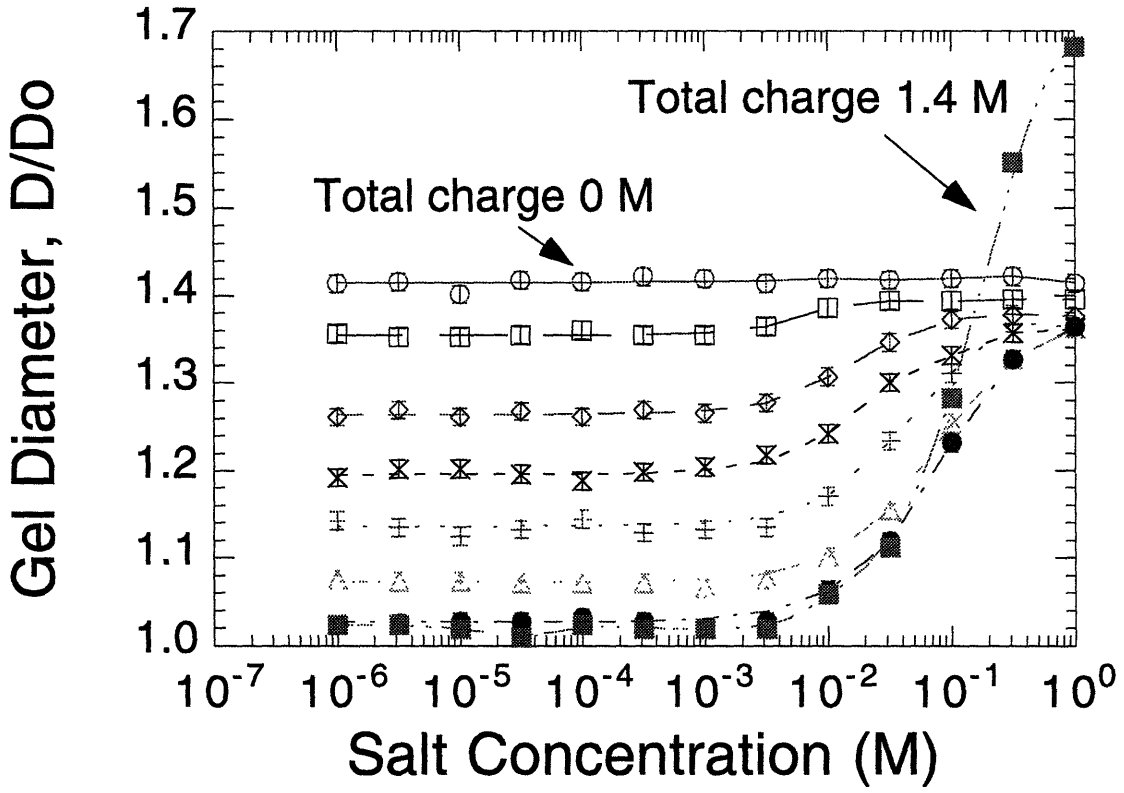

Figure 5-5: Charge dilution of balanced polyampholytes versus bath salt concentration. Balanced polyampholytes with varying concentrations of neutral spacers show a monotonically increasing swelling pattern as a function of bath salt concentration.

Figure 5-6 shows the equilibrium swelling response of polyampholytes with a 1.4% positive charge offset as a function of neutral monomeric spacer concentra-

tion. A 1.4% positive charge offset corresponds to a +20 mM charge offset when the total concentration of charged monomers is 1.4 M. This data illustrates the the very subtle effects of ion dissociation equilibrium that manifest themselves in unbalanced hydrogels at very low ionic strengths. Despite the fact the MAPTA-OH is undissociated up to extremely high pH values, one clearly sees the effects of ion dissociation equilibrium at low bath ionic strengths. The total time required to obtain this data was several weeks. Although other physical mechanisms such as solvent sorption must be considered, these results are more consistent with ion dissociation effects.

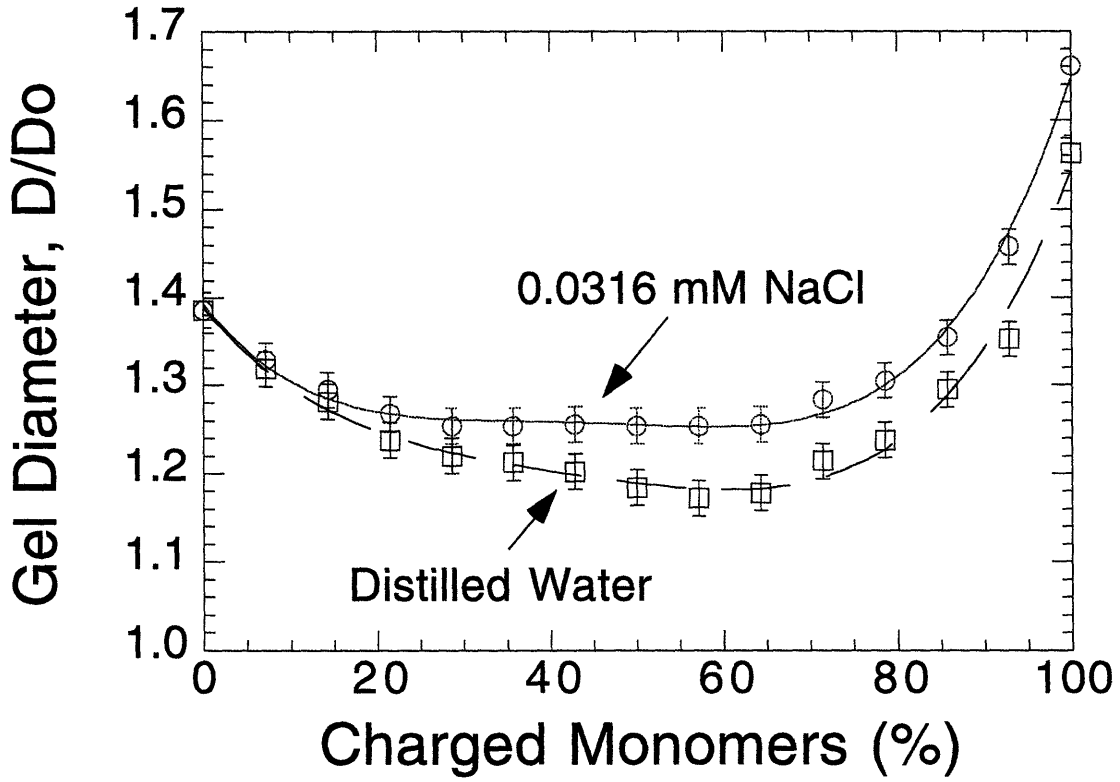

Figure 5-6: Polyampholyte swelling with a 1.4% charge offset (+20 mM offset at a total charge concentration of 1.4 M) with varying neutral monomeric composition at low ionic strengths. Increasing proportions of total charge show swelling effects consistent with base dissociation.

Figures 5-7 and 5-8 illustrate the multiple swelling effects in positively charged hydrogels over a wide range of bath salt concentrations. The complete set of mea-

surements took approximately three months to acquire in order to ensure that equilibrium had been obtained at each point. Without neutral monomers polyampholytes with a charge offset of +20 mM show characteristic swelling patterns with increasing bath salt concentrations consistent with hydroxide ion exchange, polyelectrolyte shielding, polyampholyte shielding and solvent effects which vary with monomeric composition. If solvent and elastic effects are ignored, at low bath ionic strengths increasing the proportion of neutral monomers will drive the internal pH towards that of the bath as the total charge concentration falls. The effect of internal pH on the swelling equilibrium of unbalanced polyampholytes will thus be more pronounced at high relative total charge concentrations and low bath salt concentrations. As Figs. 5-7 and 5-8 illustrate, however, solvent and elastic effects of the network complicate the swelling pattern.

Figure 5-9 shows the internal pH as a function of bath salt concentration for hydrogels with different total fixed charge concentrations. The total fixed charge concentration can be altered by changing the proportion of neutral monomers, the network elastic and solvent pressures, or through the application of external pressures. The top set of curves represent hydrogels with a 1.4% positive charge offset and the bottom those with a 1.4% negative charge offset. The asymmetry is due to both differences in dissociation constants and the effects of competing bicarbonate ions that result from dissolved CO_2. At high bath salt concentrations the internal pH becomes that of the surrounding bath. At low ionic strengths hydrogen ions balance hydrogels with excess acidic groups and hydroxide and bicarbonate ions balance hydrogels with excess base groups.

Assuming that Donnan partitioning is a valid, one could use these curves to estimate the internal hydrogen ion concentration for a given swelling measurement. All other ion concentration follow from Donnan partitioning and hence the total internal mobile ion concentration and osmotic pressure can be estimated. Local charge inhomogeneities, however, can lead to discrepancies in the internal ion concentration

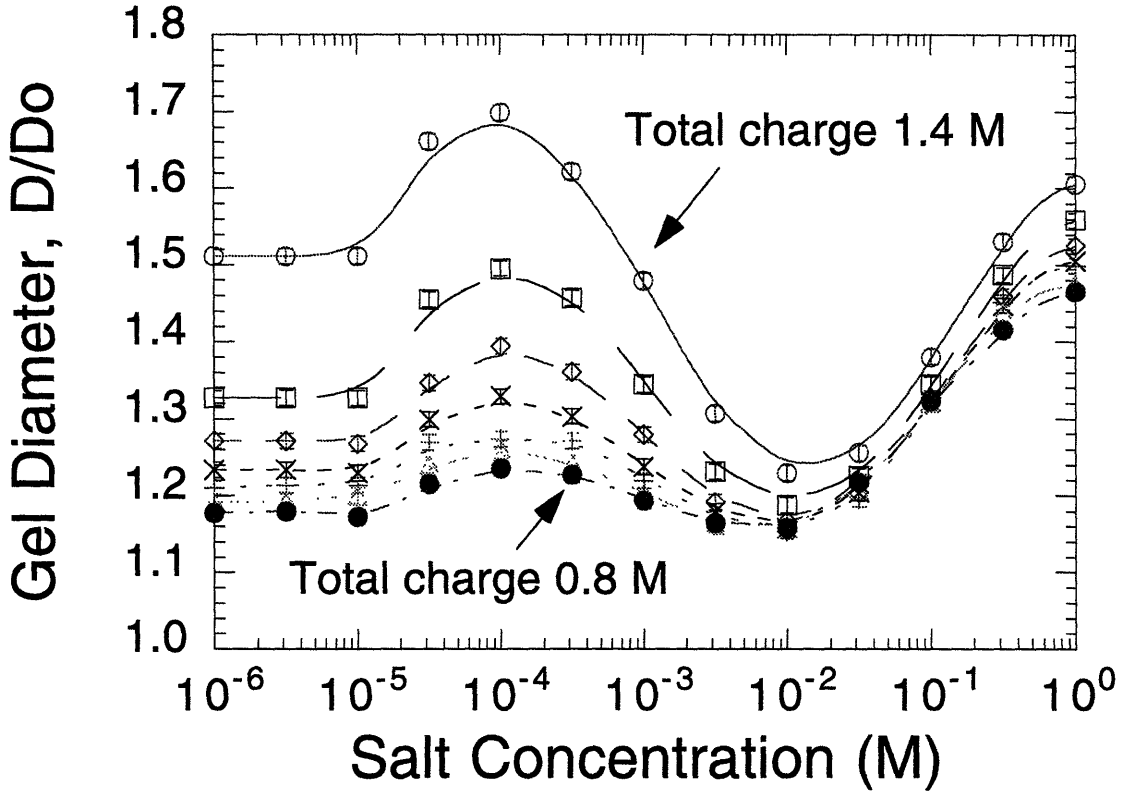

Figure 5-7: Charged polyampholyte swelling versus bath salt concentration (1.4 to 0.8 M total charge). With increasing bath salt concentrations ion dissociation, polyelectrolyte and finally polyampholyte effects are destroyed leaving only solvent and elastic interactions.

predicted by this model. In addition, with a large background of balanced positive and negative charges it will be energetically more favorable to have a higher internal salt concentration than that predicted by Donnan partitioning.

Changing the fraction of neutral monomeric spacers will alter the reference state volume fraction of the composite hydrogel. The volume fractions of pure DMAAm and AMPS-MAPTA in their reference states immediately following polymerization are significantly different. Based on the manufacturers specification, the volume fraction of DMAAm in the reference state immediately following polymerization is

$$\phi_{o\ DMAAm} = \text{Concentration} \times \text{F.W.} \ / \ \text{Density} \times \ \text{Purity}$$

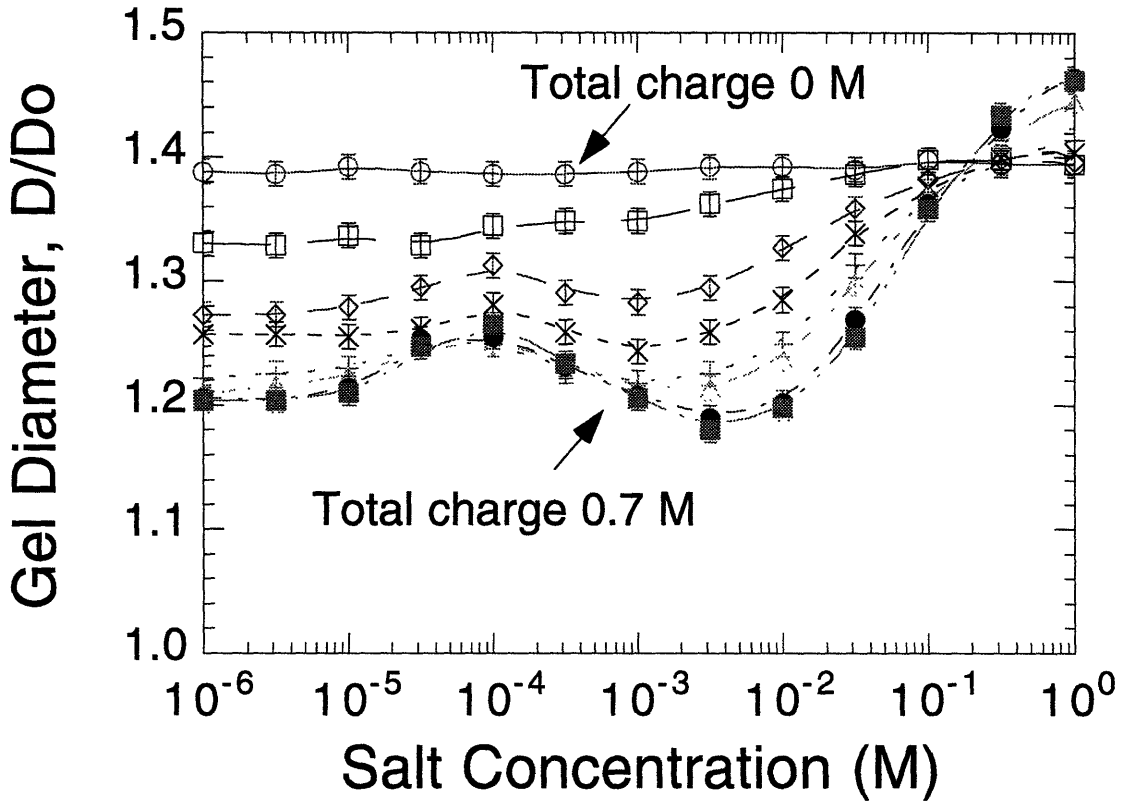

Figure 5-8: Charged polyampholyte swelling versus bath salt concentration (0.7 to 0.0 M total charge). Adding increasing proportions of neutral monomers to positively charged polyampholytes eventually eliminates all ionic effects.

$$= 1.4 \text{ mol/L} \times 99.13 \text{ g/mol} / 0.962 \text{ g/mL} \times 1000 \text{ mL/L} \times 0.99$$

$$= 0.14426.$$

A similar calculation for AMPS-H and MAPTA-Cl gives $\phi_{o\ AMPS-MAPTA} = 0.29946$. The reference state volume fraction, ϕ_{ot}, with combined neutral and charged monomeric components can in principle be estimated by interpolating the volume fraction of the pure components based on the relative composition

$$\phi_{ot}(f_N) = f_N \phi_{o\ DMAAm} + (1 - f_N)\phi_{o\ AMPS-MAPTA}. \tag{5.8}$$

Interpolating the reference state volume fraction in this manner assumes that com-

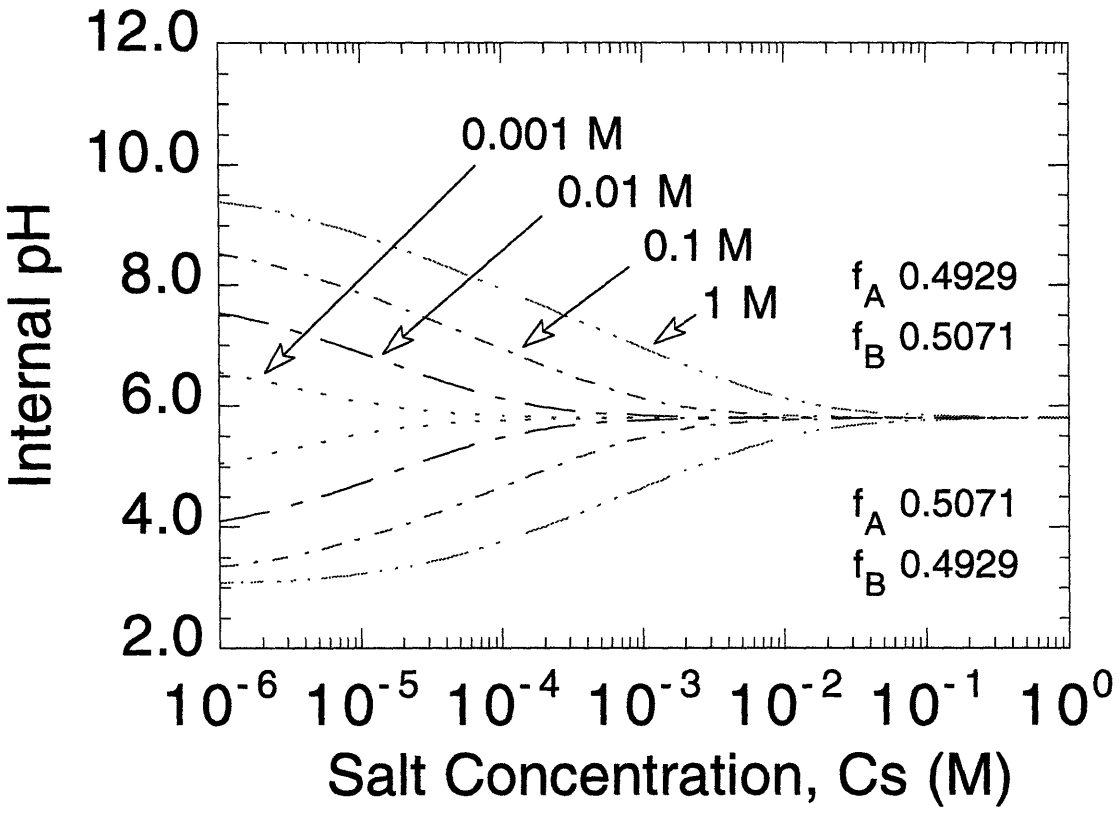

Figure 5-9: Predicted internal pH versus bath salt concentration for hydrogels with different total fixed charge concentrations. The top four curves represent a 1.4% positive charge offset and the lower four curves a 1.4% negative charge offset. The dissociation constants are $pK_a = 1.5$ and $pK_b = 11.5$ and the bath pH is 5.8.

plete polymerization has occurred. In practice, one should check this by weighing the hydrogel before and after freeze drying. However, the effects of residual ions in the network can complicate this type of measurement.[Qui93] Even with balanced polyampholytes a significant fraction of counter ions may be present inside the hydrogel.

The effective solvent interaction parameter, χ_t, will change in a complicated manner as the hydrogel composition is varied. One can estimate the Flory solvent interaction parameter by considering only the elastic and mixing contributions to the osmotic pressure. When one neglects the ion contributions to the osmotic

pressure we are left with

$$-\left[\ln(1-\phi_t)+\phi_t+\chi_t\phi_t^2\right]+\frac{\phi_{ot}}{N_x}\left[\frac{1}{2}\left(\frac{\phi_t}{\phi_{ot}}\right)-\left(\frac{\phi_t}{\phi_{ot}}\right)^{\frac{1}{3}}\right]=0. \tag{5.9}$$

Solving for χ_t gives us

$$\chi_t=\frac{1}{\phi_t^2}\left\{\frac{\phi_{ot}}{N_x}\left[\frac{1}{2}\left(\frac{\phi_t}{\phi_{ot}}\right)-\left(\frac{\phi_t}{\phi_{ot}}\right)^{\frac{1}{3}}\right]-\ln(1-\phi_t)-\phi_t\right\}. \tag{5.10}$$

Knowing ϕ_{ot} and the value of ϕ_t when ionic contributions to the osmotic pressure can be ignored allows us to calculate χ_t from

$$\phi_t=\phi_{ot}\left(\frac{D_o}{D}\right)^3. \tag{5.11}$$

The solvent interaction parameter can thus be found at high salt concentrations where polyampholyte and polyelectrolyte effects are small and the solvent and elastic effects make the dominant contribution to the osmotic pressure. Assuming high bath salt concentrations does not change the solvent interaction, we can use the D/D_o values for AMPS-MAPTA at high salt concentrations where both polyelectrolyte and polyampholyte effects are small. Since DMAAm is neutral and insensitive to variations in salt concentration we can use pure DMAAm diameter measurements at any salt concentration to estimate its effective solvent interaction.

Using the swelling diameters at high salt concentrations gives us the χ interaction parameter as a function of the number of monomers between cross-links. Figure 5-10 shows the value of χ for pure DMAAm and pure AMPS-MAPTA as a function of the number of monomers between cross-links using estimated values of ϕ and ϕ_o at high salt concentration. One notices that χ can vary significantly as a function of the number of monomers between cross-links and can even become negative. If one were to assume that the value of χ_t can be interpolated between those of the pure monomers one would conclude that χ_t is a stronger function of the number of

monomers between cross-links than the relative composition. In addition, Fig. 5-10 would suggest that for hydrogels made of both DMAAm and AMPS-MAPTA the change in χ_t with composition is smaller at low cross-linking densities. One should consider the fact that the cross-linking efficiency can easily vary as the monomeric composition is altered.

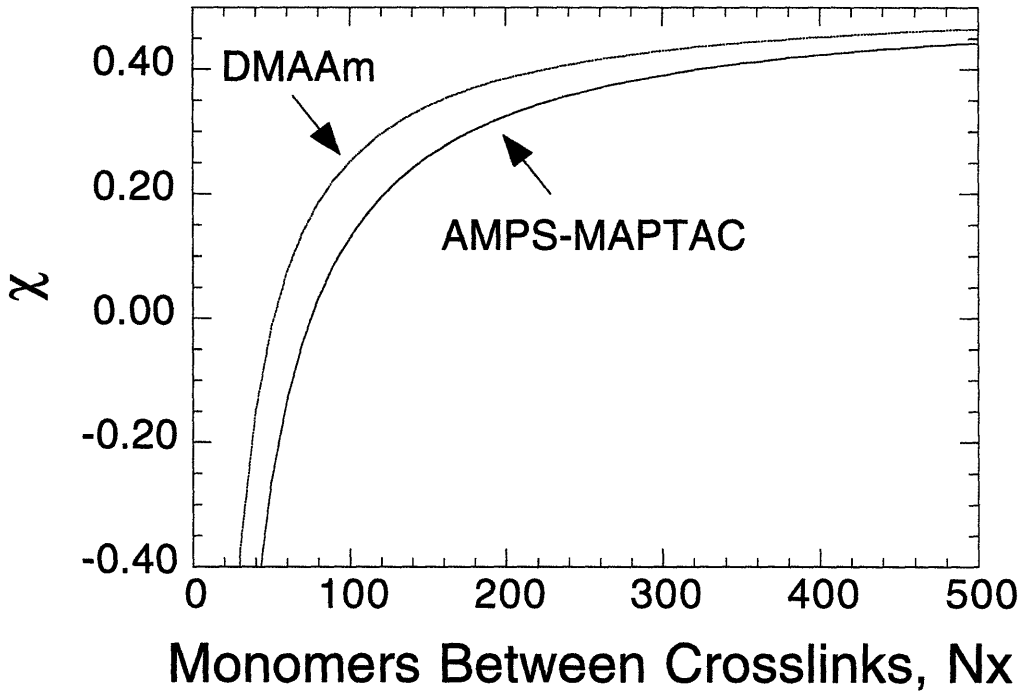

Figure 5-10: Flory solvent interaction parameter, χ, versus the number of monomers between cross-links for DMAAm and AMPS-MAPTA hydrogels based on experimental swelling measurements at high salt concentrations.

Figure 5-11 shows the mixing and elastic contributions to the osmotic pressure as a function of monomer concentration. Compared to the mixing osmotic pressure contribution over a similar concentration range the elastic osmotic pressure is comparable only for short chain lengths and low monomer concentrations. To a first order approximation reference state concentration will have little effect on the final equilibrium concentration if the number of monomers between cross-links is the same. The elastic contribution to the osmotic pressure in a Flory-Huggins model depends primarily on the number of monomers between cross-links.

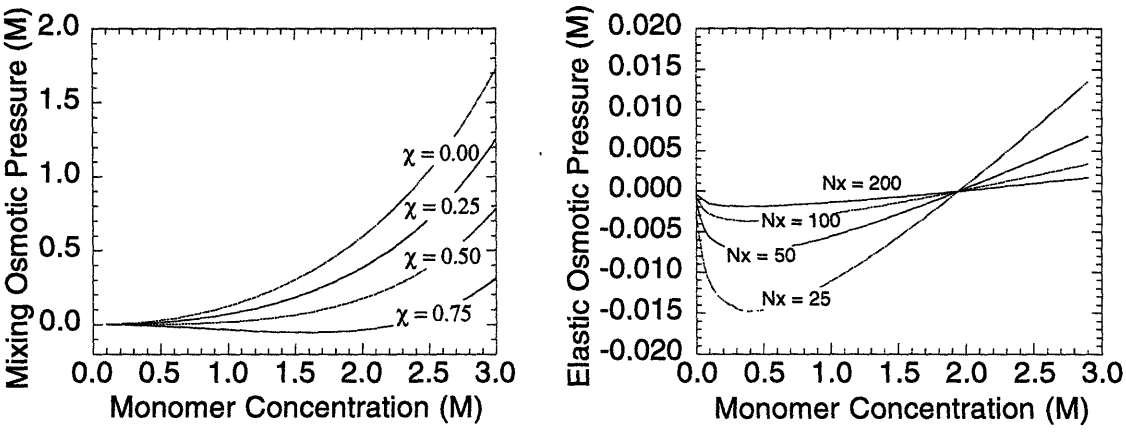

Figure 5-11: Mixing and elastic osmotic pressure components as a function of monomer concentration.

Flory-Huggins models have a number of limitations. The effects of polydispersity and entanglement are not included in this model for example. Furthermore, the Flory solvent interaction parameter will be a function of the degree of ionization of the polyampholyte network. Ionized polyions will give the polymer a low solvent interaction parameter. Unionized polyions, however, will result in lowering the quality of the solvent. The effective cross-linking density will be non-uniform and in some cases will not contribute to the elasticity of the network if the cross-links do not incorporate into the network or only one of the two bonds reacts with growing polymer chain. Varying the monomer composition can also change the effective cross-linking density and as a result the elastic contribution to the osmotic pressure will be a function of the monomer composition.

A number polyampholyte swelling equilibrium model include Debye-Hückel corrections to the free energy.[Hig91,Bak95,Yu93] Debye-Hückel corrections to the free energy lead to additional negative contributions to the osmotic pressure. At low electrolyte concentrations Debye-Hückel correction terms are acceptable and may in fact be important particularly when ion dissociation equilibria can influence the hydrogel swelling equilibrium. At the ionic concentrations of interest in this study,

however, Debye-Hückel corrections lead to catastrophic divergences. It is interesting to note that previous studies based on Debye-Hückel models use large unphysical correction factors in these models.[Yu93,Bak95]

Based on the ion concentrations within a 1.0 M polyampholyte with 20 mM excess acid groups the osmotic pressure contributions due to Debye shielding is shown in Fig. 5-12. The concentrations typical of this experiment result in a very unphysical divergence of the osmotic pressure at high ionic strength. In addition, the Debye-Hückel contribution completely dominates the ion osmotic pressure over most of the bath salt concentrations.

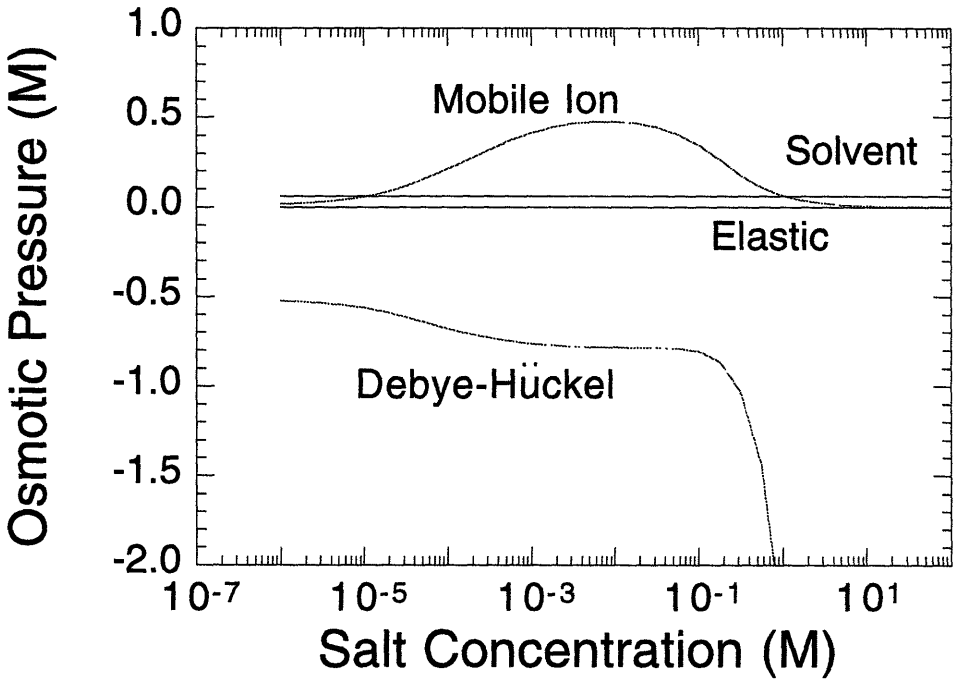

Figure 5-12: Osmotic pressure components for a 1 M acidic hydrogel as a function of bath salt concentration. The ion and Debye-Hückel osmotic pressures represents the difference between the internal and bath values. Including Debye-Hückel corrections to the osmotic pressure produces a catastrophic divergence at high bath salt concentrations.

In a previous study of polyelectrolyte behavior[Ric84a] Debye-Hückel correc-

tions to the swelling equilibrium were ignored on the account they were believed to be small corrections to the overall free energy and osmotic pressure. This treatment is motivated from ionic solution theory and is incorrect for two reasons. For fixed hydrogel ion concentrations on the order of a 1.0 mM or greater and bath salt concentrations in excess of a 1.0 mM Debye-Hückel corrections make diverging contributions to the osmotic pressure. In addition, for small charge offsets the electrostatic repulsion between interacting double layers becomes significant and the concept of small corrections to an ideal gas of solute ions is conceptually not valid.

5.5 Conclusions

At low ionic strengths acid and base dissociation and very slow kinetics dominate the swelling behavior of AMPS-MAPTA hydrogels. With increasing bath salt concentrations ion dissociation, polyelectrolyte and polyampholyte effects are shielded. Polyelectrolyte repulsion is shielded at lower ionic strengths when the charge offset is a few percent of the total charge concentration. As a result, in this study polyampholyte effects are shielded on smaller length scales than polyelectrolyte effects. Increasing relative concentrations of neutral monomers progressively reduces the effects of acid and base dissociation, polyelectrolyte and polyampholyte effects.

Debye-Hückel corrections to the osmotic pressures produce catastrophic divergences over much of the polyion and bath salt concentrations of interests in this study. The correction factors used to reduce these catastrophic divergences still fail over much of the concentration range used in this study.

Flory-Huggins lattice models provide useful insight into the contributions to the equilibrium swelling of copolymer hydrogels but are limited in a number of ways. Lattice site volumes for all monomers and solvent molecules are assumed to be equal which is clear not the case in this study. Inhomogeneities in the hydrogel structure also violate the assumption of the Flory-Huggins model. The actual concentration

of effective cross-links is also not know.

The extreme internal pH values that can be reached at low ionic strengths is an important consideration for the use and understanding of these materials. It is interesting to note that inorganic ion exchangers suffer partial decomposition from attack by acids and bases and as a result their use is restricted to a narrow pH range around pH 7.[Hel62] This could be a very important point for enzymatically controlled hydrogel swelling transitions that use enzymes that a functionally stable over a narrow pH range.

Chapter 6

Thesis Conclusions

This thesis has presented a critical study of polyampholytic phase transitions using Monte Carlo based simulations, analytical models and experimental measurements. The results of previous polyampholyte Monte Carlo simulations[Kan92,Aal94] have made important contributions to our understanding of these materials. In addition, experimental studies[Yu93,Bak95] of polyampholytic hydrogels have been of no less importance.

In agreement with previous studies, Monte Carlo simulations of single polyampholyte polymer chains show a distinct low temperature swelling transition at a critical charge offset. However, the extrapolation of these types of Monte Carlo polyampholyte simulations[Kan92] to explaining the observed swelling transitions of previous experimental studies[Yu93] is incorrect for three reasons. The coupling energy upon which these conclusions were based is much higher than that which exists in the physical system being modeled. In addition, counter ions which are present in real physical systems were completely ignored. Finally, similar to another study[Aal94], the data upon which these simulations were originally based had not completely equilibrated. As a result, unequilibrated data was used in support of models representing equilibrium thermodynamic states.

The numerical intensity of Monte Carlo simulations with Coulombic forces limits

the incorporation of counter ions in these models and as a result they are restricted to short isolated polyampholytes in non-aqueous solvents. The exclusion of counter ions in these simulations precludes the possibility of including condensation effects that become important as the charge offset increases and the temperature decreases. Furthermore, ion dissociation effects which were key to understanding the experimental results of this study, were not included in these simulations. The incorporation of Debye shielding terms to include counter ions in these models is limited to high Monte Carlo temperatures only.

Polyelectrolytes, or polymeric systems having all charges of the same sign, with dissociable ionic groups show distinct swelling patterns as a function of bath electrolyte concentration. At low bath ionic strengths ion dissociation dominates the equilibrium swelling. In aqueous solvents at low ionic strengths hydrogen ions become the only available counter ion to maintain internal charge neutrality for polyelectrolytes with fixed negative monomers. The binding of hydrogen to acidic monomeric groups results in the loss of osmotic pressure, or equivalent mutual electrostatic repulsions, and as a result the polyelectrolyte collapses at low ionic strengths. Increasing monovalent bath salt concentrations results in the exchange of internal hydrogen ions and the swelling of polyelectrolyte hydrogels due to the dissociation of hydrogen from unionized acidic monomers. Increasing bath salt concentration also contributes to polymer ion screening and reduces the osmotic pressure gradient. As a result, further increases in bath salt concentration ultimately lead to polyelectrolyte collapse.

Using acrylic acid, acylamide and N-isopropylacrylamide monomers, a polyelectrolyte copolymeric hydrogel with three distinct swelling transition regions was successfully synthesized. Swelling patterns at intermediate and low bath ionic strengths were consistent with typical polyelectrolyte behavior. At very high ionic strengths, however, the effect of ions on the neutral components produced a collapse transition. Based on the charge concentrations used in the hydrogel synthesis, the kinetic

effects due to diffusion reaction mechanisms were not long enough to compete with the mechanical response time in most cases. Varying the bivalent bath salt concentration produced a complicated swelling pattern that is both temperature sensitive and charge dependent.

Both the equilibrium and non-equilibrium swelling measurements of polyampholytic hydrogels illustrates the importance of including counter ions in the description of polyampholyte behavior. Similar to polyelectrolytes, the swelling equilibrium of unbalanced polyampholytes at low bath ion strengths is strongly influenced by acid and base dissociation. Slightly unbalanced polyampholytes show polyelectrolyte behavior at intermediate bath salt concentrations and collapse with increasing salt concentration. Unlike polyelectrolytes, however, polyampholytes swell when the bath salt concentration becomes comparable to the local concentration of positive and negative polyions. Polyelectrolyte repulsion is effectively screened at longer length scales than polyampholyte attraction.

The incorporation of neutral monomeric components into polyampholytic hydrogels produces a complicated swelling pattern as a function of bath electrolyte concentration that is the result of competing solvent, elastic and ionic interactions. The effects of ion dissociation at low ionic strengths diminishes with increasing neutral monomer concentrations. Both polyampholyte and polyelectrolyte effects are diminished, as expected, with increasing proportions of neutral monomers. The additional complication due to differences in solvent interactions between neutral and charged monomers are apparent when the polymer fixed charges are screened at high bath salt concentrations.

In closing, despite the effort to understand polyampholyte phase behavior, it is clear that much confusion still exists in this field. The limitations of the models used in this thesis are written testimony to the fact that much work is left to be done. One can conclude from the results of this work, however, that if physics truly is the study of natural phenomenon, then elaborate theories and models are of little

value if we lose contact with the real physical system we are trying to understand.

Bibliography

[Aal94] D. Aalberts, PhD Thesis, MIT (1994).

[Ann92] M. Annaka and T. Tanaka, *Nature*, **355**, 430 (1992).

[Ann94] M. Annaka and T. Tanaka, *Phase Transitions*, **47**, 143 (1994).

[Bak94] J. P. Baker, L. H. Hong, H. W. Blanch, and J. M. Prausnitz, *Macromolecules*, **27**, 1446 (1994).

[Bak95] J. P. Baker, H. W. Blanch and J. M. Prausnitz, *Polymer*, **36**, 1061 (1995).

[Bio41] M. Biot, *J. App. Phys.*, **12**, 155 (1941).

[Bor88] V. Borue and I. Erukhimovich, *Macromolecules*, **21**, 3240 (1988).

[Can87] S. J. Candau and A. Peters, *Polym. Mater. Sci. Eng. Proc.*, **57**, 270 (1987).

[Car88] I. Carmesin and K. Kremer, *Macromolecules*, **21**, 2819 (1988).

[Cor93] J. Corpart and F. Candau, *Macromolecules*, **26**, 1333 (1993).

[CRC77] *CRC Handbook of Chemistry and Physics, 58th Edition*, CRC Press Inc., B254 (1977-1978).

[DeS93] A. R. De Souza and L. Degreve, *Molecular Simulation*, **11**, 337 (1993).

[Deb23] P. Debye and E. Hückel, *Z. Physik*, **24**, 185 (1923).

[Dob95] A. V. Dobrynin and M. Rubinstein, *J. de Physique II*, **5**, 677 (1995).

[Edw80] S. F. Edwards, P. R. King and P. Pincus, *Ferroelectrics*, **30**, 3 (1980).

[Eng95] A. English, X. Yu and T. Tanaka, Abstract, *Materials Research Society*, N3.58 (1995 Fall Meeting).

[Eng96] A. English, S. Mafé, J. Manzanares, X. Yu, A. Grosberg, and T. Tanaka, *J. Chem. Phys.*, (Accepted) (1996).

[Flo53] P. Flory, *Principles of Polymer Chemistry, Ch. XIII*, Cornell University Press, Ithaca, New York (1953).

[Flo79] P. Flory, *Polymer*, **20**, 1317 (1979).

[Gri90] P. E. Grimshaw, J. H. Nussbaum, A. J. Grodzinsky, and M. L. Yarmish, *J. Chem. Phys.*, **93**, 4462 (1990).

[Gro94] A. Yu. Grosberg and A. R. Khokhlov, *Statistical Physics of Macromolecules, Ch. 5*, AIP Press, NY (1994).

[Gut95] A. M. Gutin and E. I. Shakhnovich, *Phys. Rev. E*, **50**, R3322 (1994).

[Hel62] F. Helfferich, *Ion Exchange*, McGraw-Hill, New York (1962).

[Hig91] P. G. Higgs and J. F. Joanny, *J. Chem. Phys.* **94**, 1543 (1991).

[Hil60] T. L. Hill, *Introduction to Statistical Thermodynamics*, Dover, New York (1960).

[Hir87] S. Hirotsu, Y. Hirokawa and T. Tanaka, *J. Chem. Phys.*, **87**, 1392 (1987).

[Hoo90] H. H. Hooper, J. P. Baker, H. W. Blanch, and J. M. Prausnitz, *Macromolecules*, **23**, 1096 (1990).

[Jac75] J. D. Jackson, *Classical Electrodynamics, 2nd Ed.*, John Wiley and Sons, 1020 (1975).

[Kan92] Y. Kantor, H. Li and M. K. Kardar, *Phys. Rev. Letters*, **69**, 61 (1992).

[Kan94] Y. Kantor, M. K. Kardar and H. Li, *Phys. Rev. E*, **49**, 1383 (1994).

[Kan95a] Y. Kantor and M. K. Kardar, *Phys. Rev. E*, **51**, 1299 (1995).

[Kan95b] Y. Kantor and M. K. Kardar, *Phys. Rev. E*, **52**, 835 (1995).

[Kit86] C. Kittel, *Introduction to Solid State Physics*, Wiley, New York (1986).

[Lan58] L. Landau and E. Lifshitz, *Statistical Physics*, Pergamon Press, 229 (1958).

[Lif78] I. M. Lifshitz, A. Yu. Grosberg and A. R. Khokhlov, *Rev. Mod. Phys.*, **50**, 683 (1978).

[Liu95] X. Liu, Z. Tong and O. Hu, *Macromolecules*, **28**, 3813 (1995).

[Lee80] S. W. DeLeeuw, J. W. Perram and E. R. Smith, *Proc. R. Soc. Lond. A*, **373**, 27 (1980).

[Mar83] J. E. Marsden and T. J. R. Hughes, *Mathematical Foundations of Elasticity*, Prentice-Hall, New Jersey (1983).

[May50] J. E. Mayer, *J. Chem. Phys.*, **18**, 1426 (1976).

[McQ76] D. A. McQuarrie, *Statistical Mechanics*, Harper and Row, New York (1976).

[McM45] W. G. McMillan and J. E. Mayer, *J. Chem. Phys.*, **13**, 276 (1945).

[Met53] N. Metropolis, *J. Chem. Phys.*, **21**, 1087 (1953).

[Nag61] M. Nagasawa and S. A. Rice, *Polyelectrolyte Solutions*, Academic Press, London (1961).

[Neu73] J. Neuman, *Electrochemical Systems*, Prentice-Hall, New Jersey (1973).

[Nus81] J. H. Nussbaum and A. Grodzinsky, *J. Membrane Sci.*, **8**, 193 (1981).

[Oos71] F. Oosawa, *Polyelectrolytes*, Marcel Dekker Inc. (1971).

[Osa87] Y. Osada, *Adv. Polym. Sci.*, **82**, 1 (1987).

[Out74] C. W. Outhwaite, *Statistical Mechanics - Vol. 2 Specialist Periodical Reports*, 188 (1974).

[Qui93] T. M. Quinn and A. J. Grodzinsky, *Macromolecules*, **926**, 4332 (1993).

[Ove56] J. Th. G. Overbeek, In *Progress in Biophysics and Biophysical Chemistry*, Pergamon-Press, London (1956).

[Qia88] C. Qian and A. L . Kholodenko, *J. Chem. Phys.*, **89**, 5273 (1988).

[Ric84a] J. Rička and T. Tanaka, *Macromolecules*, **17**, 2916 (1984).

[Ric84b] J. Rička and T. Tanaka, *Macromolecules*, **18**, 83 (1984).

[Sal80] J. C. Salamone, C. C. Tsai, A. P. Olson, and A. C. Watterson, *J. Pol. Sci.*, **18**, 2983 (1980).

[Sal82] J. C. Salamone, N. A. Mahumud, M. U. Mahmud, T. Nagabhushanam, and A. C. Watterson, *Polymer*, **23**, 843 (1982).

[Sal84] J. C. Salamone, C. C. Tsai, Q. Anwaruddin, A. P. Olson, M. Arnold, T. Nagabhushanam S. Sawan, and A. C. Watterson, *J. Pol. Sci.*, **22**, 2005 (1984).

[Sal88] J. C. Salamone, I. Ahmed, E. L. Rodriguez, L. Quach, and A. C. Watterson, *J. Macromol. Sci. Chem.*, **A25**, 811 (1988).

[Sim91] P. Simon, *Ion Exchange Training Manual*, Van Nostrand Reinhold, New York (1991).

[Sko94] M. Skouri, J. P. Munch, S. J. Candau, S. Neyret, and F. Candau, *Macromolecules*, **27**, 69 (1994).

[Sta71] H. E. Stanley, *Introduction to phase transitions and critical phenomena*, Oxford University Press, Oxford (1971).

[Tan73] T. Tanaka, L. Hocker and G. Benedek, *J. Chem. Phys.*, **59**, 5151 (1973).

[Tan78] T. Tanaka, *Phys. Rev. Lett.*, **40**, 890 (1978).

[Tan79] T. Tanaka and D. J. Fillmore, *J. Chem. Phys.*, **70**, 1214 (1979).

[Tan80] T. Tanaka, D. J. Fillmore, S. Sun, I. Nishio, G. Swislow, and A. Shah *Phys. Rev. Let.*, **45**, 1636 (1980).

[Tan95] T. Tanaka, C. Wang, V. Pande, A. Grosberg, A. English, S. Masamune, H. Gold, R. Levy, K. King, *Faraday Discuss.*, **102** (1996).

[Val89] J. P. Valleau, *Chem. Phys.*, **129**, 163 (1989).

[Vas86] V. V. Vasilevskaya and A. R. Khokhlov, *Polymer Science U.S.S.R.*, **28**, 348 (1986).

[Vic93] J. M. Victor and J. B. Imbert, *Europhys. Lett.*, **24**, 189 (1993).

[Wal75] F. T. Wall and F. Mandel, *J. Chem. Phys.*, **63**, 4592 (1975).

[Whi93] J. Whittmer, A. Johner and J. F. Joanny, *Europhys. Lett.*, **24**, 263 (1993).

[Yu93] X. Yu, PhD Thesis, MIT, (1993).